1. Report No.	2. Government Accession No.	3. Recipient's Catalog No.
FHWA/TX-04/0-4162-2		

4. Title and Subtitle	5. Report Date
DYNAMIC RESPONSE OF GUARDRAIL SYSTEMS ENCASED IN PAVEMENT MOW STRIPS	January 2004
	6. Performing Organization Code

7. Author(s)	8. Performing Organization Report No.
Roger P. Bligh, N. Ryan Seckinger, Akram Y. Abu-Odeh, Paul N. Roschke, Wanda L. Menges, and Rebecca R. Haug	Report 0-4162-2

9. Performing Organization Name and Address	10. Work Unit No. (TRAIS)
Texas Transportation Institute The Texas A&M University System College Station, Texas 77843-3135	11. Contract or Grant No. Project No.0-4162

12. Sponsoring Agency Name and Address	13. Type of Report and Period Covered
Texas Department of Transportation Research and Technology Implementation Office P.O. Box 5080 Austin, Texas 78763-5080	Research: September 2001 – August 2003
	14. Sponsoring Agency Code

15. Supplementary Notes

Research performed in cooperation with the Texas Department of Transportation and the U.S. Department of Transportation, Federal Highway Administration

Research Project Title: Evaluation of Barrier Systems and Placement Issues

16. Abstract

Pavement mow strips are being used to combat vegetation growth around guardrail posts. However, the effect of pavement post encasement on the crashworthiness of strong post guardrail systems has not been investigated. In this paper, we examined the performance of these systems using experimental testing and numerical simulation. Mow strip dimensions, materials, and depths are considered in addition to the presence of "leave-out" sections around posts.

Seventeen configurations of wood and steel guardrail posts embedded in various mow strip systems and confinement conditions were subjected to dynamic impact testing with a bogie vehicle. The dynamic impact tests were numerically simulated, and full-scale mow strip system models were assembled using the validated subcomponent models.

Based on predictive numerical simulations, we selected a concrete mow strip with grout-filled leave-outs for full-scale crash testing. Crash tests of a steel post guardrail system and wood post guardrail system encased in the selected mow strip configuration were successful, and implementation recommendations are provided.

17. Key Words	18. Distribution Statement
Longitudinal Barrier, Guardrail, W-Beam, Mow Strip, Mowstrip, Roadside Maintenance, Crash Testing, Roadside Safety	No restrictions. This document is available to the public through NTIS: National Technical Information Service 5285 Port Royal Road Springfield, Virginia 22161

19. Security Classif.(of this report)	20. Security Classif.(of this page)	21. No. of Pages	22. Price
Unclassified	Unclassified	166	

DYNAMIC RESPONSE OF GUARDRAIL SYSTEMS ENCASED IN PAVEMENT MOW STRIPS

by

Roger P. Bligh
Associate Research Engineer
Texas Transportation Institute

N. Ryan Seckinger
Graduate Research Assistant
Texas Transportation Institute

Akram Y. Abu-Odeh
Associate Research Scientist

Paul N. Roschke
Research Engineer

Wanda L. Menges
Associate Research Specialist

and

Rebecca R. Haug
Research Assistant
Texas Transportation Institute

Report 0-4162-2
Project Number 0-4162
Research Project Title:
Evaluation of Barrier Systems and Placement Issues

Sponsored by the
Texas Department of Transportation
In Cooperation with the
U.S. Department of Transportation
Federal Highway Administration

January 2004

TEXAS TRANSPORTATION INSTITUTE
The Texas A&M University System
College Station, Texas 77843-3135

DISCLAIMER

The contents of this report reflect the views of the authors, who are responsible for the facts and the accuracy of the data, and the opinions, findings, and conclusions, presented herein. The contents do not necessarily reflect the official view or policies of the Texas Department of Transportation (TxDOT), Federal Highway Administration (FHWA), the Texas A&M University System, or the Texas Transportation Institute (TTI). This report does not constitute a standard, specification, or regulation; its contents are not intended for construction, bidding, or permit purposes. In addition, the above listed agencies assume no liability for its contents or use thereof. The names of specific products or manufacturers listed herein do not imply endorsement of those products or manufacturers. The engineer in charge was Roger P. Bligh, P.E. (Texas, #78550).

ACKNOWLEDGMENTS

This research project was conducted under a cooperative program between the Texas Transportation Institute, the Texas Department of Transportation, and the U.S. Department of Transportation, Federal Highway Administration. The authors wish to acknowledge Mr. Robert Kovar, Mr. Mark Marek, and Ms. Rory Meza, who directed the project for TxDOT. The support and guidance of Mr. Martin Hargrave, who served as the technical representative for FHWA, is also acknowledged and appreciated.

TABLE OF CONTENTS

TABLE OF CONTENTS (CONTINUED)

Page

LIST OF FIGURES

LIST OF FIGURES (CONTINUED)

LIST OF FIGURES (CONTINUED)

FIGURE Page

LIST OF FIGURES (CONTINUED)

FIGURE Page

LIST OF TABLES

1. INTRODUCTION

1.1 BACKGROUND

1.1.1 General

Since the invention of the automobile, motor vehicle collisions have threatened public health and welfare through property damage and personal injury. Each day, more than 3000 people are killed in motor vehicle accidents worldwide. In the United States alone, approximately 42,000 people lose their lives due to traffic accidents annually. Although a majority of traffic fatalities involve multiple vehicles on a roadway, the Transportation Research Board (TRB) estimates that over 30 percent of deaths result from single-vehicle impacts with roadside structures. *(1)* These roadside structures include both manmade devices such as bridge piers and overhead sign structures, and naturally occurring features such as trees or non-traversable changes in grade. By developing devices to redirect vehicles away from hazards, or by modifying the hazards to lessen the severity of an impact, many of these fatalities can be prevented.

To this end, both the Federal Highway Administration (FHWA) and state departments of transportation such as Texas Department of Transportation (TxDOT) invest significant resources into developing better roadside devices and investigating the safety of current practices. By upgrading outdated facilities and implementing new technologies when possible, the safety of roadways can improve dramatically. In this research, the safety of one common practice, namely use of pavement mow strips, used along American roadways is evaluated through crash testing and numerical simulation in order to verify compliance with current safety performance standards. The following paragraphs in this section introduce the topics to be discussed.

1.1.2 Vegetation Control Mow Strips

Unchecked, roadside vegetation growth can impede motorist vision at intersections and degrade the appearance of a roadside guardrail (see Figure 1). In an effort to reduce maintenance costs and the safety risk to workers associated with hand mowing around guardrail, and amid recent environmental concerns regarding the use of herbicides to control roadside vegetation growth, there is a nationwide trend toward encasing guardrail posts in pavement. This pavement layer prevents vegetation growth within several feet of guardrail installations and thereby

reduces the need for hand mowing or herbicide use. However, by increasing the rigidity of the confining material around the guardrail post, the pavement "mow strip" impedes rigid-body rotation and deformation of the post. Because the energy absorbing capability of a guardrail system relies on the ability of the posts to rotate through the confining soil medium, the larger effective stiffness induced by the pavement mow strip can lead to premature post fracture and snagging or pocketing of a vehicle in the guardrail system. If not properly designed, this confinement can both decrease the effectiveness of the guardrail to safely redirect a misguided vehicle and increase repair costs after a collision.

Figure 1. Guardrail Installation Overgrown with Vegetation.

1.2 OBJECTIVE AND SCOPE

This research examines current mow strip configurations used by TxDOT in an effort to develop a standard mow strip system that meets National Cooperative Highway Research Program (NCHRP) *Report 350* criteria. *(2) NCHRP Report 350* is the standard of federal performance requirements for roadside safety hardware on the National Highway System (NHS). Evaluation of the impact performance and maintenance characteristics of mow strip systems used

subcomponent impact testing; full-scale crash testing; and the nonlinear, dynamic, finite-element analysis code LS-DYNA. *(3)*

The wide variation of mow strip materials and geometric parameters makes full-scale crash testing each configuration cost prohibitive. Thus, finite element simulation was used to reduce the number of full-scale tests required to develop a final design. The parametric variation inherent in various mow strip designs makes computer simulation an ideal tool for the design process. With rapidly increasing availability of computing power, nonlinear finite element analysis has quickly become an important design tool in the roadside safety field. Its use in this project was integral to the evaluation and selection of mow strip systems for the final full-scale crash-testing phase of this research.

1.3 STATE OF PRACTICE

1.3.1 Mow Strip Usage

For many years, standard strong post guardrail systems have effectively redirected errant vehicles. Composed of a W-beam rail mounted on either W150×13 (W6×9) steel, 178 mm (7 in.) diameter wood, or 152 mm × 203 mm (6 in. × 8 in.) wood posts embedded in soil to depths of approximately 1.1 m (3.6 ft), strong post systems provide the necessary resistance to contain and redirect an impacting vehicle. Tensile forces in the guardrail distribute impact forces along the length of the barrier. High concentrated loads can potentially rupture the steel rail, yield steel posts, or fracture wood posts. Therefore, load distribution is a key to the success of this type of barrier system.

Strong post guardrail systems embedded in soil can easily become overgrown with vegetation. Overgrown vegetation on the roadside is not only an aesthetic issue, but the height of the vegetation can obstruct the sight distance of motorists causing a potentially dangerous situation. Trimming the vegetation by hand is not only an expensive maintenance item, but also exposes workers to an increased level of risk from adjacent traffic.

In the past, herbicides have provided a solution to the guardrail vegetation problem. The ease of application, low material cost, and rapid effectiveness of spray-on herbicides caused the use of chemical vegetation control methods to gain popularity. However, in recent years environmental concerns of herbicide contamination in groundwater have led to efforts to find alternative methods of roadside vegetation control.

One such alternative method is the practice of encasing guardrail systems in pavement mow strips (see Figure 2). As a road is constructed, the paved surface is extended to encompass the guardrail system. The asphalt or concrete pavement layer prevents vegetation growth and eliminates the need for mowing between and around posts. To date, there are no state or national standards for this practice. As a consequence, many different configurations of mow strips are used with little knowledge of how they affect the impact performance of the guardrail system.

Figure 2. Wood Post Guardrail System with Asphalt Mow Strip.

Some roadside safety engineers and highway designers have recognized the implications of fully encasing guardrail posts in a stiff material such as asphalt or concrete and have installed "leave-out" sections around the posts. A leave-out section is a rectangular or circular section formed or cut around a post. This region is typically backfilled with a material that is weaker than the surrounding mow strip material but is still effective in resisting vegetation growth. An example of an existing mow strip system featuring leave-outs is shown in Figure 3. It consists of rectangular, grout-filled leave-out sections around wood posts encased in a concrete mow strip.

During an impact, the leave-out material is intended to allow for some degree of post rotation by deforming or crushing prior to generating sufficient force to cause post failure. Failure of the sacrificial leave-out backfill material also minimizes damage to the surrounding mow strip. After an impact, the damaged posts can be replaced within the leave-out region without demolishing and reconstructing the surrounding mow strip, thus providing a significant service-life cost advantage over systems without leave-outs.

Figure 3. Concrete Mow Strip System with Grout Leave-outs.

Regardless of the size or material composition of the mow strip installation, any additional constraint of the posts beyond that standard soil embedment can change the dynamic response of the guardrail system to a vehicle impact. With a wood post system the increased stiffness of pavement-post confinement can result in multiple posts fracturing during vehicle impact (see Figure 4). Multiple post fractures can quickly lead to pocketing of the vehicle within the guardrail system and rupture of the W-beam rail as it is forced to resist an increased load.

Figure 4. Mow Strip Guardrail System after Impact.

An increase in the stiffness of the post-confining material can also significantly alter the performance of steel post systems. By reducing the ability of the post to rotate and displace at the groundline during impact, the chance for the vehicle to snag on the posts and subsequently roll over or climb the rail is greatly increased. By changing the fundamental properties of the strong post guardrail system, the practice of encasing guardrail posts in pavement mow strips creates a unique guardrail system that requires analysis and testing of its own.

As mow strip systems increase in number, both the dangers and costs associated with these devices are becoming more apparent. Therefore, both FHWA and TxDOT are interested in developing mow strip systems that meet *NCHRP Report 350* impact performance guidelines. A secondary objective is to develop a mow strip system that will have good maintenance performance and require minimal repair after an impact.

1.3.2 Literature Review

1.3.2.1 Testing of Roadside Safety Devices

Roadside safety engineers have long employed destructive full-scale crash testing to evaluate performance of roadside safety devices. In order to establish a set of standard criteria for these tests, FHWA adopted the guidelines presented in *NCHRP Report 350* to evaluate roadside safety devices. In addition, FHWA requires that all new roadside features installed on the NHS after September 1998 meet *NCHRP Report 350* recommended safety performance guidelines.

Since the inception of *NCHRP Report 350* compliance requirements, numerous guardrail systems have undergone full-scale performance crash testing. *(4)* Although a number of variations of the strong post guardrail system have been tested, no systems encased in pavement have been formally evaluated for compliance with *NCHRP Report 350* criteria.

The modified G4(1S) is the most common guardrail system in use in the United States; moreover, this design is one of the standard guardrail systems used in Texas. For these reasons, it was selected as a baseline system for use in the mow strip research. The modified G4(1S) system consists of 1.8 m (6 ft) long W150×13 (W6×9) steel posts embedded in *NCHRP Report 350* standard soil and spaced at 1.9 m (6.25 ft) on center. The posts support 12-gage W-beam rail segments separated from the posts by 203 mm (8 in.) deep routed wood blockouts. A typical cross-section of this guardrail system is shown in Figure 5.

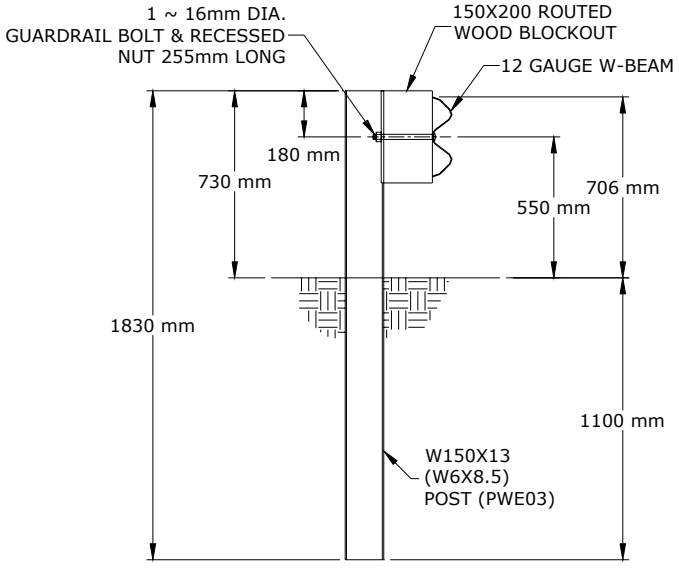

Figure 5. Left Elevation View of G4(1S) Guardrail System.

Several alternative materials have been used for guardrail blockouts in addition to the generic wood blockouts described above. These include various designs manufactured from both virgin and recycled polymers and rubber. With several passing tests available on comparable systems with different blockouts, a response envelope can be developed to provide a range of expected behavior for tests of modified G4(1S) systems. Researchers can use this response envelope to better understand test variability and help establish the validity of baseline finite element models of the modified G4(1S) system. With confidence in the guardrail model established, the effects of adding a confining mow strip layer can be examined.

In addition to the steel post systems, wood posts are also commonly used in strong post guardrail systems. Strong post guardrail systems have been successfully crash tested using 178 mm (7 in.) diameter wood posts and 152 mm × 203 mm (6 in. × 8 in.) rectangular wood posts. Details of these systems are similar to those of the modified G4(1S) guardrail, but with substitution of the wood posts for the W150×13 (W6×9) steel posts. Being slightly less expensive than steel posts, wood posts are often selected for new guardrail construction. The TxDOT standard detail sheets make provisions for use of both systems.

The United States Forest Products Laboratory has done extensive material testing of southern pine, the type of wood commonly used for round guardrail posts. A report titled "Moisture Content and the Properties of Clear Southern Pine" presents results of this material testing. *(5)* We used values from this reference for this research in the implementation of a finite element model for the wood posts as discussed in subsequent sections of this report.

Another important factor for predicting behavior of guardrail posts is the soil structure interaction between the post and the confining soil layer. Standard soil used in roadside hardware installations is sandy, cohesionless, crushed limestone road base material. The soil is well-graded and contains a maximum aggregate size of between 25 mm and 50 mm (1 in. and 2 in.). Because of the large aggregate size, it is difficult to perform traditional geotechnical tests for shear and triaxial strength. To overcome this difficulty, Dewey et al. used the gradation curve, the maximum particle size, the relative density, and the overburden pressure of a sample of the cohesionless soil to correlate the shear strength and cohesion properties. *(6)* Using these properties as a reference, a finite element model of the interaction between the soil and the guardrail post was developed as discussed in a later section.

1.3.2.2 Finite Element Simulation

Vehicle impacts with guardrail involve significant material and geometric nonlinearites. Both the vehicle and the barrier undergo large deformations in an extremely short span of time, often less than 0.5 second (s). In order to accurately simulate the behavior of a vehicle impact with a guardrail system using finite element analysis, a sophisticated nonlinear, dynamic, explicit finite element code should be used for numerical simulation. LS-DYNA is the most widely used numerical simulation software in the roadside-safety engineering community. *(7)* It possesses a large material database, many available element formulations including discrete, shell, and solid elements, and an advanced set of contact algorithms.

As computer processing power has increased over the past several years, finite element analysis has become a valuable tool for roadside hardware design. The computer simulation can reduce development cost by providing an evaluation of design alternatives in a predictive manner prior to any full-scale testing. Several finite element models of guardrail systems have been developed using LS-DYNA. Because material properties for steel can be readily obtained and modeled, the emphasis of recent research has been on the soil-post interaction.

In the past, the high computational expense of processing a continuum of solid soil elements caused researchers to use less expensive methods of modeling soil-structure interaction. Habibagahi and Lagner proposed a method of discretization whereby subgrade soil reactions are represented by an array of nonlinear springs. *(8)* The nonlinear stiffness of the springs is defined by the horizontal subgrade modulus and is dependent upon the physical properties of the soil, the displacement, and the depth below ground level. This subgrade modulus approach was used by Patzner et al. to model interaction between timber guardrail posts and a sandy, cohesionless soil. *(9)* Tabiei and Wu used a cylindrical mesh of solid, Lagrangian finite elements to simulate soil structure interaction in an attempt to more accurately model soil response. *(10, 11)* This research examines the effectiveness of these methods.

Wood post guardrail systems have also been modeled using LS-DYNA. Plaxico et al. presented finite element models of both the G4(1W) and G4(2W) wood post guardrail systems. *(12)* They calibrated simulations of a G4(2W) crash test against existing crash test data in order to develop a predictive model of the G4(1W) to evaluate it for compliance with *NCHRP Report 350* criteria. Since Plaxico et al. completed that research, several new material models capable of simulating the orthotropic properties of wood have been incorporated into LS-DYNA. In

addition to developing a round wood post model, the research examines these new material models.

2. RESEARCH METHODOLOGY

2.1 OVERVIEW

The previous section introduced the problem of encasing roadside guardrail systems in mow strips. In order for a roadside barrier to comply with *NCHRP Report 350* guidelines, it must pass a series of full-scale crash tests; the most demanding test is a 100 km/h (62 mph) impact of a full-sized, 2000 kg (4400 lb) pickup truck with the barrier at an angle of 25 degrees. As each of these tests requires an extensive setup, instrumentation, and destruction of a test vehicle, the cost per test is substantial. In order to minimize the number of such test runs, the research methodology focuses on identifying common mow strip configurations, evaluating these configurations using finite element analyses, and choosing a representative system for crash testing using predictive full-scale simulation. This section presents the research plan that the research team used to study the effect of encasing guardrail posts in pavement mow strips. Each step in the research plan is briefly discussed. Implementation of the test plan and results from the tests performed for this research are presented in subsequent sections.

2.2 SYSTEM IDENTIFICATION

The first step in analyzing performance of mow strip systems is to determine the mow strip configurations and range of variables currently in use throughout Texas. To this end, ther research team conducted a survey of the TxDOT districts. Standard mow strip specifications and engineering drawings were collected. In addition to the drawings and specifications, information concerning standard mow strip construction practices was gathered. The research team developed typical mow strip layouts using these data. These typical layouts were selected such that they represent the mow strip materials and dimensions deemed most critical to the performance of the guardrail system. A test matrix of various mow strip design configurations was developed for use in the subcomponent evaluation phase of the project.

2.3 SUBCOMPONENT EVALUATION

The test matrix developed from the TxDOT district surveys identifies several variables that distinguish different mow strip designs from one another. Full-scale crash testing of the entire test matrix would be both cost-prohibitive and unnecessary. Subcomponent-level tests

were performed to develop an understanding of the dynamic response of the selected mow strip systems. The subcomponent evaluation phase consisted of both dynamic impact testing and finite element simulation.

Following the test matrix, mow strip installations with embedded guardrail posts were constructed for dynamic impact testing using the TTI bogie impact vehicle. By isolating individual post installations, salient characteristics of each mow strip design were examined. The bogie impact vehicle is equipped with an accelerometer that provides time-history data useful for understanding the behavior of the embedded post.

The impact tests were reproduced using a finite element model of a bogie vehicle developed by the National Crash Analysis Center (NCAC). *(13)* In order to accurately represent the mow strip systems using finite element simulation, material models, meshing patterns, contact algorithms, and element formulations are examined. Qualitative and quantitative data from the impact tests assisted with the calibration and validation of the subcomponent finite element models from which the full system model was assembled.

2.4 FULL SYSTEM EVALUATION

2.4.1 Baseline Simulation

As discussed earlier, several full-scale crash tests on soil-embedded strong post guardrail systems have been performed at TTI. *(4, 14, 19)* To study effects of the addition of the confinement of a mow strip layer to a guardrail system, it is necessary to establish a guardrail performance baseline without mow strip confinement. Using results of the subcomponent evaluation and available crash test data, a baseline, full-scale crash test was simulated. This simulation was used to validate behavior of the posts, W-beam guardrail, soil, and other aspects of the baseline full-scale guardrail model.

2.4.2 Predictive Simulation

The researchers developed finite element models of several mow strip systems based on designs selected from the subcomponent testing phase. These systems were selected for their anticipated performance in the crash test, cost of construction, and ease of maintenance and repair. Because full-scale crash tests are extremely expensive to run, we used numerical

simulation to predict the behavior of each selected system. Full-scale models were assembled using subcomponent models validated by dynamic impact testing.

2.4.3 Full-scale Crash Testing

Based on results of the predictive simulations, two mow strip configurations were selected for full-scale crash testing to assess compliance with *NCHRP Report 350* requirements. Structural adequacy tests of a steel post and wood post guardrail system encased in concrete mow strip were conducted.

3. SYSTEM IDENTIFICATION

3.1 MOW STRIP USAGE SURVEY

3.1.1 General

The lack of state or national standards for the practice of encasing guardrail posts in mow strips has led to the use of many different designs. In order to quantify the extent of mow strip usage and identify details of the mow strip systems currently in use throughout Texas, the research team distributed a state of practice survey to each of the 25 TxDOT districts (see Appendix A). Of the 25 surveys distributed, 20 were completed and returned.

A key purpose of the state of practice survey was to quantify the usage of mow strips throughout Texas. As shown in Figure 6, 65 percent of participating TxDOT districts utilize vegetation control mow strips. Of the seven districts that do not use mow strips, two are located in regions dominated by desert-type terrain. These districts indicate on the survey that roadside vegetation growth is not a problem due to the dry climate. Even where roadside vegetation occurs in these districts, wind-blown sand would quickly cover a mow strip and allow vegetation to grow on top of it. With a majority of districts using some form of vegetation control mow strip, it is important to establish a statewide standard design that meets the criteria of *NCHRP Report 350*.

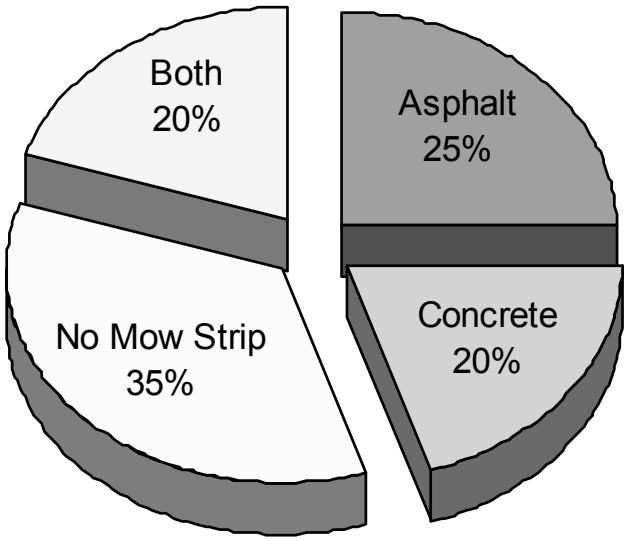

Figure 6. Mow Strip Usage in TxDOT Districts.

3.1.2 Mow Strip Materials

When installing a new road, mow strips are often built by extending the paved surface of the road beyond the shoulder to encompass the guardrail posts. Although hot mix asphalt and Portland cement concrete are the most commonly used mow strip materials, any material other than *NCHRP Report 350* standard soil placed around guardrail posts and intended to prevent or discourage vegetation growth can be classified as a mow strip.

3.1.2.1 Asphalt

Commonly used for road construction throughout Texas, hot mix asphalt is also frequently used in the construction of mow strips. Forty-five percent of TxDOT districts report using asphalt mow strips on a regular basis. During construction of a new road, pavement is typically extended over the area designated for guardrail placement. Hot mix asphalt for the mow strip is compacted with the same process and equipment used in the construction of the road. Using either a 305 mm (12 in.) or 457 mm (18 in.) diameter auger, crew then drilled postholes through the asphalt into the soil. They set posts into the holes, and backfilled the void around the posts with hand-tamped soil. The top several inches of backfill around the post is often filled with hand-tamped hot mix asphalt to prevent vegetation growth.

Asphalt is composed of two major components, bituminous binder and limestone aggregate. Bituminous binders are classified using a performance grade system. For each binder grade, a temperature range is given over which the asphalt binder possesses certain physical properties. TxDOT typically uses PG64-22 asphalt binder for new highway construction. This performance grade specifies that the binder possesses adequate physical properties over a range of pavement temperatures from 64°C to –22°C. The second characteristic of asphalt cement is the gradation of aggregate. Aggregates are classified by the distribution of stone sizes according to results of a standard sieve test. TxDOT specifications for asphalt aggregate classify coarse to fine aggregate gradations from A to F. *(20)* Type C or D aggregate is typically used for new highway construction, and consequently, for mow strips.

3.1.2.2 Concrete

Portland cement concrete is another material commonly used in both roadway and mow strip construction. According to the survey, concrete mow strips are used by approximately

40 percent of TxDOT districts. TxDOT specifications define 13 classes of concrete delineated by strength, material composition, and intended use. Class B concrete is the most commonly used grade of concrete for mow strip construction. Often referred to as riprap, Class B is required to have a minimum 28-day compressive strength of 14 MPa (2031 psi). This relatively low strength concrete is typically used in foundations for small roadside signs and other types of anchors. To avoid shrinkage cracking and separation from the adjacent roadway, mild steel reinforcement is sometimes used in concrete mow strips. Reinforcement typically consists of #3 bars at 305 mm (12 in.) center-to-center or W6×W6 or W3×W3 welded wire fabric. Sometimes the mow strip concrete is placed without reinforcement.

Unlike the construction of an asphalt mow strip, guardrail posts are typically installed prior to placing the concrete mow strip. An auger cannot be used to drill through cured concrete in the same manner as it can asphalt, and therefore crews set posts into the soil and place concrete around them. Where leave-outs are not used, crews place concrete directly around posts over the entire mow strip area. When leave-outs are incorporated into the design, they are formed around the posts and typically backfilled with a grout mixture.

3.1.2.3 Alternative Materials

Although a majority of mow strips consist of either concrete or asphalt pavement, other materials can be used to inhibit the growth of roadside vegetation. Reclaimed asphalt pavement or concrete pavement is sometimes used around posts for this purpose. This recycled material consists of broken-up pieces of demolished pavement, and can be classified as course gravel. Only one of the 25 TxDOT districts reported using alternative mow strip materials.

3.1.3 Mow Strip Geometry

Regardless of whether asphalt or concrete pavement is used to construct a mow strip, the depth and width of the mow strip installation has a significant effect on the response of the guardrail system to an impact event. Concrete mow strips are typically constructed throughout Texas with depths ranging from 75 mm (3 in.) to 127 mm (5 in.). Asphalt mow strips range in depth from 102 mm (4 in.) to 203 mm (8 in.) with 152 mm (6 in.) being the most common depth.

Depending on the type of post and blockout used, the depth of W-beam guardrail installations typically range from 432 mm (17 in.) to 480 mm (19 in.). Guardrails are sometimes

installed such that traffic face of the W-beam is at the edge of the travelway or shoulder. Therefore, practically speaking, a mow strip must be a minimum of 607 mm (24 in.) wide to encase the guardrail system. According to the survey, mow strip widths typically range from 0.6 m (2 ft.) to 1.5 m (5 ft.). Provided there are no obstructions to limit the width of the mow strip, TxDOT maintenance personnel prefer to have a mow strip that is wide enough for the tire of a shredder/mower to ride on the mow strip behind the guardrail posts. This allows crew to cut vegetation up to the mow strip without the need for herbicides or hand mowing.

3.1.4 Leave-out Materials

Because of maintenance issues discussed later, some districts began to utilize leave-outs around posts. Approximately one-half of the participating TxDOT districts indicate that they use some form of leave-out in new mow strip construction (see Figure 7). In a concrete mow strip system, a leave-out is created by forming a region around the posts using either wooden formwork or a circular Sonotube to keep the concrete away from the posts. A leave-out is created in an asphalt mow strip when postholes are augered through the asphalt. The size of the leave-out can be increased by using a larger auger.

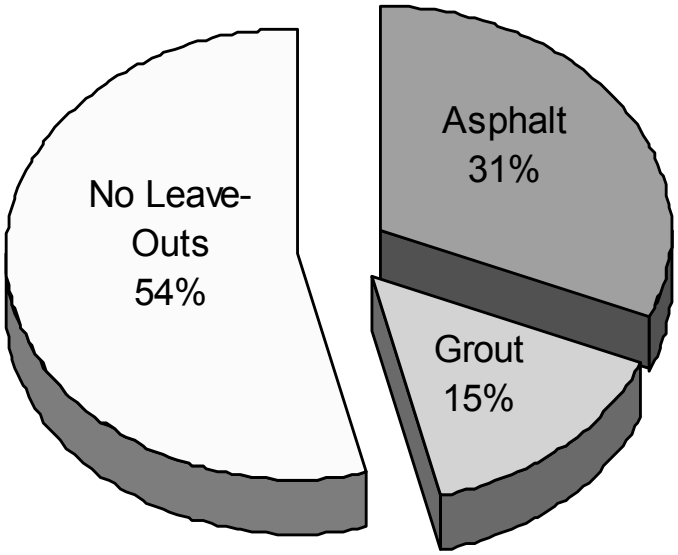

Figure 7. Leave-out Usage among TxDOT Districts

To permit rotation of the posts during impact, it is preferable that the backfill material used in the leave-out region be weaker than the post and surrounding mow strip material. The presence of a sacrificial material around the posts during an impact can also prevent damage from occurring to the mow strip material, thereby reducing repair costs. However, leave-out backfill materials should not allow vegetation growth around the posts, as this would defeat the purpose of the mow strip system. According to the survey, TxDOT districts most commonly use grout and asphalt as leave-out materials.

3.1.4.1 Grout

With a low material cost and a well-established history of use, grout is a practical and economic choice as a leave-out backfill material. Two-sack grout consisting of fine sand aggregate, Portland cement, and water is used by 15 percent of TxDOT districts. With a compressive strength of approximately 0.85 MPa (120 psi), two-sack grout is durable enough to prevent vegetation growth over the life of the guardrail installation, yet weak enough to allow post rotation during an impact. With no course aggregate, grout is a very workable material. After a concrete or asphalt mow strip system has been constructed, grout can be poured into the leave-out region around each post. As an additional benefit for concrete mow strip systems, the grout is similar in appearance to the mow strip, thereby improving aesthetics of the design.

3.1.4.2 Asphalt

Hot mix asphalt is the most common leave-out backfill material used by TxDOT districts. Of participating districts, 31 percent report using hot mix asphalt as a leave-out material. Unlike the asphalt used for the construction of a mow strip, the hot mix asphalt used in leave-out sections is not compacted using a heavy rolling device but, rather, is hand-tamped around the post. If the hot mix is not tamped or compacted around the posts in some manner, vegetation can eventually grow in or through the leave-out material. The depth of asphalt used in the leave-out is also an important consideration. The survey results indicate that hot mix asphalt is usually placed around the post in the leave-out to the full depth of the mow strip layer. From a performance standpoint, the asphalt should only be deep enough to prevent vegetation growth in order to facilitate movement of the post.

3.2 TEST MATRIX DEVELOPMENT

The goal of this research is to develop a mow strip installation design that meets the crashworthiness requirements of *NCHRP Report 350*. In doing so, installation and maintenance cost requirements for the system must be taken into consideration and balanced with system performance. The research team created a test matrix of mow strip layouts (see Table 1) using data from the state-of-practice survey and in consultation with TxDOT engineers. The layouts represent the mow strip materials and dimensions deemed most critical to the performance of the system.

Table 1. Mow Strip Test Matrix Configurations.

Case (1)	Mow Strip Material (2)	Post Type (3)	Leave-Out Material (4)	Leave-Out Size (5)	Leave-Out Depth (6)
1	None	Wood	N/A	N/A	N/A
2	None	Steel	N/A	N/A	N/A
3	Asphalt	Wood	Asphalt	305 mm Dia.	200 mm
4	Asphalt	Wood	Asphalt	457 mm Dia.	200 mm
5	Asphalt	Steel	Asphalt	305 mm Dia.	200 mm
6	Asphalt	Steel	Asphalt	457 mm Dia.	200 mm
7	Concrete	Wood	N/A	N/A	N/A
8	Concrete	Wood	Grout	457x457 mm	100 mm
9	Concrete	Wood	Grout	457x607 mm	100 mm
10	Concrete	Steel	N/A	N/A	N/A
11	Concrete	Steel	Grout	457x457 mm	100 mm
12	Concrete	Steel	Grout	457x607 mm	100 mm
13	Asphalt	Wood	Grout	457 mm Dia.	100 mm
14	Asphalt	Steel	Grout	457 mm Dia.	100 mm
15	Asphalt	Wood	Asphalt	457 mm Dia.	100 mm
16	Asphalt	Steel	Asphalt	457 mm Dia.	100 mm
17	Asphalt	Steel	Rubber Mat	457 mm Dia.	N/A

Researchers selected the most commonly used mow strip materials, PG64-22 Type D hot mix asphalt and TxDOT Class B riprap concrete for use in the subcomponent impact tests. The hot mix asphalt mow strip was compacted with the same process and equipment used in road construction. Using either a 305 mm (12 in.) or 457 mm (18 in.) diameter auger, postholes were then drilled through the asphalt into the soil. Posts were set into the holes, and the void around the posts was backfilled with hand-tamped soil meeting the specifications of *NCHRP Report 350*

standard soil. The top several inches of backfill around the post were formed with various materials (hand-tamped hot mix asphalt, grout, etc.) intended to prevent vegetation growth.

We selected TxDOT Class B riprap concrete as the other mow strip material investigated. As mentioned previously, Class B concrete is required to have a minimum 28-day compressive strength of 14 MPa (2031 psi). To help avoid shrinkage cracking and separation of the mow strip from the adjacent test apron, a single layer of W6×W6 welded wire fabric was used to reinforce the concrete mow strip.

To minimize the number of tests required, the research team examined the most severe (i.e., most stiff) mow strip systems. To this end, a maximum practical thickness for both mow strip materials was selected. A 127 mm (5 in.) thick concrete mow strip and a 203 mm (8 in.) thick asphalt mow strip were chosen for dynamic impact testing. Furthermore, in order to satisfy the maintenance requirements, provide room for leave-out sections around the posts, and encase the full depth of guardrail in the mow strip material, a mow strip width of 1.1 m (3.5 ft) was selected.

Wood posts and steel posts have vastly different failure mechanisms, and the geometric differences between the two types of posts can effect the interaction between the post, guardrail system, and vehicle. For this reason, each mow strip material was investigated using both wood and steel posts. Based on common guardrail installation practice and equipment typically available for use in the field, 305 mm (12 in.) and 457 mm (18 in.) diameter augers were used to create leave-outs in the asphalt mow strips. In the concrete mow strips, 457 mm × 457 mm (18 in. × 18 in.) and 457 mm × 607 mm (18 in. × 24 in.) leave-out sections were formed around the posts. As a baseline, direct soil embedment and concrete embedment without a leave-out section around the post were chosen for testing to develop a full range of post responses.

The maintenance and possible performance advantages of leave-out sections make them an important part of this research. Both grout and hot mix asphalt were selected for dynamic impact testing based on their low cost and availability. Alternative leave-out materials such as foam and recycled rubber mats were also considered.

4. TESTING OF SUBCOMPONENTS

4.1 OVERVIEW

Dynamic impact testing is performed using the bogie impact vehicle constructed by TTI. *(21)* Intended for low cost component testing, the TTI bogie consists of a sliding nose mounted on a vehicle frame and the suspension. Various sizes and strengths of crushable, metallic honeycomb are staged in a crushable nose assembly that is calibrated to represent the frontal crush stiffness of a small passenger car. After an impact, the expendable honeycomb cartridges are replaced and the vehicle is reused. Thus, the bogie vehicle provides an inexpensive method for performing multiple dynamic impact tests.

The dynamic subcomponent tests have two primary objectives. First, dynamic response of guardrail posts (e.g., force-deflection response, failure mode, etc.) in various mow strip configurations is obtained. This permits a preliminary assessment of the ability of the various mow strip configurations to meet *NCHRP Report 350* impact performance criteria. Second, the test results can be used to calibrate and validate finite element models of the mow strip components prior to their implementation in a full-scale model.

4.2 BASELINE TESTS

To understand the effect of encasing guardrail posts in mow strips, it is necessary to have a point of reference from which to compare changes in performance. Both the modified G4(1S) steel post guardrail and the G4(2W) wood post guardrail installations meet *NCHRP Report 350* criteria when posts are installed following standard soil embedment procedures. To compare performance of posts embedded in mow strips to post configurations that have been successful in crash tests, standard soil embedment is used as the baseline test configuration (see Figure 8).

4.2.1 Test Description

The research team performed two baseline impact tests. These are test cases 1 and 2 in the test matrix shown in Table 1. A W150×13 (W6×9) steel post was embedded to a depth of 1.1 m (3.6 ft). A 457 mm (18 in.) diameter hole was augered in the soil to the desired embedment depth, and the post was placed into the hole. The void surrounding the post was backfilled with *NCHRP Report 350* standard soil that was compacted through hand-tamping. The same

procedure was followed to install a 178 mm (7 in.) diameter wood post to the same embedment depth. As mentioned previously, TxDOT permits the use of both 178 mm (7 in.) diameter and 152 mm × 203 mm (6 in. × 8 in.) wood posts in its strong post W-beam guardrail installations. A 178 mm (7 in.) diameter wood post was selected over the 152 mm × 203 mm (6 in. × 8 in.) wood post because it has a slightly lower flexural strength, thereby making it more critical (i.e., more likely to fail) in a mow strip application.

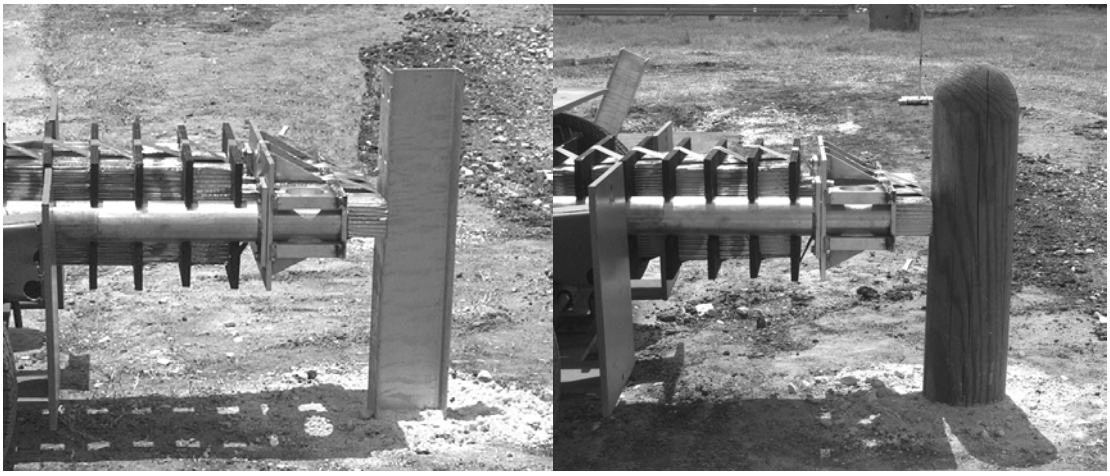

(a) **(b)**

Figure 8. Baseline Impact Tests: (a) Steel Post Test; (b) Wood Post Test.

4.2.2 Test Results

The bogie vehicle impacted each post head-on at a speed of 35 km/hr (21.7 mph). Accelerometer data obtained from the bogie vehicle during the baseline tests are shown in Figure 9. The peak acceleration on the bogie vehicle for both the wood post and the steel post tests was approximately 9 g. In the steel post test, the bogie vehicle climbed the post and came to rest on top of it. In the wood post test, the nose of the bogie dug into the face of the post, thus preventing the bogie from climbing the post. Because the bogie did not become airborne, the area under the acceleration-time curve was larger.

Figure 10 shows both posts after impact. Both posts deflected steadily through the soil as the bogie vehicle progressed forward. The steel post experienced some permanent deformation below ground near the point of maximum moment. The wood post rotated as a rigid body and did not fracture.

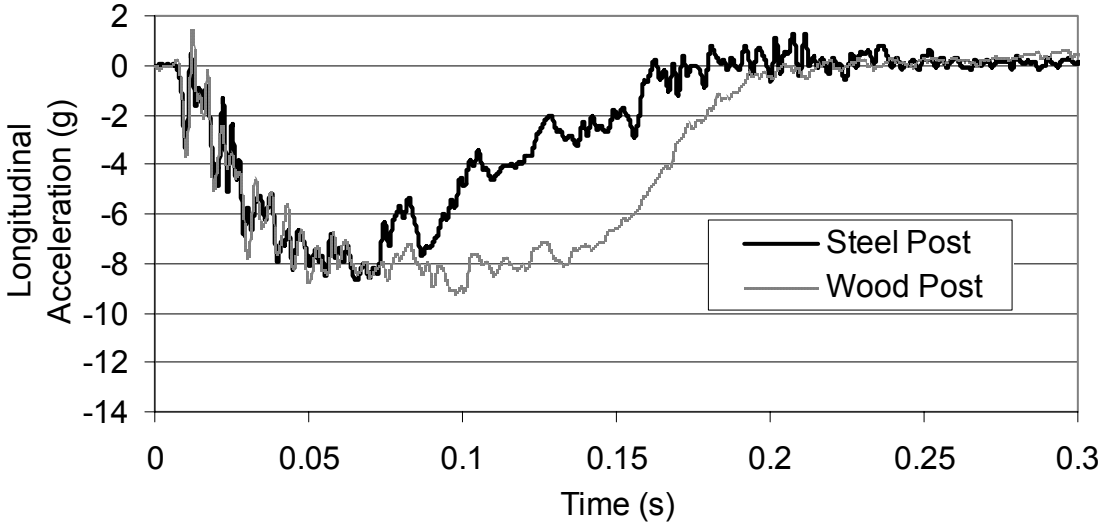

Figure 9. Accelerations of Bogie for Baseline Impact Tests.

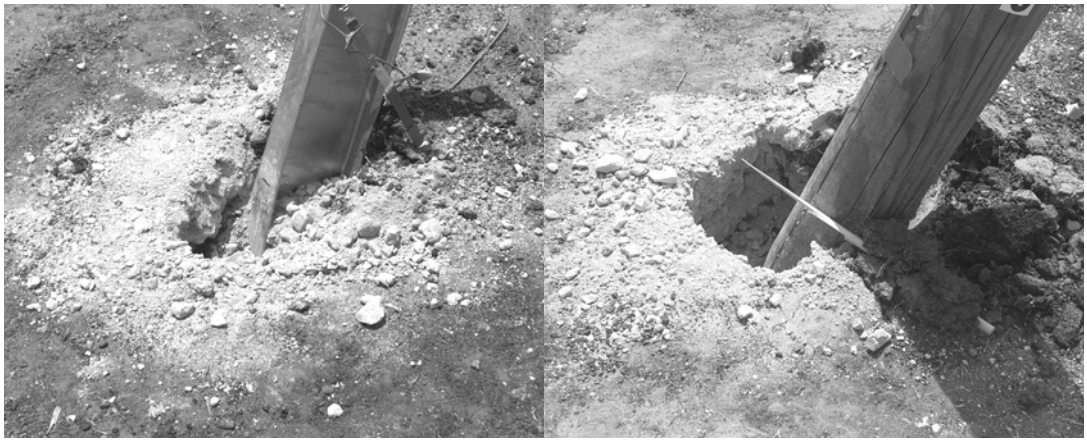

(a) **(b)**

Figure 10. Baseline Test Posts after Impact: (a) Steel Post; (b) Wood Post.

4.3 ASPHALT MOW STRIP TESTS

4.3.1 Test Description

An asphalt mow strip was constructed according to standard procedures followed by TxDOT as determined by the state of practice survey. Performance grade PG64-22 asphalt was used with Type D aggregate. The mow strip was 9.5 m (31.3 ft) long and accommodated four guardrail posts with a spacing of 1.9 m (6.3 ft). This spacing is standard for strong post guardrail

installations. The asphalt is 203 mm (8 in.) deep, and 1.1 m (3.5 ft) wide. To permit proper compaction, 305 mm (12 in.) of standard road base material was placed below the asphalt.

Using a mechanical roller, the asphalt was compacted to approximately 90 percent of its lab density. The in-place density of the asphalt was measured using a nuclear densitometer and was determined to be 2425 kg/m^3 (151.4 lb/ft^3). After compaction of the asphalt, two 305 mm (12 in.) and two 457 mm (18 in.) diameter holes were drilled through the asphalt using an auger.

Two sets of impact tests evaluated posts embedded in the asphalt mow strip. For the first set of asphalt mow strip tests, cases 3 through 6 (refer to Table 1), asphalt filled leave-outs were used. The posts (two steel and two wood) were set in holes to depth, and the void around the posts was backfilled with hand-tamped *NCHRP Report 350* standard soil to 203 mm (8 in.) below the surface of the asphalt. The top 203 mm (8 in.) surrounding the posts was filled with hot mix asphalt. The asphalt was hand-tamped around the posts in an effort to create a weaker layer of material in the leave-out region around the post. Drawings for all subcomponent impact test installations are provided in Appendix B. A typical test setup is shown in Figure 11.

Figure 11. Typical Setup for Asphalt Mow Strip Test Cases.

In the second set of asphalt mow strip tests, cases 13 through 17 (refer to Table 1), several different leave-out materials were used. All of the holes used for placement of the posts were 457 mm (18 in.) in diameter. This increased the distance between the back of the post and the mow strip, providing more room for post rotation before bottoming out on the inside edge of the mow strip layer. Both wood and steel posts were tested for each mow strip configuration evaluated. The posts were set to depth in augered holes, and the voids around the perimeters of the posts were filled to within 102 mm (4 in.) of the pavement surface with hand-tamped *NCHRP Report 350* standard soil. Two-sack grout (test cases 13 & 14) and hand-tamped hot mix asphalt (test cases 15 & 16) were placed in the top 102 mm (4 in.) of the 457 mm (18 in.) diameter leave-out region.

A final test with the asphalt mow strip was performed using a steel post with a recycled rubber mat surrounding the base of the post as shown in Figure 12. The mat was a Durotrim anti-vegetation tile obtained from Welch Products, Inc. The 607 mm × 607 mm (24 in. × 24 in.) mat was 25 mm (1 in.) thick, and consisted of recycled rubber tire pieces bonded with a urethane binder. The mat was provided in two interlocking pieces that were cut to fit snugly around the post. A urethane bonder supplied by the manufacturer was then used to bond the two pieces of mat together, bond the perimeter of the mat to the asphalt mow strip surface, and to seal the perimeter of the steel post. The rubber mat is intended to provide an alternative to the two-sack grout for preventing vegetation growth around guardrail posts encased in mow strip.

Figure 12. Asphalt Mow Strip Bogie Test with Rubber Mat.

4.3.2 Test Results

The bogie vehicle impacted the posts in asphalt mow strip by using the same impact conditions as the baseline tests. Acceleration-time histories for these tests are shown in Figures 13 and 14. The 203 mm (8 in.) thick hand-tamped hot mix asphalt leave-out layer prevented rotation of both the wood and steel posts. The steel posts yielded at the groundline and allowed the bogie vehicle to slide up and over the posts. While the posts in the 457 mm (18 in.) diameter leave-outs had slightly lower acceleration values, the difference in performance between the 305 mm (12 in.) and 457 mm (18 in.) diameter leave-outs was negligible, and neither allowed any significant post deflection.

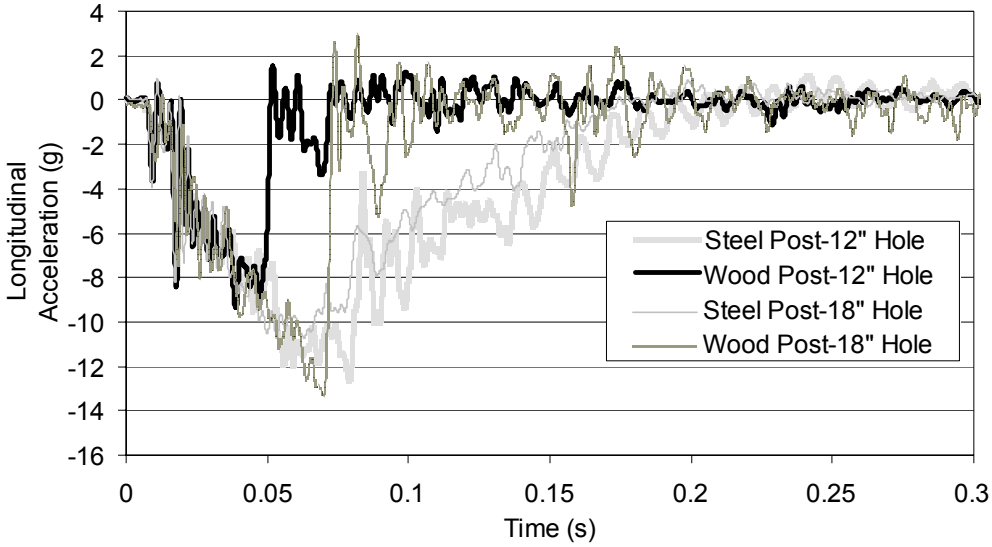

Figure 13. Accelerations of Bogie for First Set of Asphalt Mow Strip Tests.

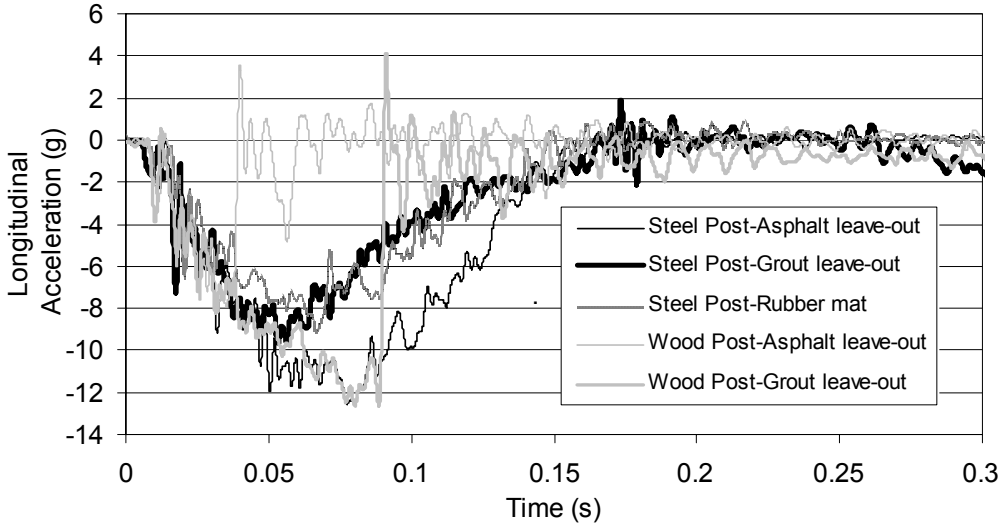

Figure 14. Accelerations of Bogie for Second Set of Asphalt Mow Strip Tests.

The wood posts fractured at ground level and failed to bring the bogie vehicle to a stop. The wood post in the 305 mm (12 in.) diameter leave-out system broke off cleanly at the groundline, whereas the post in the 457 mm (18 in.) diameter leave-out system deflected slightly before splintering and fracturing. This difference is visible in the respective acceleration histories obtained from the bogie vehicle. The peak acceleration for the wood post in the 305 mm (12 in.) diameter leave-out occurs 0.025 s earlier than for the wood post in the 457 mm (18 in.) diameter leave-out.

Even when the thickness of the hand-tamped asphalt backfill was reduced from 203 mm (8 in.) to 102 mm (4 in.) in the second series of tests, the material was still too stiff and did not allow either the wood or steel posts to translate in a substantial manner. Just as in the first set of tests, the wood posts fractured cleanly at the groundline and the steel post yielded at the groundline without significant translation.

The two-sack grout leave-out backfill material greatly improved the performance of both the wood and steel posts under impact by the bogie. The grout broke up shortly after each post was impacted and allowed the posts to deflect to the back of the leave-out before yielding or fracturing. Figure 15 shows bogie accelerations for three of the wood post bogie tests in asphalt mow strip. Although the performance of the grout-filled leave-out does not match the performance of the soil-embedded post, it greatly enhances performance of the post over a fixed condition in regard to post displacement and energy dissipation, approximately doubling the time over which the wood post is effective before fracture.

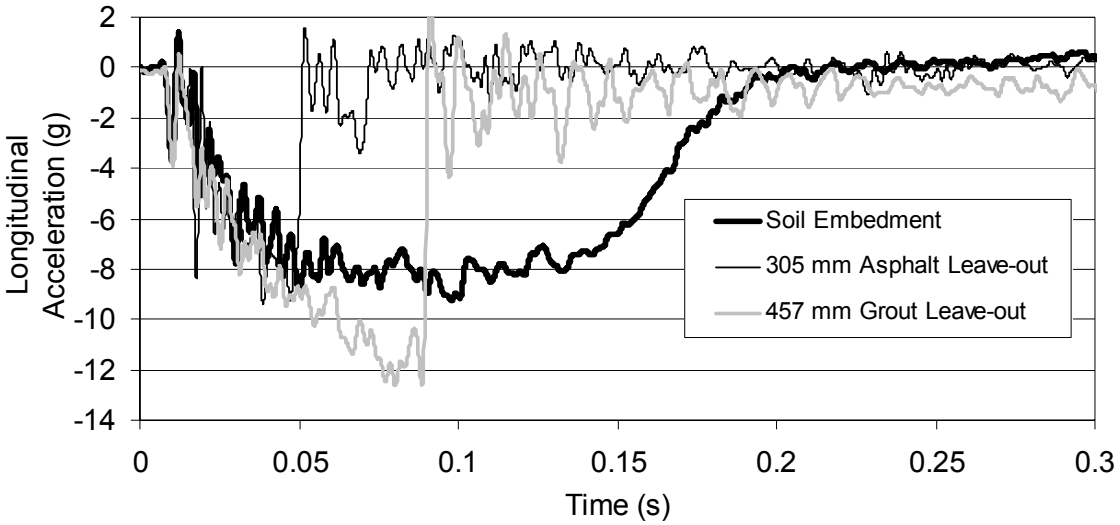

Figure 15. Accelerations of Bogie for Asphalt Mow Strip Wood Post Tests.

It is expected that a larger leave-out diameter could further improve the impact performance and would more closely match the behavior of soil embedment; however, 457 mm (18 in.) is considered to be the largest size for augering through the asphalt using equipment commonly available to contractors and TxDOT maintenance crews.

The final asphalt mow strip configuration tested incorporates a recycled rubber mat. As the post is impacted, the rubber mat tears and allows the post to rotate to the back of the leave-out. While the amount of post rotation allowed by the rubber mat is desirable, the amount of damage incurred by the mat may preclude its reuse (see Figure 16). A cost effectiveness analysis could be conducted to determine when or if such an option is viable.

Figure 16. Deformed Steel Post Surrounded by Rubber Mat after Bogie Impact.

4.4 CONCRETE MOW STRIP SYSTEM TESTS

4.4.1 Test Description

The research team performed six bogie vehicle impact tests on posts embedded in a concrete mow strip. The concrete mow strip was 1.1 m (3.6 ft) wide and 127 mm (5 in.) deep. The length was 13.3 m (43.8 ft), which was sufficient to install six guardrail posts at a standard spacing of 1.9 m (6.3 ft). The mow strip was placed on top of 305 mm (12 in.) of compacted road base material. It was constructed using TxDOT Class B riprap concrete with a minimum

28-day compressive strength of 14 MPa (2031 psi). The concrete was reinforced throughout with welded-wire mesh reinforcement with the exception of the leave-out sections formed around the posts. Both wood and steel posts were tested in direct concrete confinement and with grout-filled leave-outs around the perimeters of the posts.

The posts were installed prior to pouring the concrete mow strip following typical TxDOT installation procedures. The posts were embedded to a depth of 1.1 m (3.6 ft) in 305 mm (12 in.) diameter augered holes. The holes were backfilled with hand-tamped *NCHRP Report 350* standard soil. As a baseline, one wood post and one steel post were directly encased in the concrete mow strip without a leave-out section. Two sizes of rectangular leave-outs were included in the test matrix: 457 mm × 457 mm (18 in. × 18 in.) and 457 mm × 607 mm (18 in. × 24 in.). Due to its low cost, ease of installation, overall effectiveness, and matching appearance, a two-sack grout mixture was used as the backfill material in the top 102 mm (4 in.) of the leave-outs. The test installation is shown in Figure 17, and drawings are provided in Appendix B.

Figure 17. Concrete Mow Strip Test Installation.

4.4.2 Test Results

As expected, direct concrete confinement of the posts (cases 7 & 10 in Table 1) represented a severe impact scenario. Figure 18 shows steel and wood posts embedded in the concrete mow strip after impact. The acceleration-time histories are given in Figures 19 and 20 for the wood and steel post tests, respectively. The bogie impact caused severe damage to the concrete mow strip around the steel post with little movement of the post. By contrast, the wood post fractured rapidly upon impact, thereby reducing damage to the concrete mow strip, but permitting the bogie vehicle to pass through relatively unimpeded. In both cases, the concrete mow strip allowed minimal deflection of the post at the groundline and created a costly repair situation.

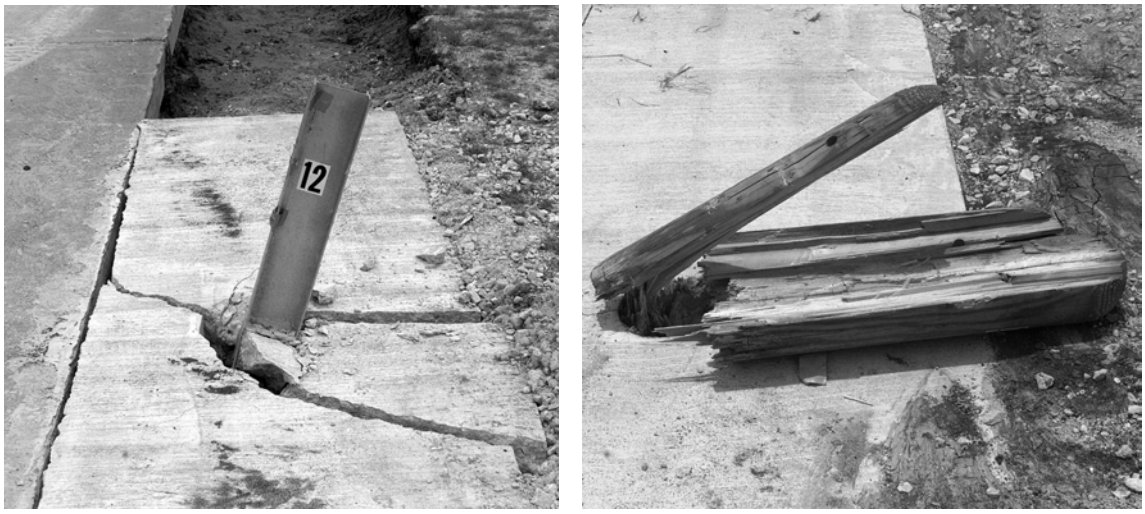

(a) **(b)**

Figure 18. Posts Embedded in a Concrete Mow Strip: (a) Steel Post; (b) Wood Post.

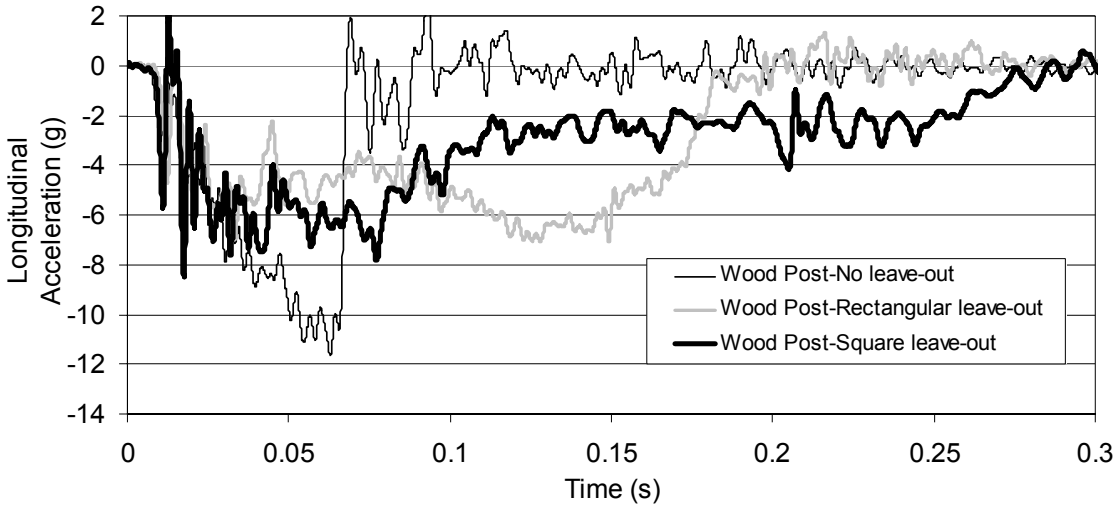

Figure 19. Accelerations of Bogie for Concrete Mow Strip Wood Post Tests.

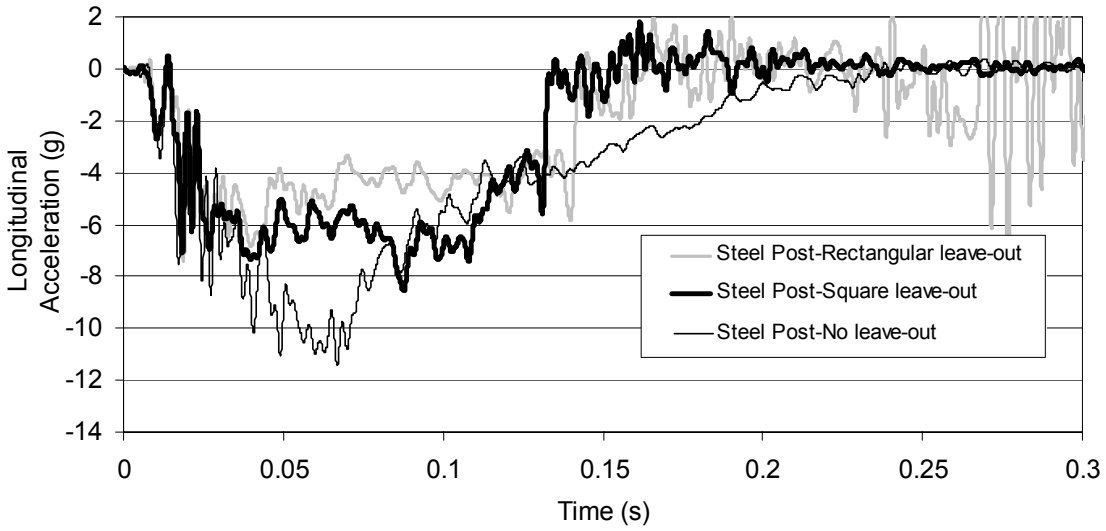

Figure 20. Accelerations of Bogie for Concrete Mow Strip Steel Post Tests.

The second configuration tested within the concrete mow strip were the wood and steel posts surrounded by 457 mm × 457 mm (18 in. × 18 in.) grout-filled leave-outs. As observed in the asphalt mow strip tests, the addition of the grout-filled leave-outs dramatically improves post performance. As shown in Figures 21(a) and 22(a), both the steel and wood posts rotated through the grout to the back of the leave-out and contacted the concrete mow strip.

The contact of the wood post with the back of the mow strip caused the back of the mow strip to fracture. The steel post also causes concrete fracture at the back of the leave-out.

However, the bogie vehicle is able to ride over the steel post, and therefore, damage to the mow strip is not as severe. Although the damage to the mow strip in these tests is significant, it is important to keep in mind that the posts were impacted in a head-on condition. In a redirective impact, the guardrail works together as a system to dissipate the energy of the impacting vehicle and the post deflections are not expected to be as severe. Thus, the 457 mm × 457 mm (18 in. × 18 in.) grout-filled leave-outs may indeed provide a viable alternative for the concrete mow strip system.

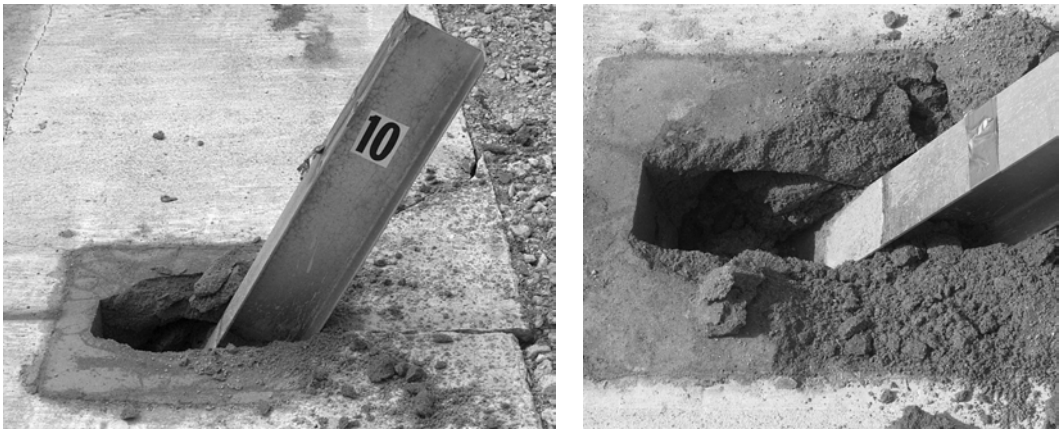

(a) **(b)**

Figure 21. Steel Posts in Concrete Mow Strip with Grout-Filled Leave-out: (a) Square Leave-out; (b) Rectangular Leave-out.

(a) **(b)**

Figure 22. Wood Posts in Concrete Mow Strip with Grout-filled Leave-out: (a) Square Leave-out; (b) Rectangular Leave-out.

Figures 19 and 20 show that significant reductions in peak acceleration of the bogie and increase in energy dissipation were achieved with the addition of the square leave-outs around the post compared to the direct concrete confinement condition.

Figures 21(b) and 22(b) show steel and wood posts in rectangular 457 mm × 607 mm (18 in. × 24 in.) grout-filled leave-outs after impact by the bogie vehicle. As in the square leave-out case, the rectangular grout leave-out allows significant post deflection with both posts deflecting to the back of the leave-out area. The additional 152 mm (6 in.) of grout behind the posts provided by the rectangular leave-outs results in a substantial decrease in damage to the mow strip system with only minor cracks observed in the concrete.

5. NUMERICAL SIMULATION OF SUBCOMPONENTS

5.1 OBJECTIVES

The research team performed seventeen dynamic impact tests on a series of mow strip configurations. By testing single post installations in this manner, the behavior of individual guardrail system subcomponents such as the posts, soil, and leave-out backfill material can be studied. This section describes development and validation of subcomponent finite element models for several impact tests as a first step in modeling full-scale guardrail installations encased in a mow strip. Results from numerical simulation of these models form a comparison with the impact tests to validate accuracy of the models.

5.2 BOGIE VEHICLE MODEL

The physical vehicle used for dynamic impact testing is a bogie developed by TTI. *(21)* The TTI bogie is similar to the Federal Outdoor Impact Laboratory (FOIL) bogie, but has one key difference. *(22,24)* To bring the bogie vehicle up to the desired impact speed, TTI uses a steel cable guidance and reverse tow system. To accommodate this type of guidance system, the TTI bogie is built using the frame and suspension of a car. By contrast, the FOIL bogie is mounted on a track and built with a rigid frame. The flexible suspension included in the TTI bogie introduces some additional compliance in frontal impacts that is not present in the FOIL bogie.

A finite element model of the FOIL bogie was created by Eskandarian et al. for use with LS-DYNA. *(13)* The model consists of 1844 elements and 2985 nodes. The frame of the vehicle is modeled using both rigid and linearly elastic Belytschko-Schwer beam elements (LS-DYNA 2001) with rectangular cross-sections. *(3)* The metallic honeycomb cartridges are modeled with an anisotropic, nonlinear, elastoplastic material model formulated for honeycomb and foam materials (LS-DYNA 2001). Three-dimensional, single-point, corotational elements (LS-DYNA 2001) are used to model the honeycomb cartridges. The single-point, corotational element formulation is available in LS-DYNA to accommodate severe deformations in honeycomb materials.

An impact with an instrumented rigid pole calibrated the TTI bogie vehicle. *(21)* Force transducers from the rigid pole and accelerometer data from the bogie vehicle were used to compare performance of the TTI bogie with frontal impact characteristics of a small passenger vehicle. This rigid pole impact test was simulated using the FOIL bogie model. Figure 23 shows the FOIL bogie model impacting a rigid pole.

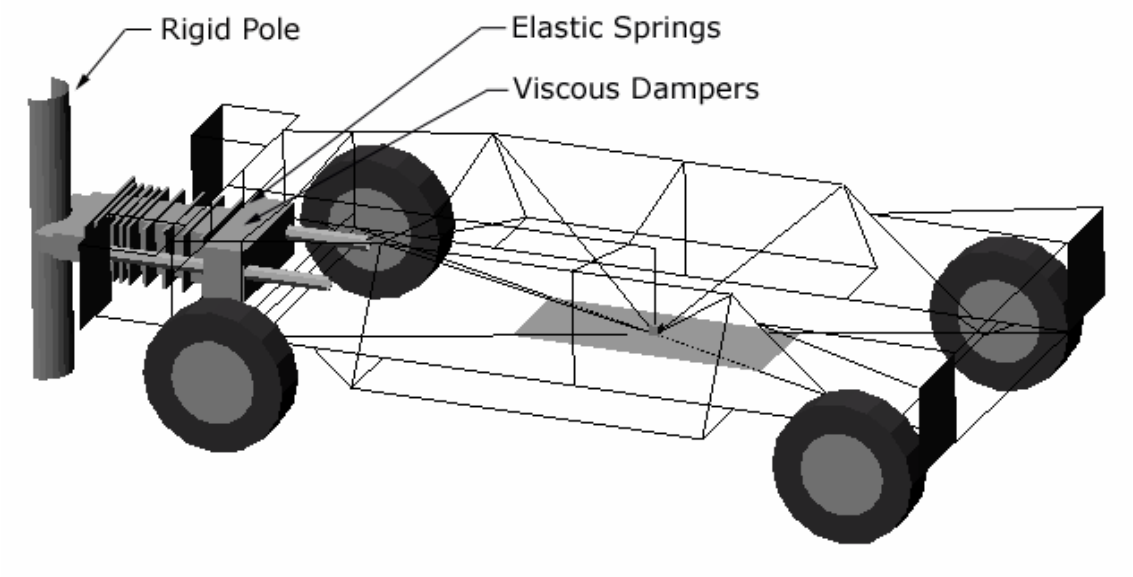

Figure 23. Simulation of Bogie Vehicle Impacting Rigid Pole.

Figure 24 shows time histories of longitudinal acceleration from the TTI rigid pole test and the FOIL bogie simulation. The frame of the TTI bogie includes a flexible suspension not included in the FOIL bogie or the FOIL bogie model. Consequently, the TTI bogie absorbs energy through elastic deformation of the flexible suspension. Therefore, the TTI bogie sustains lower peak accelerations over a longer duration. The FOIL bogie model collapses the crushable honeycomb cartridges more quickly and bottoms out on the pole approximately 40 milliseconds (ms) sooner than the TTI bogie. In order to use the FOIL bogie model to simulate impact tests performed with the TTI bogie, it was necessary to modify the model to account for the effects of the suspension on the frontal crush response.

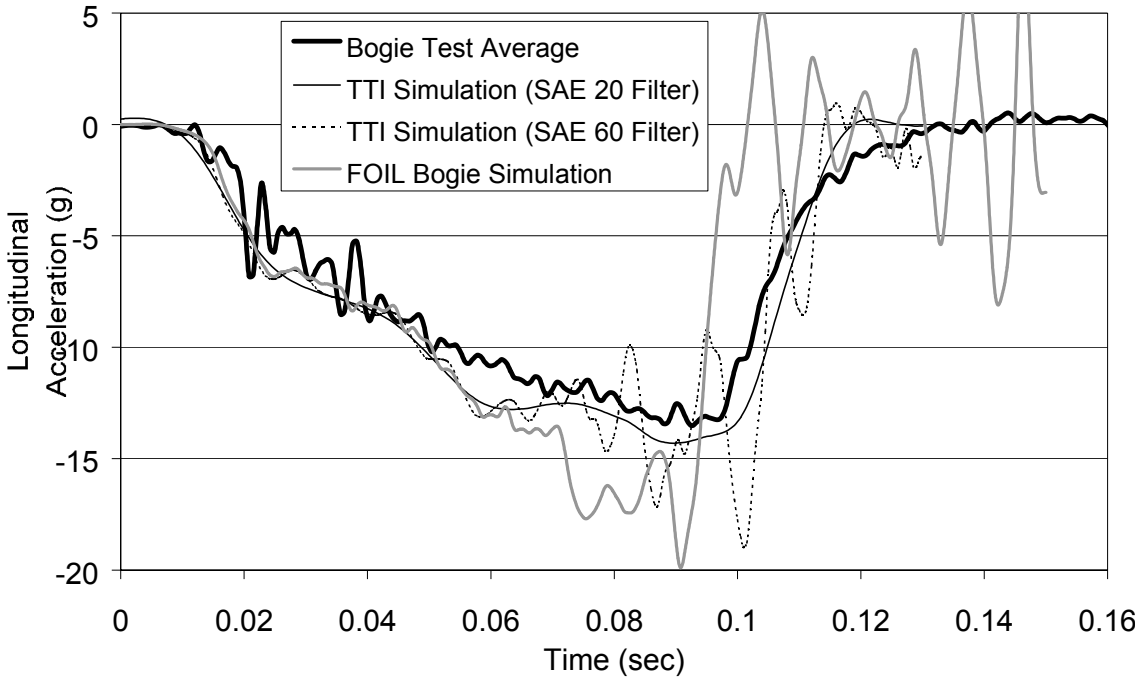

Figure 24. Accelerations of Bogie for Simulation Calibration.

Linear elastic springs and viscous damper elements were added behind the compressible nose of the FOIL model. The springs and dampers are placed in parallel, and are located at each corner of the final back-up plate comprising the nose assembly. A parametric study was performed to calibrate the properties of the springs and dampers to achieve better correlation of the acceleration response of the bogie model to the TTI bogie test. The stiffness for the spring elements is 1571 N/mm (107.6 kip/ft), and the damping constant for the dampers is 10 N-sec/mm (0.685 kip-s/ft). Figure 24 shows bogie accelerations from the FOIL bogie model simulation, the modified FOIL bogie model simulation including springs and dampers, and an average of TTI bogie test results.

Before the addition of springs and dampers, the FOIL bogie model bottoms out on the post approximately 40 ms before the TTI test average. With the addition of springs and dampers, response of the bogie model more closely follows the test average.

5.3 BASELINE SIMULATIONS

As discussed in Section 4, dynamic impact tests were performed on posts embedded in soil to serve as a baseline for comparison with mow strip configurations. To develop finite

element models of both soil and post subcomponents, these tests were numerically simulated in LS-DYNA. The isotropic, elastoplastic behavior of steel is considerably more straightforward to represent in a numerical model than the anisotropic, nonlinear behavior of wood. In addition, the failure mechanisms of steel guardrail posts, including yielding and buckling, are more reliably modeled than fracture and splitting of wood. In order to concentrate on the soil model and soil-post interaction, the finite element modeling efforts initially focused on steel post systems.

5.3.1 Steel Post Model

The model for the W150×13 (W6×9) steel post, shown in Figure 25, consists of 452 elements and 508 nodes. The steel post is 1.8 m (6 ft) long, and has two 22 mm (7/8 in.) diameter holes through one flange centered 178 mm (7 in.) from the top of the post to accommodate the attachment of the blockout. Post dimensions and section properties are readily available. *(25)* The post was meshed with four-noded Belytschko-Tsay shell elements (LS-DYNA 2001). Gauss quadrature numerical integration was used with two integration points through the thickness of the element. This underintegrated formulation reduces the computation time requirements but can lead to zero-energy hourglass modes depending on mesh and geometry. Behavior of the steel posts was monitored closely during simulation for the presence of such numerical instabilities.

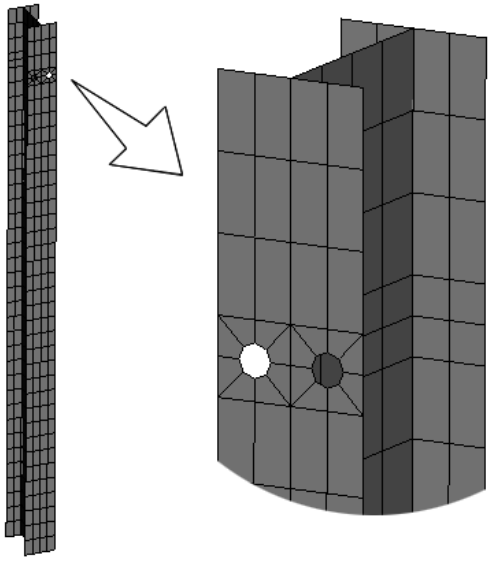

Figure 25. Finite Element Model of W150×13 Steel Post.

The posts are numerically modeled using a *Piecewise Linear Plasticity* material model. This is material number 24 in LS-DYNA (2001). Before yield, the material is assumed to be linearly elastic. After yielding, the steel can undergo plastic deformation and strain hardening. To numerically evaluate the nonlinear behavior of the steel after yield, the stress/strain constitutive relationship can be defined using either a tangent stiffness modulus or, more accurately, with a series of stress and strain data points.

Although nominally graded A36, actual properties of steel posts can vary. To determine values for the material properties needed to numerically model a steel post, Hamilton performs a series of three tensile tests on steel coupons taken from guardrail posts. *(26)* Material properties for the post are summarized in Table 2. Using the test data, a true stress-true strain curve for the steel is developed. True strain values (see Table 3) are calculated from engineering strain using the following equation:

$$\epsilon_{xx}^{plastic} = \left[\ln\left(1 + \epsilon_{xx}^{engr}\right) \right] - \frac{\sigma_{xx}}{E} \qquad (1)$$

Table 2. Summary of Material Properties for Steel Post.

Mass Density (kg/m^3) (1)	Young's Modulus (MPa) (2)	Poisson's Ratio (3)	Yield Stress (MPa) (4)
7.13	200,000	0.29	336

Table 3. Stress-Strain Curve for Yielded Steel.

Effective Plastic Strain (mm/mm) (1)	True Stress (MPa) (2)
0.000	336.72
0.024	336.05
0.042	401.15
0.057	434.28
0.141	527.22
0.213	589.56
0.250	675.00
0.259	677.36

The mesh was designed to balance computation cost and numerical accuracy. Elements comprising the web are 51 mm (2 in.) tall and 37 mm (1.5 in.) wide. The flange elements are 51 mm (2 in.) tall and 25 mm (1 in.) wide. Two separate components are used to model each post in order to accommodate the separate web and flange thicknesses. The elements along the boundary of the web and flange are equivalenced to join the parts, thereby eliminating coincident nodes.

5.3.2 Wood Post Model

Since they cost less than steel posts, wood posts are frequently used in guardrail installations throughout Texas. Wood is a complex fibrous material with anisotropic, nonlinear properties. In addition, wood properties can vary with time, loading rate, moisture content, and temperature. During an impact, response of a wood post has a significant impact on the behavior of the mow strip guardrail system. Sudden fracture of a wood post can induce pocketing of the vehicle and increased tensile stresses in the W-beam rail, eventually leading to vehicle climb or rail rupture. Therefore, a numerical model of wood posts must not only provide accurate force-deflection characteristics, but must also accurately predict failure of the post.

Although wood is anisotropic, it is a fibrous material possessing three major directional material axes. For analysis and design purposes wood can be considered to be an orthotropic material. Reviewing the available material models in LS-DYNA, six potential models are identified for modeling wood posts (see Table 4). Material models were selected based on support for solid elements, orthotropic constitutive relationships, and element failure criteria. With reference to Table 4, material models with the word "*Option*" in the material name are capable of modeling multiple constitutive relationships such as orthotropic, isotropic, or anisotropic.

Each of the material models with the exception of Material 13 (see Table 4) is valid for modeling orthotropic material behavior in solid elements. Material 13 is an isotropic material model with a simple plastic strain failure model (LS-DYNA 2001). Plaxico et al. used experimental data to develop equivalent isotropic properties for modeling wood guardrail posts. *(12)* An isotropic material model is not capable of capturing the actual mechanism of failure for a wood post subject to bending; however, equivalent isotropic properties can be used as an approximation for the complex behavior of wood.

Table 4. LS-DYNA Material Models Considered for Wood Post.

Material Number (1)	Material Name (2)
2	*Option* tropic Elastic
13	Isotropic Elastic Plastic with Failure
22	Composite Damage
26	Honeycomb
59	Composite Failure *Option* Model
126	Modified Honeycomb

The other five material models considered can represent orthotropic material behavior. Materials 26 and 126 are intended for use with metallic honeycombs and can be used to model materials with three independent, uncoupled axes. These models require extensive material property input that is not readily available for wood. In addition, honeycomb materials are prone to hourglass formation and numerical instability. For these reasons, Materials 26 and 126 were not further considered.

Materials 2, 22, and 59 are intended for orthotropic, solid elements. Material 2 is an orthotropic elastic material model capable of representing the linearly elastic behavior of wood. To include element failure with this material model, an *Add Erosion* card can be added in the LS-DYNA input file. The *Add Erosion* card can impose element failure criteria on any material model that does not already include such criteria. The limitation of the *Add Erosion* card is the requirement of failing elements by principle stress or strain, equivalent stress or strain, shear strain, or pressure. These failure criteria are not readily available for wood and neglect to consider the differences in strength along each of the material axes.

Materials 22 and 59 support linear elastic orthotropic material behavior, as well as orthotropic brittle failure. Compressive, tensile, and shear strengths for each principle axis are input, and failure is determined using the Chang and Chang criteria (LS-DYNA 2001). The difference between Materials 22 and 59 is the implementation of element failure. Material 59 erodes failed elements, whereas Material 22 leaves failed elements in the model (see Figure 26). Because element erosion provides a more accurate visual representation of the actual failure mechanism of a wood post, it was selected over Material 22.

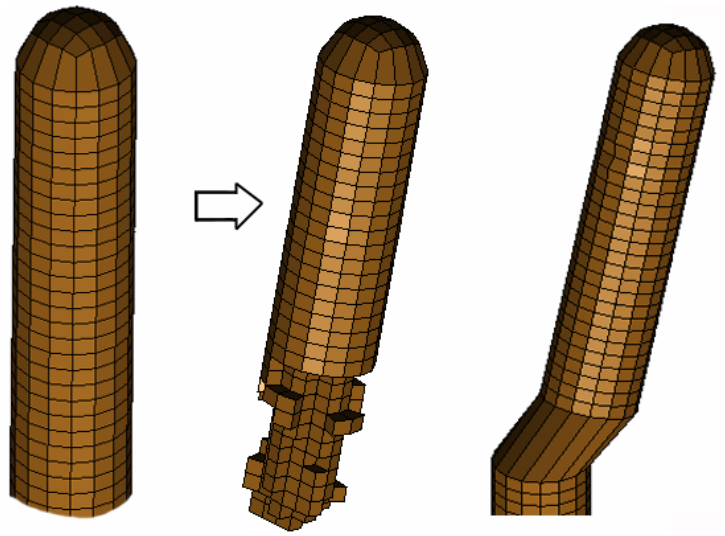

(a) **(b)**

Figure 26. Wood Post Failure: (a) Material 59; (b) Material 22.

The model for the 178 mm (7 in.) diameter wood post, shown in Figure 27, consists of 2304 elements and 2993 nodes. The wood post is 1.8 m (6 ft) long. Material 59 does not support fully integrated elements, thus eight-node constant stress solid elements (LS-DYNA 2001) are used for simulations. Behavior of the wood posts was monitored closely during the simulations for the presence of numerical instabilities incited by the underintegrated element formulation.

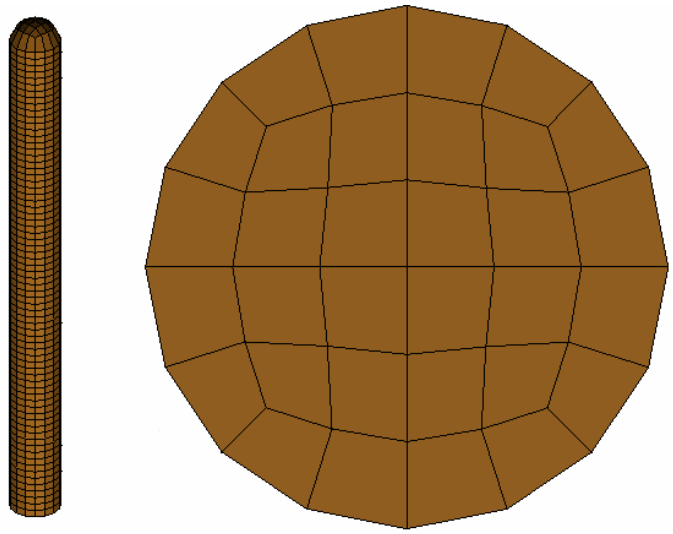

(a) **(b)**

Figure 27. Finite Element Mesh of Wood Post: (a) Isometric; and (b) Bottom Views.

5.3.3 Soil Model

Guardrail systems rely in part on soil deformation to absorb energy during a vehicle impact. Variations in soil strength and post embedment depth have a significant effect on system performance. *(27)* Therefore, accurate numerical modeling of the soil and its interaction with the guardrail system is essential for a reliable model. Development of a numerical model for the soil structure interaction of guardrail posts is discussed by Seckinger and Roschke, a summary of which follows. *(28)*

Standard soil used in crash testing of roadside guardrails is basically an American Association of State Highway and Transportation Officials (AASHTO) designated road base material. *(29)* As mentioned previously, Dewey et al. and Jeyepalan developed correlations of shear strength and cohesion properties for this soil type using a gradation curve, maximum particle size, relative density, and overburden pressure. *(6, 30)* An engineering manual published by the United States Army Corps of Engineers gives average values for Young's modulus, elastic shear modulus, and Poisson's ratio for different types of soils. *(31)* These studies were used to establish a range of appropriate material property values for a numerical model of soil for use in simulations of guardrail systems. A summary of the soil material properties used in the simulations performed under this study is given in Table 5.

Table 5. Summary of Material Properties for Soil Model.

Mass Density (kg/m^3) (1)	Elastic Shear Modulus (MPa) (2)	Poisson's Ratio (3)	Failure Surface Shape Parameter (4)	Internal Friction Angle (rad) (5)	Cohesion (6)	Dilation Angle (rad) (7)
1,922.0	9.00	0.40	0.80	0.75	0.00	0.00

In the past, the computational expense of processing a continuum of solid soil elements has caused researchers to use less expensive approximations for modeling soil structure interaction. For example, Patzner et al. used a subgrade modulus approach to model interaction between timber guardrail posts and a cohesionless soil. *(9)* Figure 28 shows the finite element representation of this model including the nonlinear springs used to represent the soil. While the subgrade modulus approach can efficiently represent the reactions of soil on a loaded post,

changes to the overburden pressure or confinement during the simulation, such as can occur during impact of a guardrail encased in mow strip impact, can result in inaccuracies.

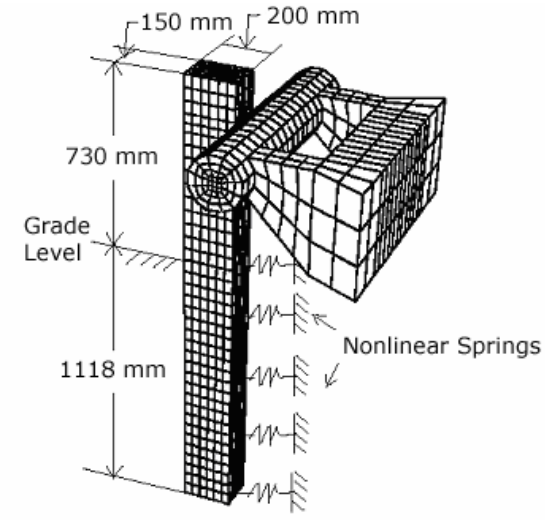

Figure 28. Post Impact Using Subgrade Modulus Soil Discretization.

Several material models are available in LS-DYNA to represent solid, Lagrangian elements with material characteristics of soil (LS-DYNA 2001). The material models considered for this research are listed in Table 6. Unlike most other soil structure interaction problems, roadside guardrail applications typically have low confinement. Many of the numerical material models developed for soil are intended for high-confinement, deep foundation problems. The material behaves as a fluid and requires confinement within a geometric boundary. Low confining stresses cause numerical instabilities in these models. This limitation is present for material numbers 5, 14, and 78. Of the remaining material models, several require extensive experimental material data not readily available, or use complex algorithms too computationally costly for use in this research.

Soil can be numerically modeled assuming linear elastic material behavior up to a state of stress at which slip or yield occurs. The yield point and ultimate strength of soil are pressure dependent. *(32)* An *Isotropic Elastic Plastic* constitutive relationship (Material 12) is available in LS-DYNA (2001), and can be used to model a continuum of soil elements. However, the yield surface used for this model is pressure independent (see Figure 29), and can result in inaccuracies when the confinement or normal stress on the soil changes during an impact event.

Table 6. LS-DYNA Material Models Considered for Soil Modeling.

Material Number (1)	Material Name (2)
5	Soil and Foam
12	Isotropic Elastic Plastic
14	Soil and Foam with Failure
16	Pseudo Tensor Geological Model
25	Inciscid Two Invariant Geological Cap
26	Honeycomb
72	Concrete Damage
78	Soil Concrete
79	Hysteretic Soil
126	Modified Honeycomb
192	Soil Brick
193	Drucker-Prager

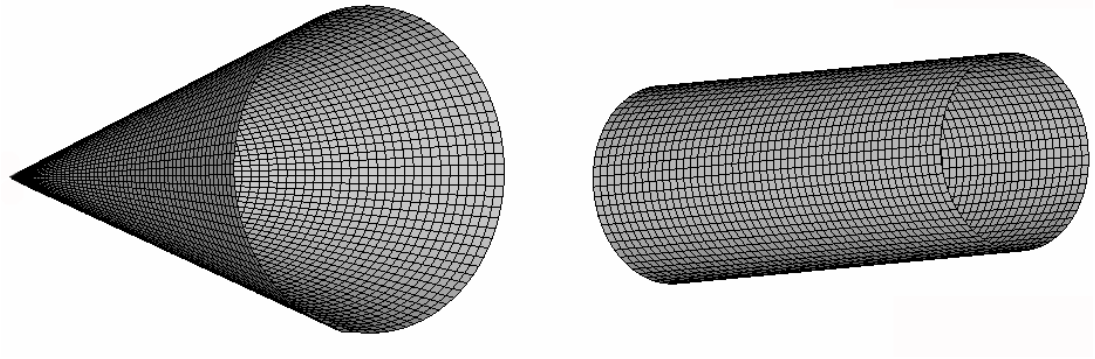

(a) **(b)**

Figure 29. Yield Surfaces for Plasticity Models: (a) Drucker-Prager (Pressure Dependent); (b) Von Mises (Pressure Independent).

In order to capture the increase of strength under normal stress demonstrated by sandy soils, Drucker and Prager proposed a modification of the Mohr-Coulomb criterion to take into account the inability of a cohesionless soil to resist tensile loading. *(33)* The model also accounts for volumetric expansion as a result of shear deformation. The yield surface is defined by the following equation:

$$3\sigma_m \sin(\phi) + J_2 - c = 0 \qquad (2)$$

where σ_m is the mean stress, J_2 is the second stress invariant, c is cohesion, and ϕ is the friction angle of the material. A *Drucker-Prager* material model is available in LS-DYNA (2001), and requires input parameters readily available in published literature. Because of its computational efficiency and ability to accurately model important characteristics of soil mechanics, this model was used for the numerical simulation of soil under this study.

A continuum of 888 solid elements modeled a cylinder of soil for numerical simulation of the dynamic post impact tests. A typical mesh is shown in Figure 30. In order to maximize the distance between the post and the outer boundary of the soil layer with the least number of elements, a cylinder of soil elements is used. The soil cylinder is 1.6 m (5.3 ft) deep and provides ample depth of material below the post. For dynamic impact simulations, a diameter of 1.5 m (4.9 ft) was used for the soil cylinder. During the full-scale simulation phase, the diameter of the soil cylinders in the impact region was increased to 2.7 m (8.6 ft) to eliminate edge effects caused by severe deflection of the posts.

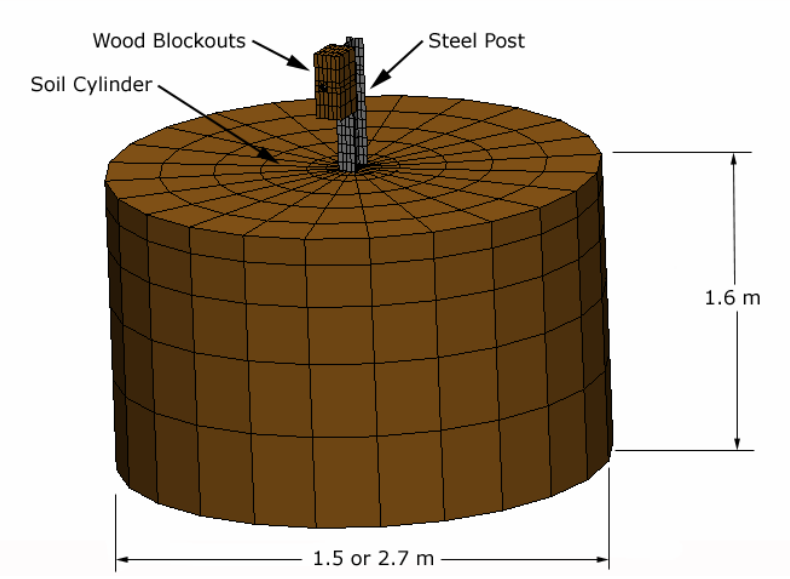

Figure 30. Finite Element Model of Steel Post in Soil.

Constant stress solid elements are more computationally efficient than fully integrated selectively reduced (S/R) solid elements. In addition, the *Drucker-Prager* material model in LS-DYNA currently does not support fully integrated elements. Therefore, constant stress, eight-noded solid elements (LS-DYNA 2001) were used to numerically model the soil. This is an underintegrated element formulation that can lead to zero energy hourglass modes. Behavior of the elements must, therefore, be carefully monitored during simulation for the presence of such modes.

To prevent contamination of data by the reflection of stress waves off of the soil cylinder boundary, a nonreflecting boundary is used around the outer face of the cylinders. Segment sets are defined for the outer surface of the soil cylinders. They consist of four node sets defining faces of solid elements. Based on linear material behavior, LS-DYNA computes an impedance matching function for all nonreflecting boundary segments (LS-DYNA 2001). Dilational and shear waves are both accounted for by the nonreflecting boundary. To accommodate this, the soil cylinder must be modeled such that all nonlinear behavior occurs away from the boundaries. The nonreflecting boundary surface is constrained from translation in the horizontal plane, but nodes are free to both rotate about any axis and to translate vertically. No constraints were placed on the top surface of the soil cylinder. The bottom of the cylinder was constrained from translation in both the horizontal and vertical planes.

Although LS-DYNA features some of the most advanced contact algorithms available in commercial finite element software, capturing interaction between solid and shell elements can be a daunting task. This task is exacerbated when the edges of shell elements are in contact with solid elements. In addition, to accurately model post embedment, any gap left between solid soil elements and post elements must be very small. In order to capture contact between post and soil, null shell elements were used (LS-DYNA 2001). Null shell elements were only included for contact purposes and were not included in the structural element processing.

The selection of contact algorithms in LS-DYNA is extremely case-specific. To capture interaction between the thin edges of the steel post and the surface of the soil, it is necessary to use a *Surface to Surface* contact with an edge-checking algorithm. The edge-checking algorithm is computationally expensive, but it is necessary to prevent penetration. This algorithm was unnecessary with the wood post, however, as only surfaces were in contact.

5.3.4 Simulation Results

Using the aforementioned steel, wood, and soil models, numerical simulations replicated the baseline dynamic impact tests. The numerical simulations validated behavior of the subcomponent finite element models. Results of these simulations are discussed below.

5.3.4.1 Steel Post System

The initial configuration for the numerical simulation of the steel post in soil is shown in Figure 31. Figure 32 shows a comparison of longitudinal accelerations of the bogie for the experimental test and numerical simulation. Results of numerical simulation follow the same trend as for the experimental test. After the peak acceleration is reached, numerical simulation demonstrates high-frequency oscillation. This oscillation is induced by the linear elastic springs added to the bogie model to account for a flexible suspension.

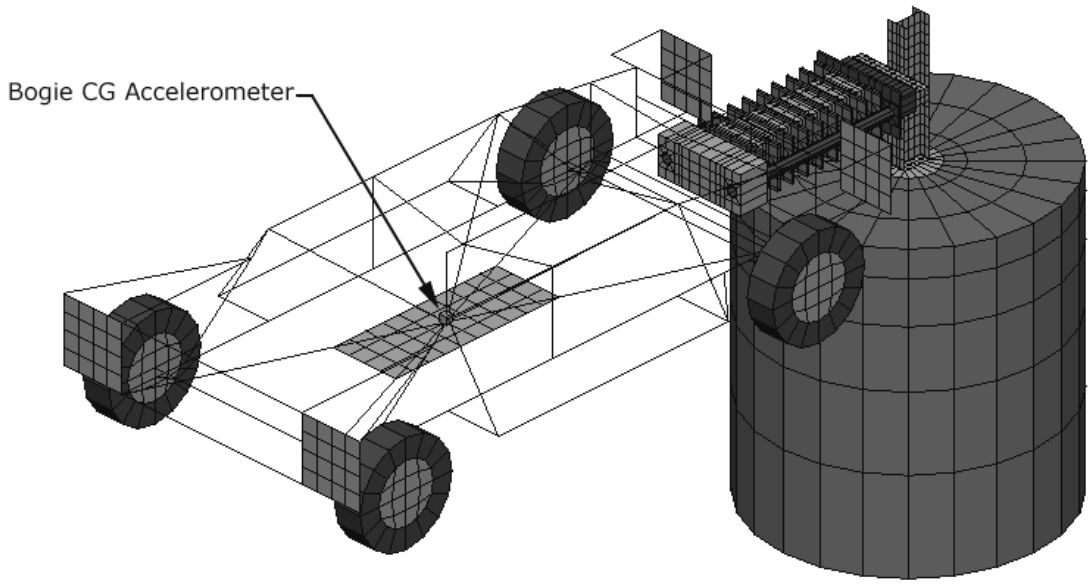

Figure 31. Initial Configuration of Steel Post Baseline Bogie Simulation.

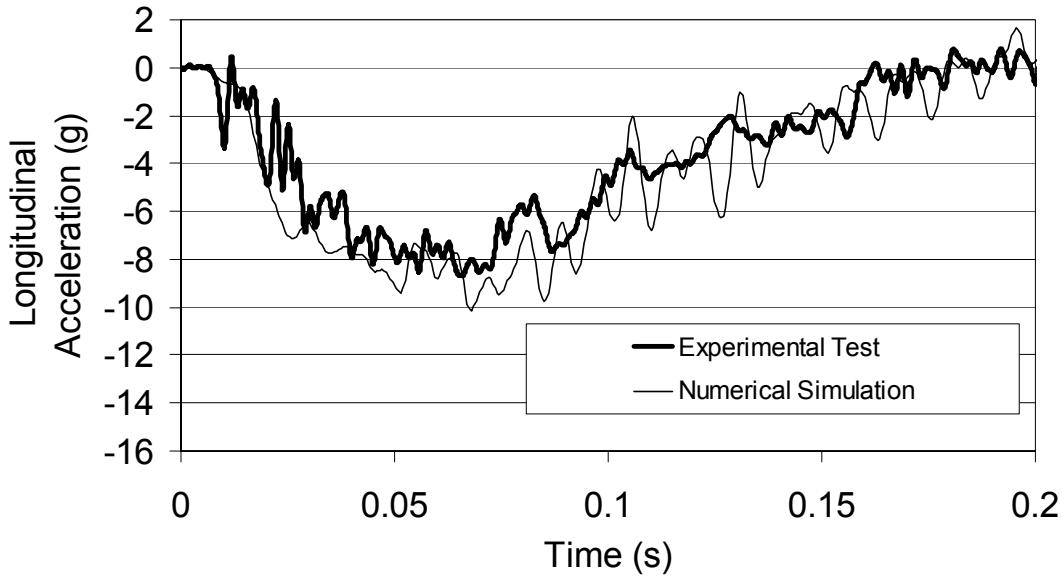

Figure 32. Comparison of Simulation and Test Accelerations of Bogie for Baseline Steel Post Impact.

Sequential images of the numerical simulation and experimental testing are shown in Figure 33. Although the bogie vehicle eventually slides up and over the post, the initial impact deflects the post back through the soil. Dilation of the soil occurs behind the post both in the experiment and during simulation. In addition to good correlation with the bogie acceleration history, the post deflection pattern is consistent between the test and simulation. The steel post undergoes some plastic deformation during impact. Final deformed states of the post in test and simulation show similar amounts of plastic deformation. This indicates that the subgrade reaction of the soil on the post in the numerical simulation provides a reasonable representation of the actual soil behavior. With good correlation between test and simulation, this model was implemented in a full-scale guardrail system.

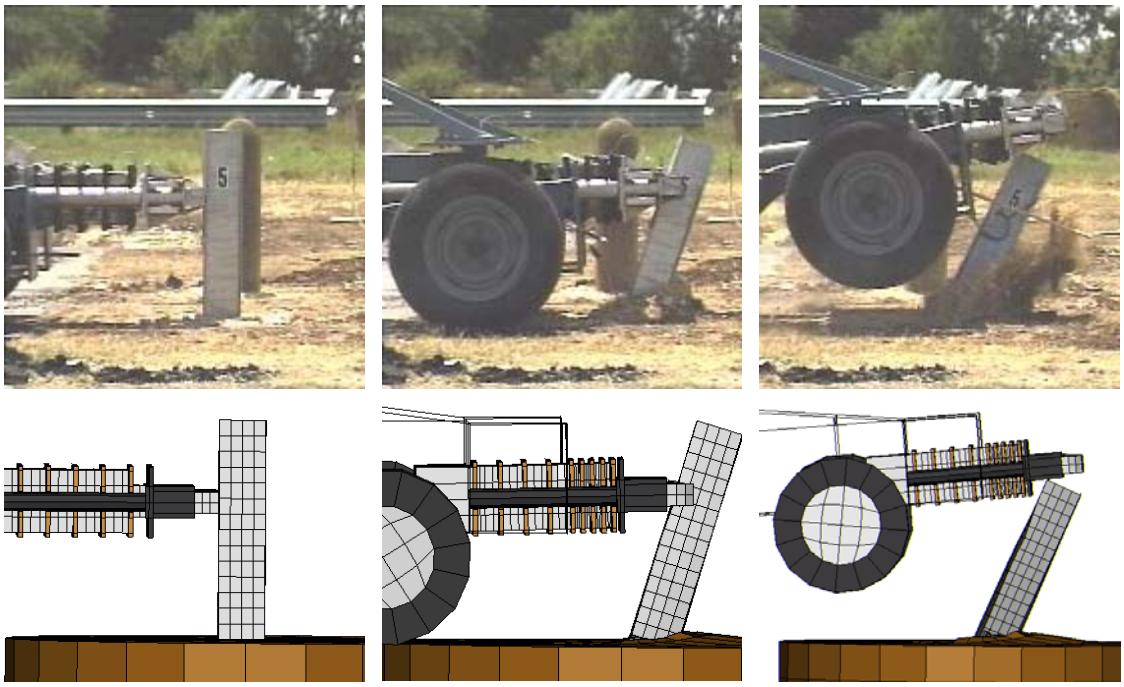

Figure 33. Sequential Comparison of Test and Simulation for Baseline Steel Post in Soil Impact.

5.3.4.2 Wood Post System

Using numerical models of a wood post and the soil as described above, conditions simulated those of the wood post dynamic impact test in soil. The initial configuration for the numerical simulation is shown in Figure 34. Sequential images of the numerical simulation and experimental testing are shown in Figure 35. Impact of the bogie vehicle causes the wood post to deflect through the soil. Soil dilation occurs behind the post both in test and simulation as with the steel post. The post deflection pattern is consistent between the experimental test and simulation.

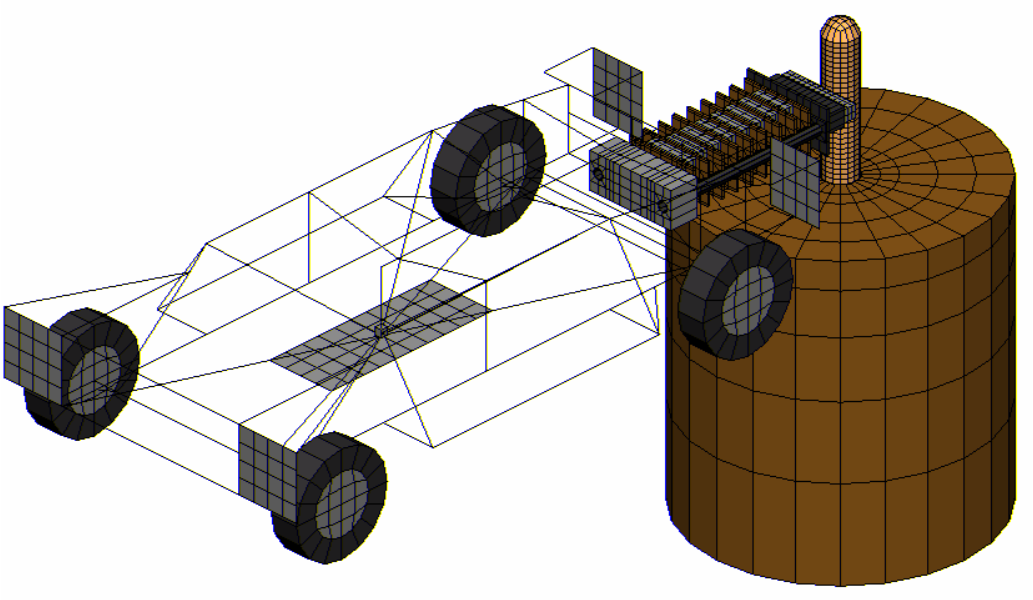

Figure 34. Initial Configuration of Wood Post Baseline Bogie Simulation.

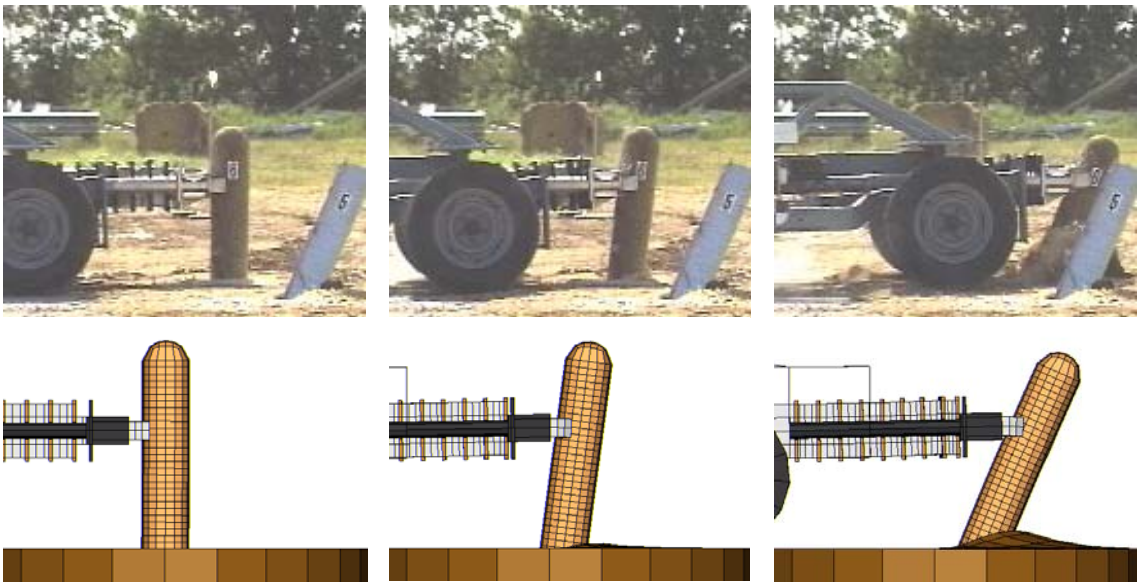

Figure 35. Sequential Comparison of Test and Simulation for Baseline Wood Post in Soil Impact.

5.4 NUMERICAL SIMULATION OF MOW STRIP INSTALLATIONS

In addition to baseline impact tests, dynamic impact tests of posts embedded in asphalt and concrete mow strips were also performed. Wood, steel, and soil models are validated by results of baseline tests. Numerical models of mow strip installations were developed by adding concrete or asphalt mow strip layers around the validated post and soil models developed from the baseline simulations.

5.4.1 Wood Post in Asphalt

As described previously, the wood post model developed for use in this study was partially validated by comparing simulation and test results obtained from the bogie test of a wood post in soil. However, to complete the validation, it is important to verify that the failure mode of the post is accurately captured. A simulation of the bogie test of a wood post in asphalt mow strip was used for this purpose. The asphalt mow strip impact test was selected to avoid the complications of concrete fracture that occurred during the concrete mow strip tests.

In the asphalt mow strip test, the post fractured with minimal displacement. Therefore, since the focus of this investigation was to capture post fracture, the asphalt mow strip was simply modeled as a rigid material.

Sequential images of the numerical simulation and experimental test are shown in Figure 36. Impact of the bogie vehicle causes the wood post to fracture. The post failure pattern is consistent between the experimental test and simulation. Based on these results, the wood post model was considered sufficiently valid for use in full-scale system models.

5.4.2 Concrete Post Embedment

The research team developed a concrete mow strip model to replicate the dimensions and properties of the configuration used in the subcomponent testing. The initial configuration of the model is shown in Figure 37. It consists of 4600 eight-noded constant stress elements and 5982 nodes. Null shell elements are used to treat contact between the steel post and concrete models. The null shell elements extend down through the concrete and into the soil cylinder below.

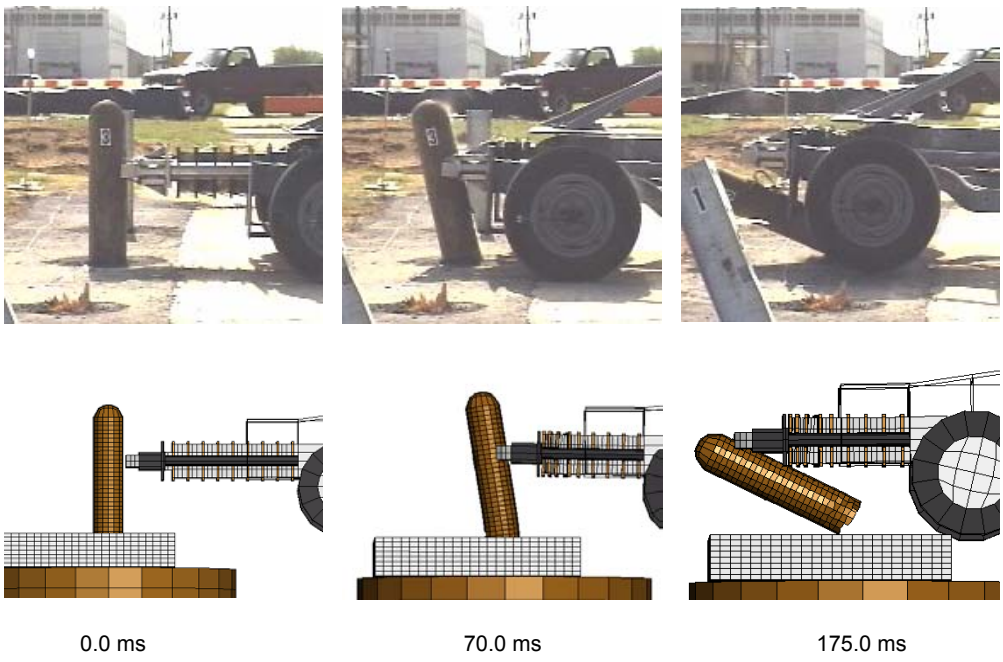

Figure 36. Comparison of Bogie Vehicle Simulation and Test Results for Wood Post in Asphalt.

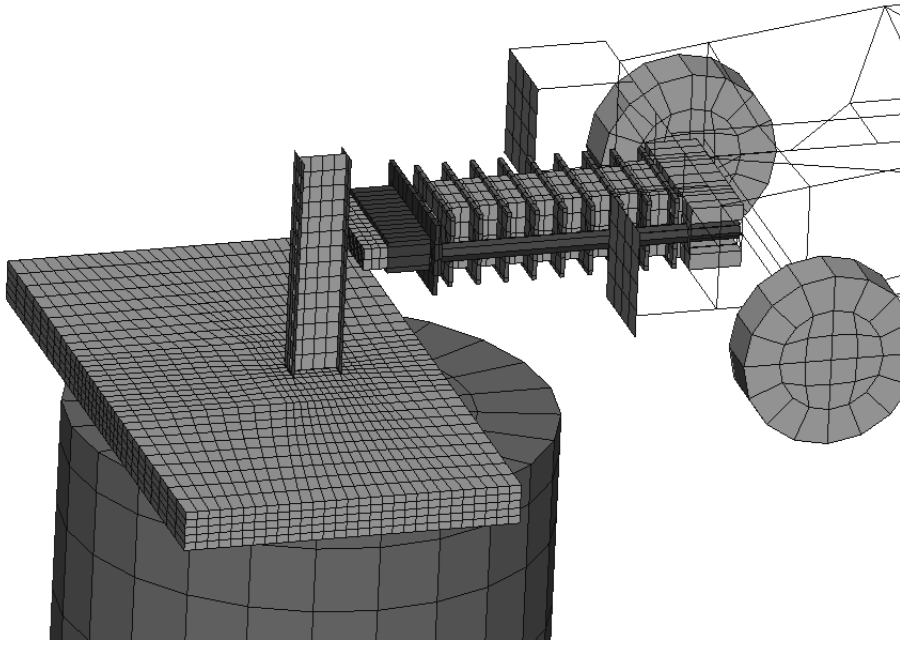

Figure 37. Initial Configuration of Steel Post in Concrete Bogie Simulation.

Dynamic impact testing of the posts embedded in concrete resulted in significant fracture and cracking to the concrete mow strip. To accurately capture the force-deflection characteristics of the posts in these tests, it is necessary to model the concrete with a material model capable of extensive, large-deflection concrete failure. LS-DYNA Material 84 (*Winfrith Concrete*) is a smeared crack (or pseudo crack) model that can be used to capture crack initiation and propagation in concrete. Figure 38 shows a visual representation of concrete failure modeled with the Winfrith concrete model. The black marks displayed on the concrete mow strip surface represent crack formation. Although the crack pattern in the numerical simulation is consistent with damage observed during the test, the *Winfrith Concrete* model does not accommodate large deflections in a stable manner. As a result, the steel post in the numerical model is not able to rotate through the failed concrete as in the test.

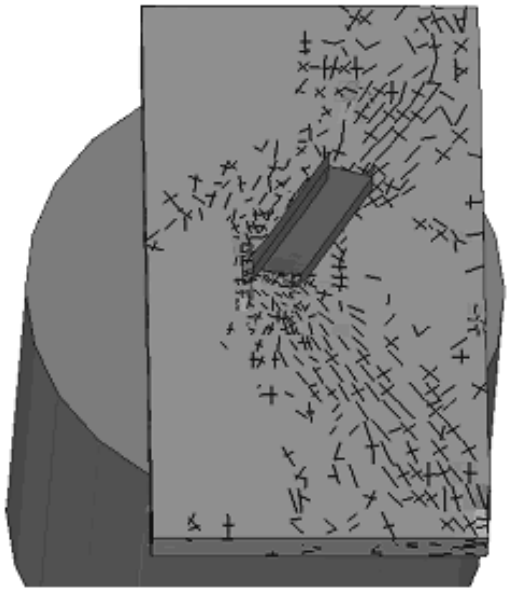

Figure 38. Concrete Failure in Numerical Simulation.

Further, the *Winfrith Concrete* model does not support fully integrated element formulation (LS-DYNA 2001). Because of this, significant hourglass behavior develops after the concrete becomes damaged. Numerical instability associated with hourglass modes causes simulation to terminate. In addition, the mesh density required to accurately model concrete failure makes implementation in a full-scale model impractical. The increase in system size

from a 1.9 m (6.3 ft) long strip of concrete in a bogie simulation to a 30 m (100 ft) long strip of concrete in a full-scale system amplifies the stability and computational problems exponentially.

In order to focus on the effects of mow strips on guardrail performance rather than maintenance issues associated with the extent of damage to the mow strip, the concrete mow strip layer was ultimately assumed to be rigid. With this assumption, difficulties associated with numerical instabilities and computational costs are eliminated and full-scale implementation becomes practical.

5.4.3 Grout-Filled Leave-Outs

The two-sack grout mixture used in the experimental tests had a measured compressive strength of 0.85 MPa (120 psi). Observation of the bogie tests indicates that the grout in a leave-out shears up and out of the leave-out region prior to developing its full compressive strength. Two methods for numerically modeling this failure are available in LS-DYNA (see Figure 39). Element erosion can be used to delete elements when a failure criterion has been met. Material 12 *Isotropic Elastic Failure* is one material model that allows the user to specify a failure pressure for element erosion. Also, LS-DYNA has an *Add Erosion* card that allows the user to add element erosion failure to an existing material model that does not have this option built in. The *Add Erosion* option allows for seven different failure criteria that trigger element erosion.

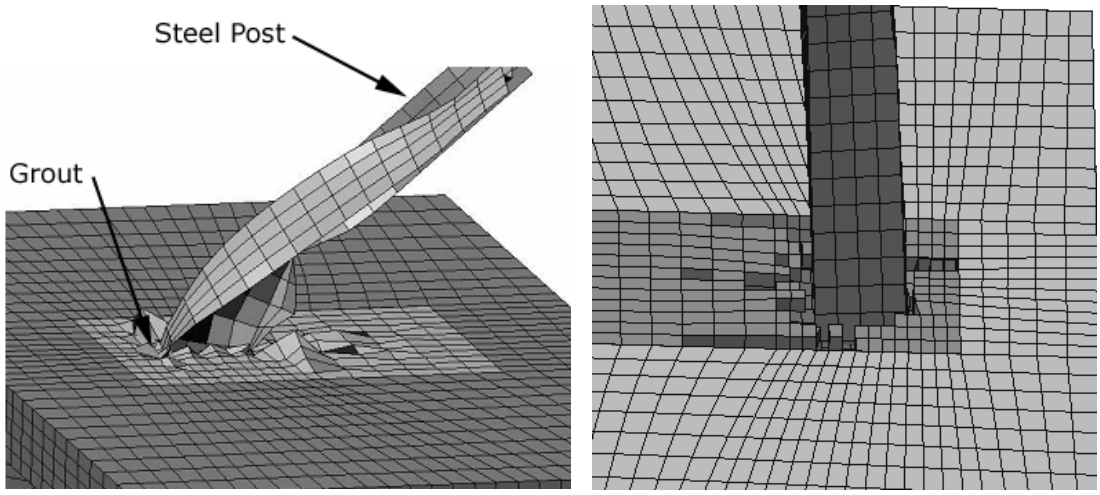

(a) **(b)**

Figure 39. Numerical Modeling of Grout Failure: (a) Winfrith Concrete Model; (b) Element Erosion.

Another method of modeling the grout failure around the posts is by using a material model that deforms in such a way that the behavior of the grout is effectively represented. This material model does not erode elements, but undergoes severe deformations as the post rotates through the material. Several concrete material models such as *Winfrith Concrete*, Type 84, were examined as candidates for this application. However, when the low strength parameters of the grout were input into these material models, severe hourglass deformation occurred and the large deformations displayed by the grout in experimental tests were not replicated. Because of this difficulty, element erosion was used to simulate failure of the grout material.

The grout material model was validated using a bogie impact simulation of a steel post encased in a 203 mm (8 in.) thick asphalt mow strip with a 457 mm (18 in.) diameter grout-filled leave-out (see Figure 40). The researchers used the asphalt mow strip impact test for validation to avoid the complications of concrete fracture that occurred during the concrete mow strip tests.

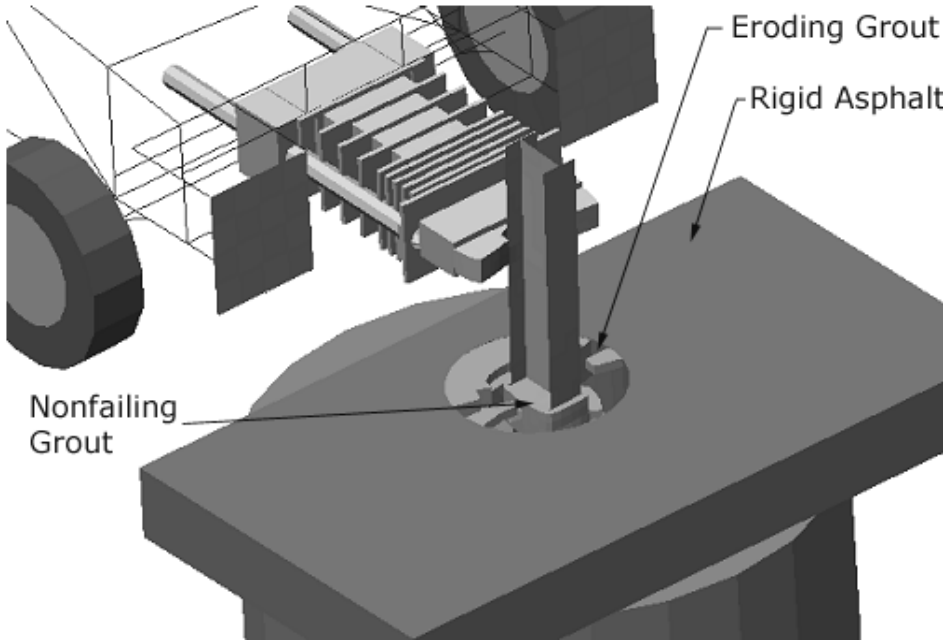

Figure 40. Bogie Impacting Steel Post Surrounded by Eroding Grout Elements.

The compressive strength of the grout as tested is 0.85 MPa (120 psi). When compressed in a leave-out, however, the grout is not able to reach its full compressive strength. A shear failure causes the grout to buckle vertically out of the leave-out. Without a direct way to calculate the strength of this shear-buckling mode, the 0.85 MPa (120 psi) compressive strength

value was used as a starting point to calibrate the material model. An *Isotropic Elastic Failure* material model was used with element erosion to model failure of the grout elements. When the pressure in an element reaches a specified failure value, the element is eroded.

A layer of elements directly around the post is not assigned a failure criterion. These elements are in contact with the steel post, and are equivalenced to the failing grout elements around them. An eroding contact is defined for the failing and nonfailing elements that triggers automatic contact surface updates. This definition allows the exposed grout surfaces to be in contact with one another as elements are eroded. Nonfailing elements around the post simplify the interaction between the post and the grout, and make possible the null shell contact method described earlier.

After simulating numerous pressure failure values, results indicated that a pressure failure of −0.23 MPa (33 psi) allows the grout to fail in a manner that is consistent with the bogie testing. The maximum acceleration placed on the bogie vehicle directly corresponds to failure of the grout. When the grout begins to fail, the reaction force placed on the bogie by the mow strip and post begins to decrease. Figure 41 shows slight variation between the experimental test and simulation. However, there is good correlation between both the maximum acceleration and the rate of change of acceleration. Future simulations can improve the grout model by implementing a more sophisticated failure criterion; however, by modeling the peak capacity of the grout before failure, an accurate representation of post deflection can be achieved with this grout model.

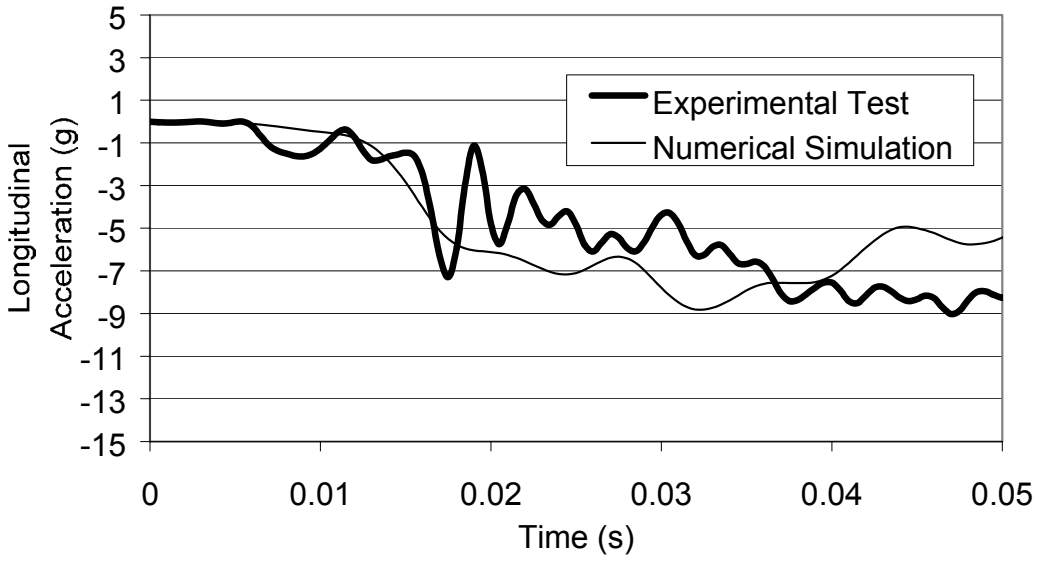

Figure 41. Comparison of Simulation and Test Accelerations of Bogie for Steel Post in 457 mm Diameter Grout Leave-out Impact.

6. PREDICTIVE FULL-SCALE SYSTEM SIMULATIONS

In order to study the performance of guardrail systems in various mow-strip configurations, the research team devised several simulation scenarios based on the results of the subcomponent analysis and testing. Four numerical models of mow strip guardrail configurations were constructed. These models include a steel post guardrail in rigid mow strip, steel post guardrail in concrete mow strip with grout-filled leave-outs, wood post guardrail in rigid mow strip, and wood post guardrail in mow strip with grout-filled leave-outs. Additionally, a full-scale system model of a modified G4(1S) guardrail was conducted to help establish validity of the system model and serve as a verified baseline response for comparison with the mow strip configurations. Development and analysis of these full-scale guardrail system models is discussed below.

6.1 NUMERICAL SIMULATION OF STEEL POST GUARDRAIL IN SOIL

6.1.1 Numerical Model of Guardrail

As the most commonly used strong post guardrail system in the United States, the G4(1S) has undergone extensive full-scale crash testing. Consequently, it is convenient to base an analysis of the effect of mow strip confinement on this system. Using the numerical model of a steel post embedded in a soil, a full-scale model of a modified G4(1S) system was developed. The full system, which is 30 m (100 ft) long, consists of 90,573 elements and 108,782 nodes, not including the vehicle model (see Figure 42). Crash tests of the modified G4(1S) system with routed wood and polymer blockouts serve as the basis for evaluating the numerical model.

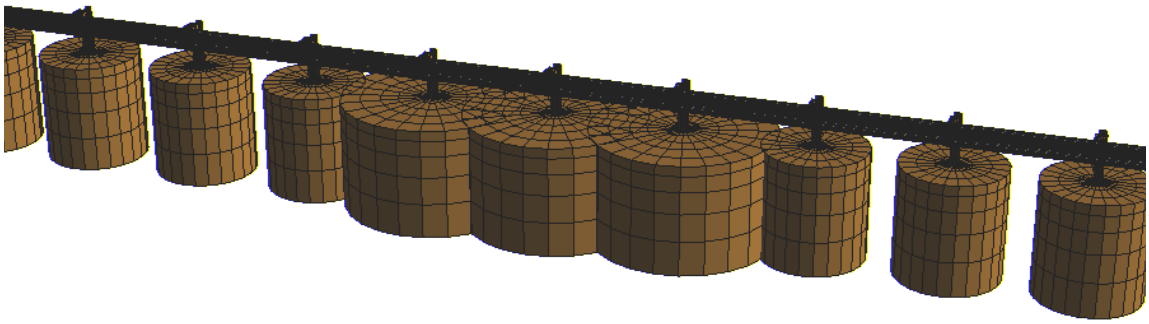

Figure 42. Initial Configuration of Finite Element Model of G4(1S).

Consistent with the full-scale crash tests and the guidelines in *NCHRP Report 350,* the impact location was selected to be 4.5 m (15 ft) upstream from the rail splice near the one-third point of the installation. As mentioned previously, the three most severely impacted posts are embedded in a soil cylinder with an increased diameter of 2.7 m (8.6 ft). This modification is made to eliminate edge effects caused by severe deflection of the posts in the vehicle impact region and to prevent nonlinear soil behavior near a nonreflecting boundary.

Routed wood blockouts were explicitly modeled and attached to the flanges of the steel posts (see Figure 43). Because failure of wood blockouts is not common, they were modeled using simple linearly elastic elements. The blockout and post assembly are joined together using a rigid carriage bolt. To model elongation of the bolt, the nut is allowed to slip freely along the shaft of the bolt. The bolt is linked to the nut by a linear elastic spring. The spring constant is calculated using the following formula:

$$k = \frac{EA}{l} \qquad (3)$$

where E is the Young's Modulus of the bolt, A is the cross-sectional area of the bolt, and l is the length of the bolt. Using this equation, the spring stiffness is calculated to be 185 kN/mm (1056 kip/in.). A deflection failure of 0.24 mm (0.01 in.) is defined for the spring to model bolt failure induced by combined tension and bending.

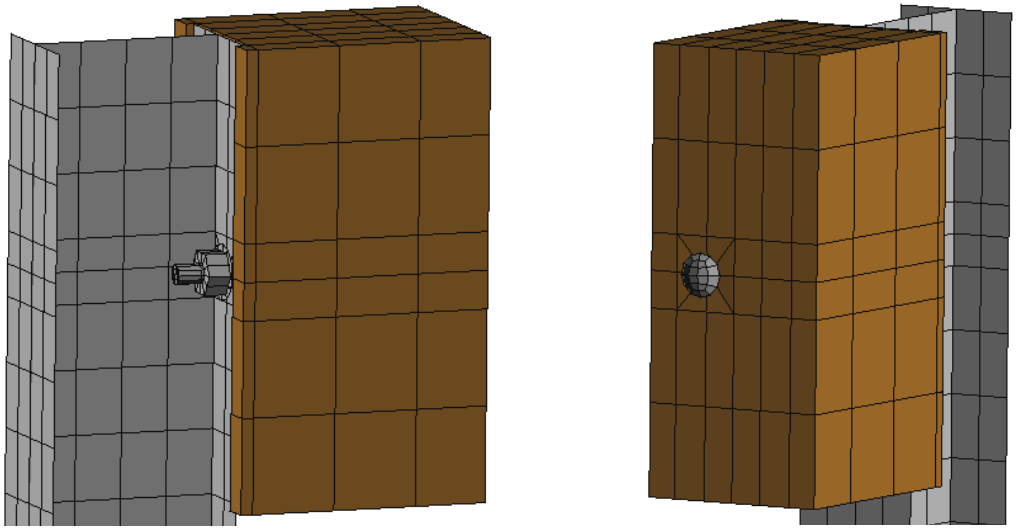

Figure 43. Finite Element Model of Routed Wooden Blockout Bolted to Steel Post.

The W-beam guardrail model used in the study is shown in Figure 44. Dimensions of the cross-section are readily available. *(34)* Slotted post bolt holes are modeled for connecting the rail to the blockouts and posts. Eight splice bolt holes are meshed at each end of the rail segment for splicing adjacent rails. It is particularly important to model these splice bolt holes because this is the region of the rail subjected to the greatest stresses and is, therefore, the most likely location for failure of the rail to occur.

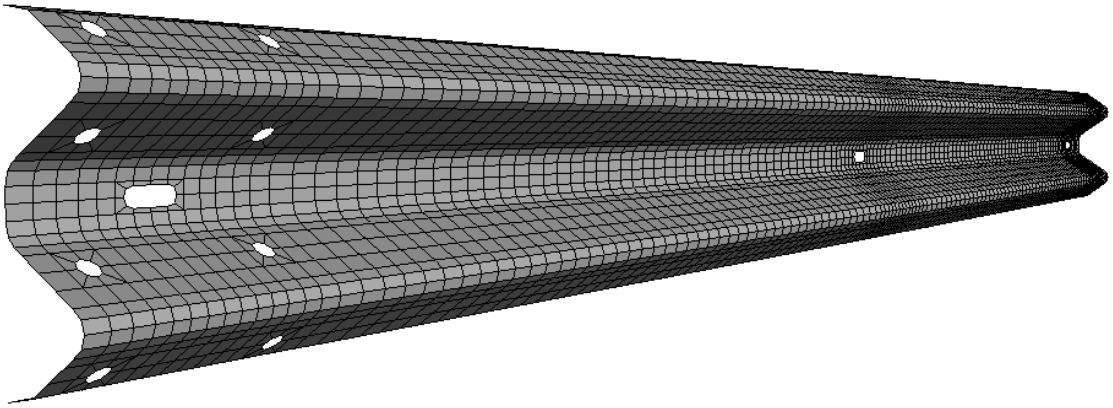

Figure 44. Finite Element Mesh of W-beam Guardrail.

The numerical model of each rail segment consists of 4036 elements and 4262 nodes. Underintegrated Belytschko-Tsay shell elements were used with two Gauss integration points through the element thickness. Material properties for the steel rail are given by Reid and Sicking based on experimental tests of guardrail specimens. *(35)* A *Piecewise Linear Plasticity* material (LS-DYNA 2001) is used to model the behavior of the steel rail. Although a failure model was not used for the W-beam rail steel, the stresses and strains were compared to nominal yield strength, ultimate strength, and ductility of the AASHTO M-180 steel to determine whether failure of the rail is likely.

Guardrail segments are joined with splice bolts (see Figure 45). As with the post bolts, splice bolts are modeled as rigid, and the same method of modeling bolt elongation is used. By explicitly modeling bolts at splices and guardrail-to-post connections, the natural slack inherent to the system is modeled.

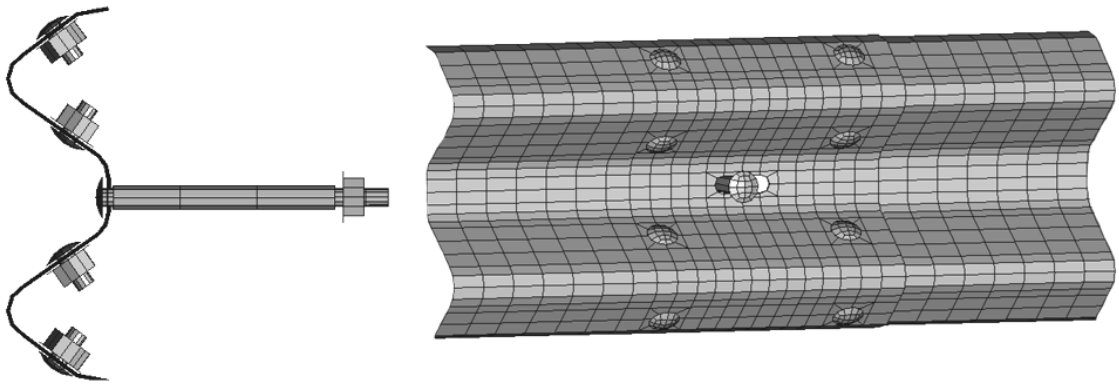

Figure 45. Finite Element Model of Guardrail Splice.

Because the lateral load of an impact is carried in part by tension in the guardrail, accurate modeling of the end constraints of the rail are important for simulating performance of the system. In an actual guardrail installation, end terminals are used at either end of the system. Hamilton approximates the stiffness of an end terminal by performing numerical simulations of uniaxial loading tests. *(26)* Data from these simulations are used to develop equivalent stiffness parameters for a W-beam cross-section of shell elements. Material and section properties derived by Hamilton were used as a starting point for this study. Because the response of a guardrail system to impact is extremely sensitive to end constraints on the rail, properties of the constrained shells were calibrated to match experimental test data.

6.1.2 Simulation Results

The numerical simulation showed the vehicle is smoothly redirected without severe snagging or pocketing, and it exits the system in a stable manner without considerable roll. Overall dynamics of the vehicle were consistent between test and simulation. Table 7 presents a summary of results from the numerical simulation and five similar crash tests. Figures 46 and 47 show images of the simulation.

The maximum dynamic deflection of the guardrail in the numerical simulation is slightly less than the average for the five full-scale crash tests (see Table 7). However, it is well within the range of values established by the tests. Similarly, occupant impact velocity (OIV) and maximum 50-ms average acceleration values for the simulation are within the range of values observed in the five crash tests (see Table 7). Two posts separated from the rail in the numerical simulation. This occurs as the head of the bolt pulls through its slot in the guardrail. Typically,

between one and three posts separate from the rail with an average of two posts separating in each test. Plastic strain contours of the rail, shown in Figure 48, indicate localized concentrations of high strain around the post bolts slots and moderate plastic strain throughout the rail segment. This condition indicates that rupture of the rail segment is not probable and only few tears around the slots are likely to develop. Overall dynamics of the vehicle are consistent between test and simulation as well. The vehicle redirects without snagging or overriding, and subsequently exits the system with only a small roll angle.

Table 7. Summary of G4(1S) Crash Test and Simulation Results

Guardrail System (1)	Maximum Dynamic Deflection (mm) (2)	Number of Separated Posts (3)	Maximum Occupant Impact Velocity (m/s) (4)	Maximum 50-ms Acceleration (g) (5)
Bligh et al. (17)	750	1	7.38	-7.76
Bullard et al. (15)	1,000	2	7.10	-7.90
Alberson et al. (18)	890	3	4.30	-9.30
Bligh & Menges (16)	1,130	2	6.74	-9.08
Williams et al (19)	937	2	7.90	-10.90
Test Average	921	2	6.08	-8.99
Numerical Simulation	862	2	4.70	-10.70

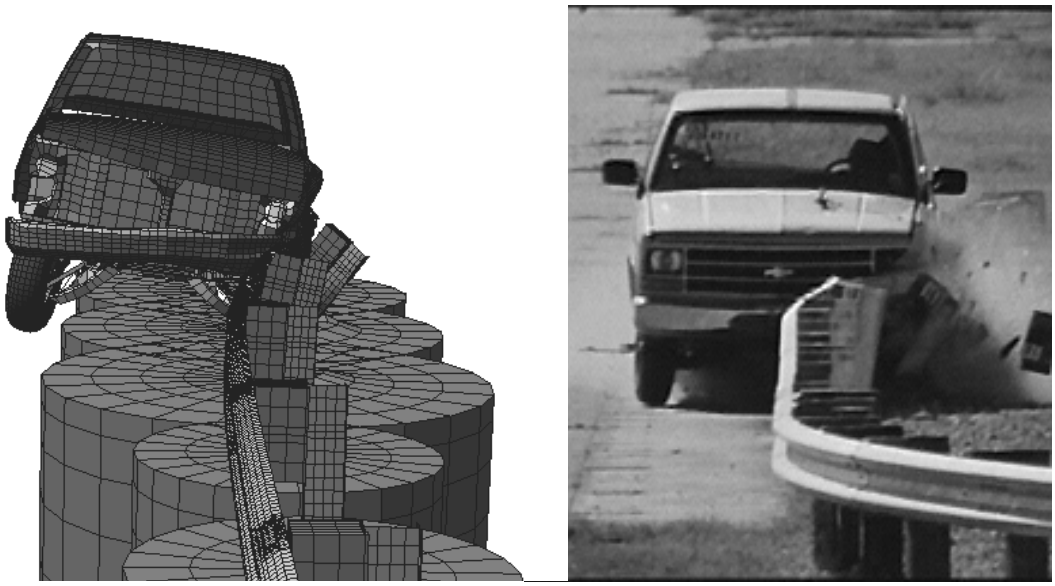

Figure 46. Side-by-Side Comparison of Numerical Simulation and Crash Test.

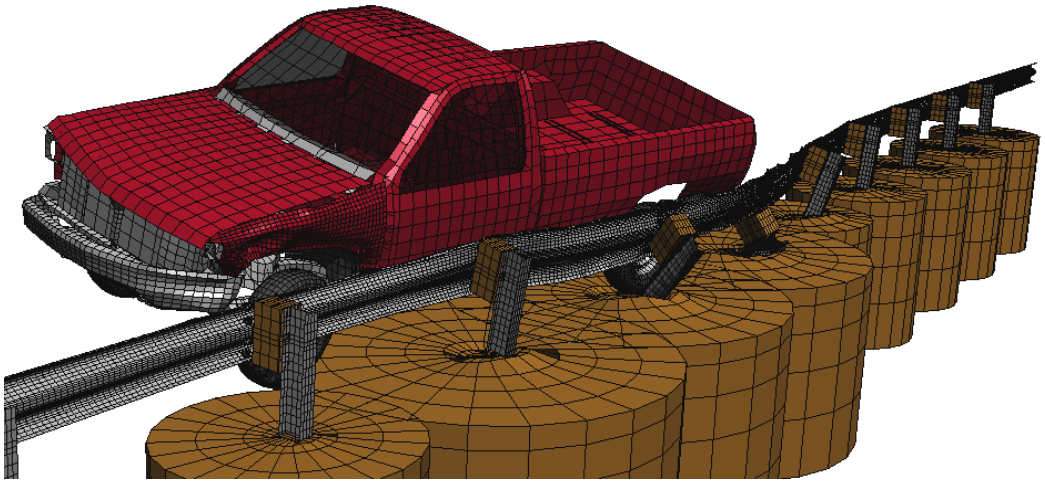

Figure 47. Vehicle Impacting G4(1S) Guardrail System.

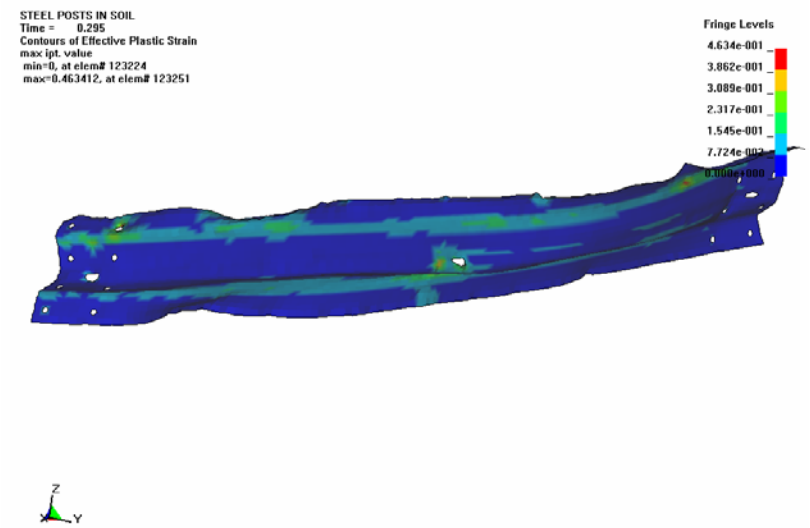

Figure 48. Contour of Plastic Strain in Rail Element – Soil Embedded System.

One difference between the experimental tests and numerical simulation is the separation of several blockouts from the steel posts. This separation occurs as the bolt is subjected to combined axial tension and bending moment when the vehicle pries the blockout away from the post. The threshold of the failure criterion for the bolt spring was decreased to account for this observation; however, the rigid bolt and nut were unable to capture this phenomenon. Because this failure only occurs on posts that have already separated from the guardrail, and it does not adversely affect the response of the vehicle in the tests, modeling the blockout failure is not viewed as essential to establishing fidelity of the numerical simulation.

6.2 PREDICTIVE SIMULATION USING LS-DYNA

With numerical simulation of the modified G4(1S) guardrail system demonstrating behavior that is typical of full-scale crash tests, the numerical model was used as a baseline model to construct other finite element models of mow strip guardrail system variations. Four numerical models of mow strip guardrail configurations were developed for use in predictive simulations to assess their ability to meet *NCHRP Report 350* criteria. These models include wood and steel post guardrail encased in a rigid concrete mow strip, and wood and steel post guardrail encased in a concrete mow strip with grout-filled leave-outs around the posts. The rigid concrete mow strip was selected because its use is widespread and it is believed to represent a worst-case scenario in regard to pavement-post confinement. Simulations of the concrete mow strips with grout-filled leave-outs were selected as viable candidates for full-scale crash testing.

6.2.1 Steel Post Guardrail in Rigid Concrete Mow Strip

To investigate the impact performance of a steel post guardrail completely encased in concrete or asphalt, a finite element model of a full-scale steel post guardrail system encased in a rigid mow strip was constructed (see Figure 49). This assumption is realistic given that relatively thick concrete and asphalt mow strip are often used in practice and no signs of distress in the asphalt mow strip were observed in some of the subcomponent testing.

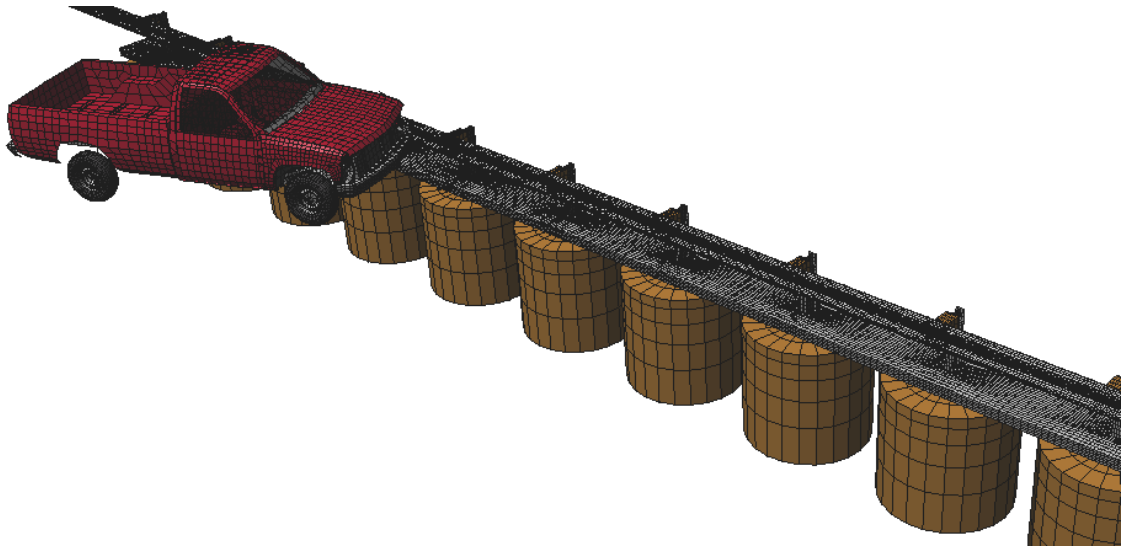

Figure 49. Initial Configuration of Steel Post Guardrail in Rigid Concrete Mow Strip.

The model consists of 90,492 elements and 95,031 nodes. On a two processor Dell Xeon workstation, 450 ms of impact time takes 135 CPU hours (67.5 clock hours) to simulate. The mesh of elements representing the concrete is the same mesh used in the subcomponent simulations described in Section 5. In addition, the same contact definitions and constraints used for the subcomponent simulations are used in the full-scale model.

As expected, the rigid concrete mow strip system produces a severe impact response. As shown in Figure 50, the rigid mow strip restricts the bases of the posts from deflecting. The severe post snagging that ensues destabilizes the vehicle, causing it to climb above the top of the rail. Figure 51 presents a comparison between the soil-embedded guardrail (i.e., modified G4(1S)) and the guardrail encased in a rigid mow strip at the same instant in time during the simulations. As seen in this figure, the soil-embedded guardrail system (Figure 51(a)) has stably redirected the vehicle, while the guardrail in rigid mow strip (Figure 51(b)) is overriding the rail in an unstable manner.

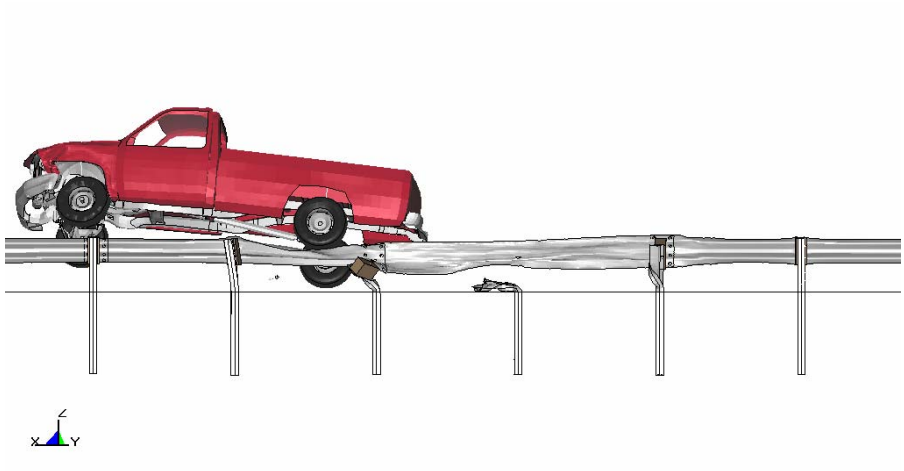

Figure 50. Vehicle Instability during Impact of Steel Post Guardrail in Rigid Mow Strip.

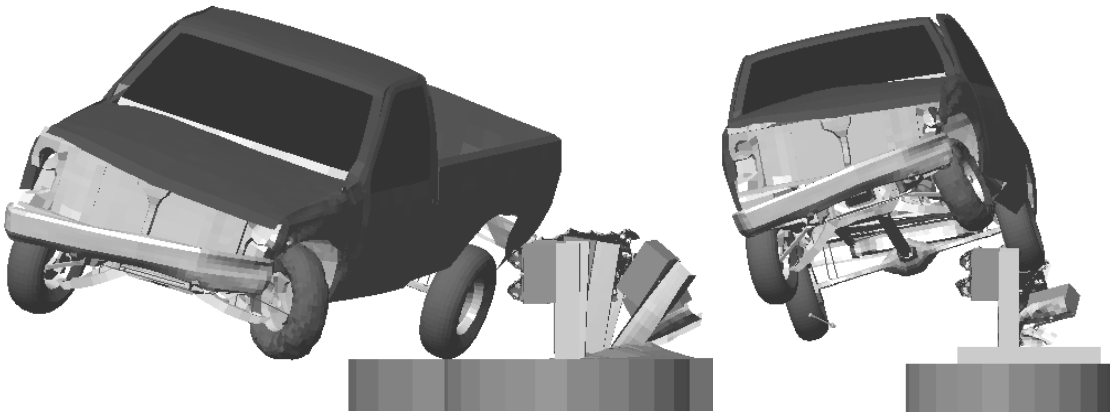

(a) (b)

Figure 51. Vehicle Model Response after Impact with Guardrail Systems: (a) Baseline Soil Embedment; (b) Rigid Concrete Mow Strip.

The lack of post rotation also causes increased stresses in the W-beam rail and increased deformation of the lower edge of the rail. As shown in Figure 52, the plastic strain contours in the rail, which are in excess of 30 percent over substantial portions of the rail, indicate a high probability of rail rupture. In summary, the results indicate that this system has a low probability of passing *NCHRP Report 350* evaluation criteria and the research team highly discourages its use.

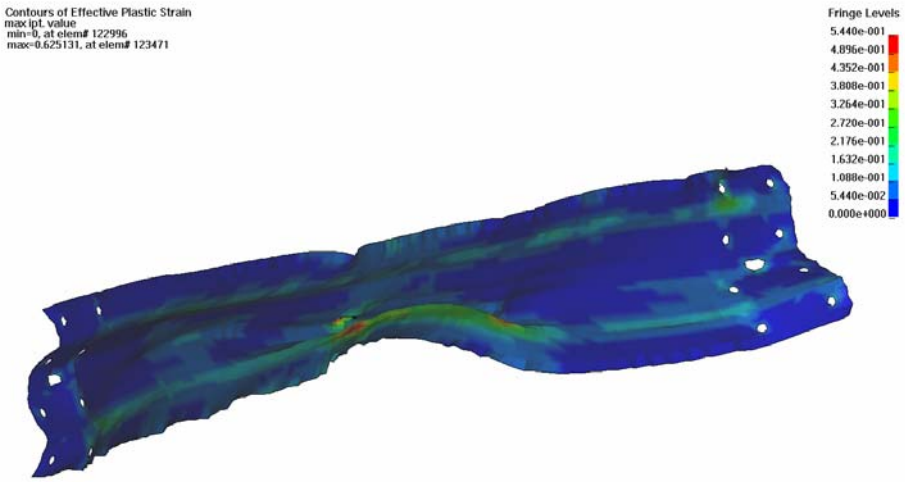

Figure 52. High Plastic Strains in W-beam Segment for Fully Rigid Mow Strip.

6.2.2 Wood Post Guardrail in Rigid Concrete Mow Strip

To investigate the impact performance of a wood post guardrail completely encased in concrete or asphalt, the researchers constructed a finite element model of a full-scale wood post guardrail system encased in a rigid mow strip. The model was similar in detail to the previously described steel post guardrail system but with the validated wood post model substituted for the steel posts. Again, the mow strip is assumed rigid to represent the critical case where no movement (rotation) of the post is allowed.

As shown in Figure 53, the constraint imposed by the rigid mow strip caused four wood posts to fracture during the impact. Because the posts fractured in advance of the vehicle, there was no snagging contact between the vehicle and the posts and, therefore, the vehicle remained relatively stable However, the loss of four posts did produce some pocketing of the vehicle in the rail system as evident in Figure 54. This pocketing behavior led to some kinking and high plastic strains along a cross-section of the rail located at the post at the downstream end of the pocket. These strains, shown in Figure 55, indicate a high probability of W-beam rupture at this post, particularly if it happens to coincide with a rail splice location. In summary, the results indicate that this system has a low probability of passing *NCHRP Report 350* evaluation criteria and the research team highly discourages it use.

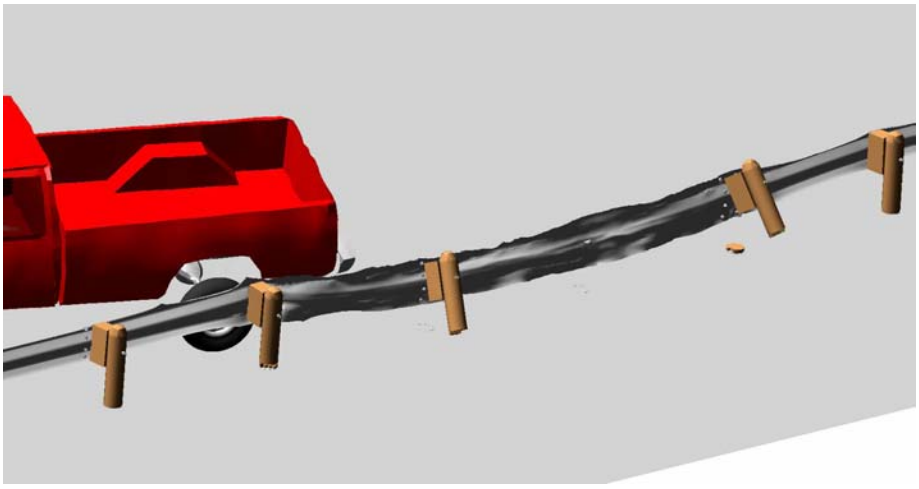

Figure 53. Fracture of Wood Posts due to Confinement in Rigid Mow Strip.

Figure 54. Vehicle Pocketing during Impact of Wood Post System in Rigid Mow Strip.

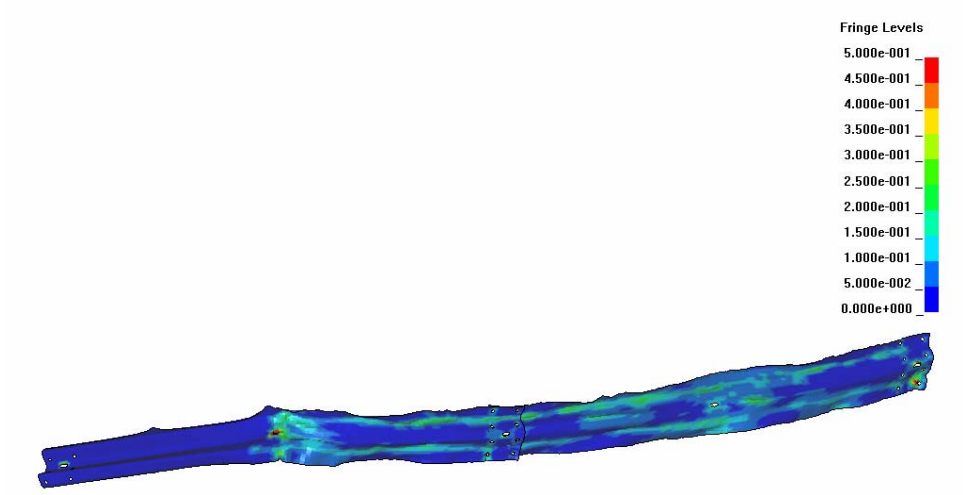

Figure 55. Plastic Strain Distributions for Wood Post System in Rigid Mow Strip.

6.2.3 Steel Post Guardrail in Concrete Mow Strip with Grout-filled Leave-outs

A finite element model of a steel post guardrail encased in concrete mow strip with grout-filled leave-outs was modeled and used in a predictive crash simulation to assess the ability of the system to meet *NCHRP Report 350* performance requirements (see Figure 56). The dimensions of the leave-outs were 457 mm × 457 mm (18 in. × 18 in.). The top 102 mm (4 in.) of the leave-out was backfilled with two-sack grout. The traffic face of the steel guardrail posts were offset 75 mm (3 in.) from the front edge of the leave-out. The same mesh, material models,

contact definitions, and constraints used in the subcomponent simulations of the grout leave-out configurations described in Section 5 were used in the full-scale system model. On a four processor Compaq Alpha ES40, 600 ms of impact time takes 305 CPU hours (76 clock hours) to simulate.

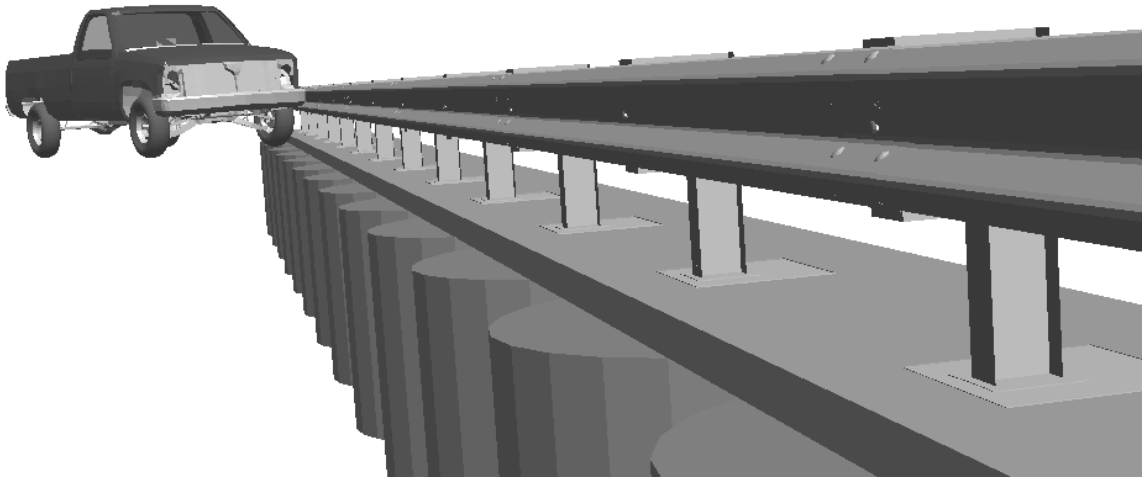

Figure 56. Initial Configuration for Steel Post Guardrail System in Concrete Mow Strip with Grout-filled Leave-outs.

As shown in Figure 57, the steel posts are able to rotate and deflect within the mow strip due to the failure of the weak grout backfill material inside the leave-outs. The post movement mitigated the severe vehicle-post snagging observed in the rigid mow strip simulation. Consequently, the vehicle is redirected in much smoother manner without significant climb or roll. Two posts disengage from the rail, and some were deflected and twisted in a manner reminiscent of soil-embedded steel posts. Plastic strain contours of the rail, shown in Figure 58, indicate localized concentrations of high strain around bolts slots and moderate plastic strain throughout the remainder of the rail segment. This indicates that rupture in the rail segment is not probable and only a few small tears around the slots are likely to develop.

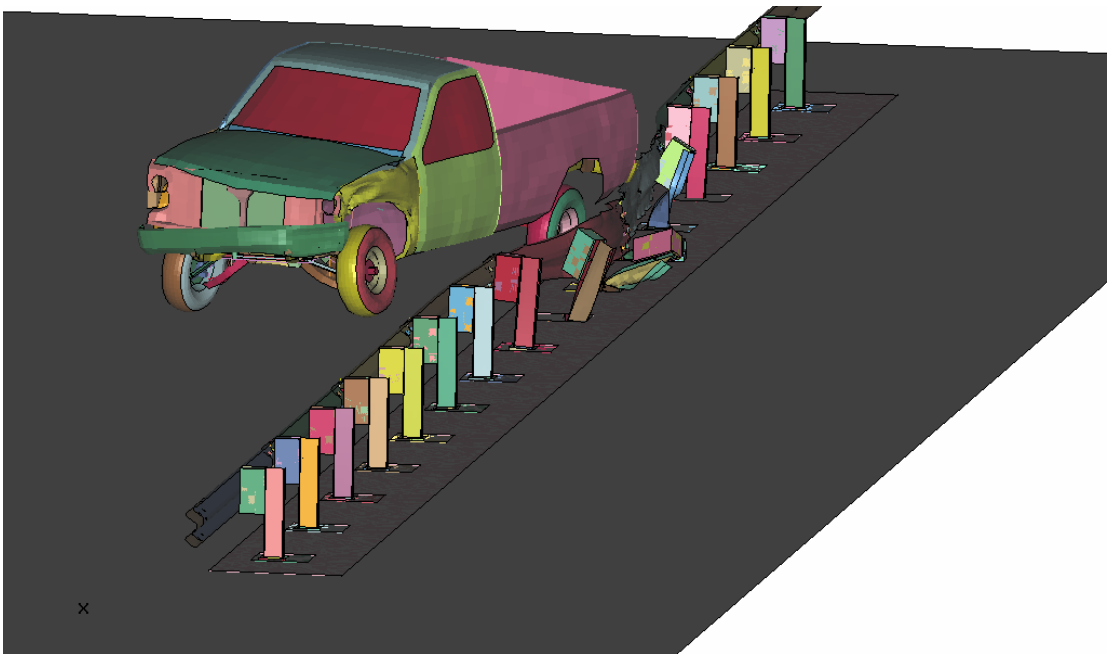

Figure 57. Simulation of Steel Post Guardrail System in Concrete Mow Strip with Grout-filled Leave-outs.

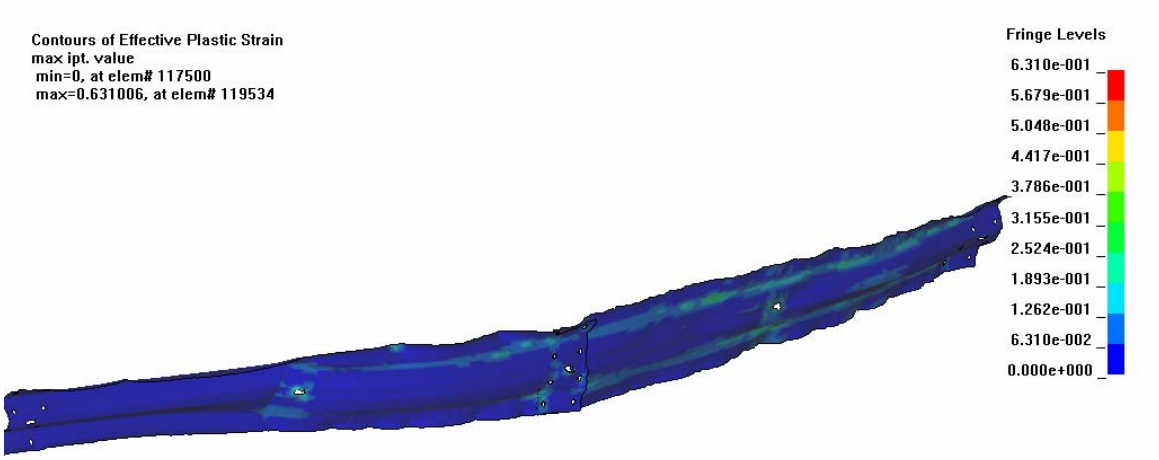

Figure 58. Contour of Maximum Plastic Strain for Steel Post Guardrail in Concrete Mow Strip with Grout-filled Leave-outs.

The numerical simulation shows that the grout-filled leave-outs provide significant improvement in impact performance over direct concrete embedment. The post snagging is still more severe than for the soil embedded system, but the vehicle is much more stable and the rail stresses and strains are within acceptable levels. The steel post guardrail system encased in

concrete mow strip with grout-filled leave-outs is considered to have a high probability of passing *NCHRP Report 350*.

6.2.4 Wood Post Guardrail in Concrete Mow Strip with Grout-filled Leave-outs

To investigate the *NCHRP Report 350* compliance of a wood post guardrail system encased in concrete mow strip with grout-filled leave-outs, a full-scale finite element model of the system was constructed (see Figure 59). The model was similar in detail to the previously described steel post guardrail system with grout-filled leave-outs, but with the validated wood post model substituted for the steel posts.

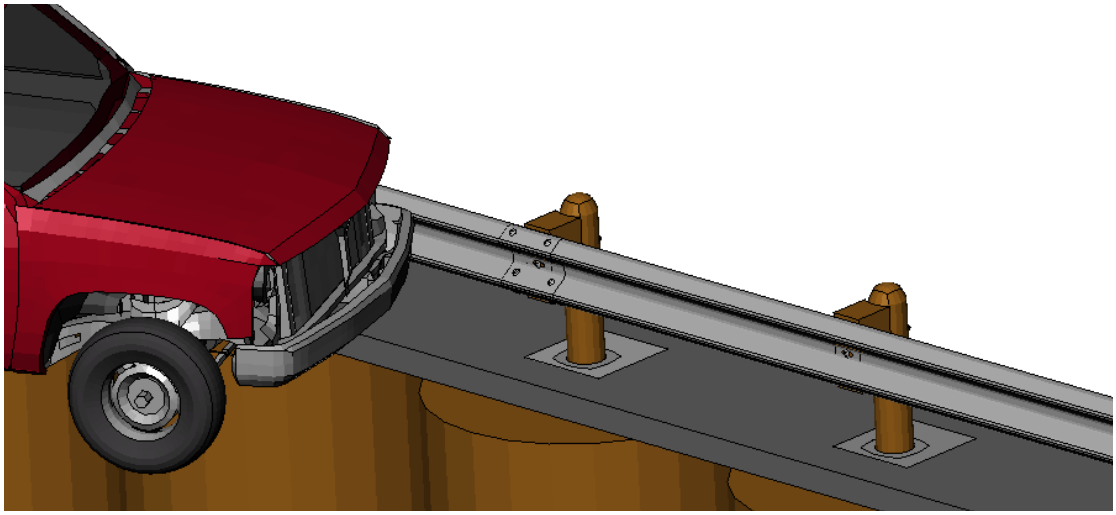

Figure 59. Finite Element Model of Wood Post Guardrail System Encased in Concrete Mow Strip with Grout-filled Leave-outs.

As shown in Figure 60, the wood posts are able to rotate and deflect within the mow strip due to the failure of the weak grout backfill material inside the leave-outs. Compared to the wood post system in rigid mow strip, the number of fractured wood posts was reduced from four to two. Further, these two posts fractured on the back edge of their leave-outs after dissipating a significant amount of energy by rotating through the soil. Consequently, the pocketing pattern did not develop in the rail, and the vehicle was redirected in a relatively smooth and stable manner.

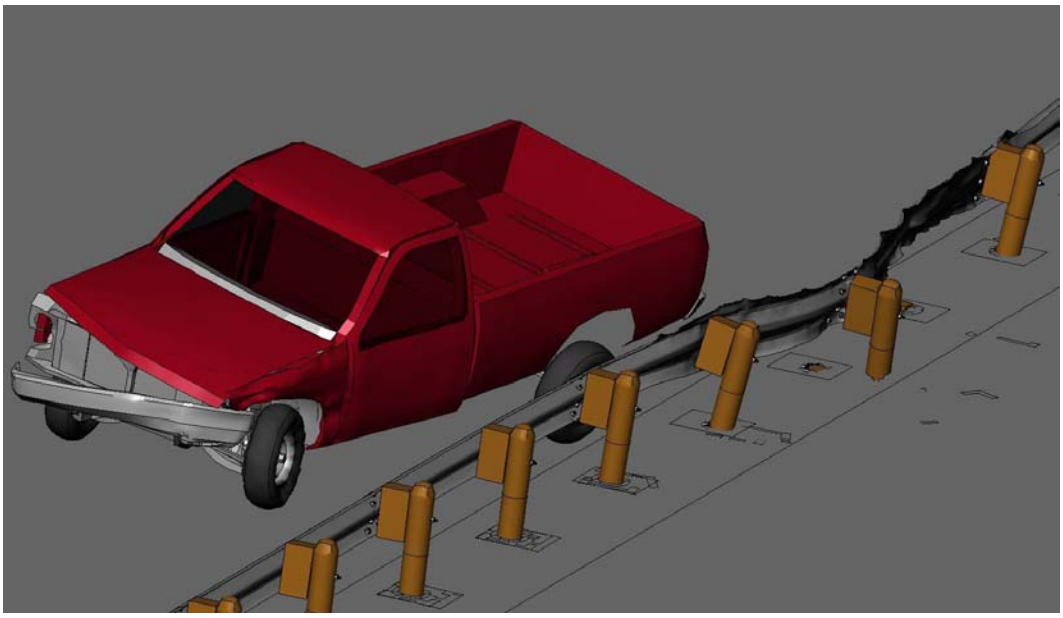

Figure 60. Vehicle Exit Where Three Wood Posts Are Broken.

Plastic strain contour shown in Figure 61 indicates localized concentrations of high strain around bolts slots and moderate plastic strain throughout the rail segment. This indicates that rupture in the rail segment is not likely and only few tears around the slots are likely to develop.

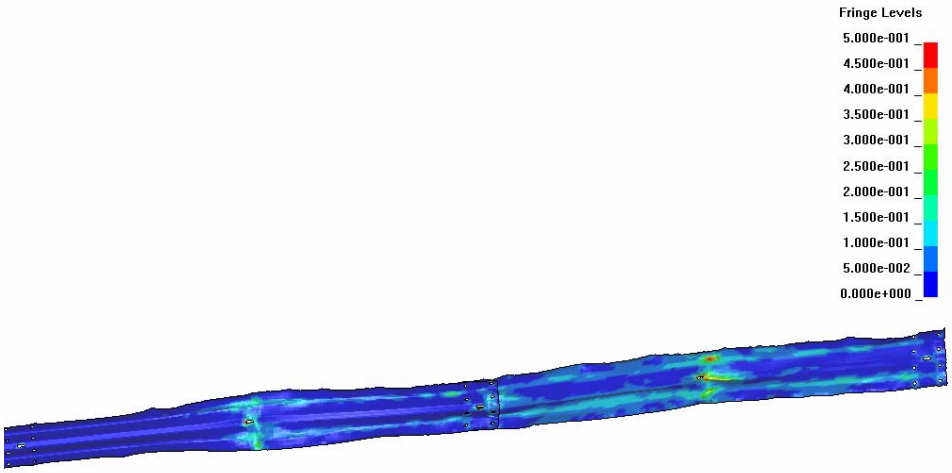

Figure 61. Plastic Strain Distributions for Wood Post System in Grout.

6.2.5 Expected Damage to Mow Strip

One important factor for judging maintenance performance of a guardrail system in mow strip is the amount of damage to the mow strip from an impact. The full-scale simulations of the

guardrail systems encased in mow strip with grout-filled leave-outs indicated that two or three posts in the impact region would contact the back edge of the leave-outs. Because the concrete mow strip was modeled as rigid, the extent of damage to the mow strip (if any) cannot be directly obtained. However, using the contact forces generated between the posts and the back edge of the leave-out, some engineering estimates can be made.

The most critical mow strip configuration from a damage perspective is a steel post encased in a concrete mow strip with square or rectangular leave-outs. Based on the results of subcomponent testing, an asphalt mow strip is not likely to incur damage. For wood post systems, the contact forces with the back edge of the leave-out are limited by the flexural strength of the post. Circular-shaped leave-outs remove the stress concentrations that exist at the corners of a square leave-out.

Using the simulation contact forces between the most severely deformed steel post and the concrete at the back edge of the leave-out, the maximum expected impact force is approximately 200 kN (45 kips). The shear strength of the concrete is calculated using the formula:

$$V_c = 4\sqrt{f_c'}A_s \qquad (4)$$

where f'_c is the compressive strength of concrete, A_s is the area of concrete in shear assuming 45 degree shear planes, and V_c is the shear strength of the concrete. *(36)* Two shear planes are assumed to radiate outward at 45 degrees from the corners of the square leave-out section. Using the ACI formula, the shear strength of the 381 mm (15 in.) deep, 127 mm (5 in.) thick concrete layer behind the back of the leave-out is 169 kN (38 kips). Using these approximations, it is possible that some damage to the concrete may occur during a design impact event.

If it is desirable to further reduce the probability of concrete damage during severe impacts, several approaches can be used. These include increasing the width of the mow strip behind the leave-out, using a circular leave-out section, increasing the level of reinforcement in the mow strip, and increasing the concrete strength. None of these options should have an adverse effect on impact performance.

7. FULL-SCALE CRASH TESTING

Based on the results of the predictive impact simulations, the research team selected two mow strip configurations for full-scale crash testing to verify their compliance with *NCHRP Report 350*: a strong steel post W-beam guardrail and strong wood post W-beam guardrail encased in a concrete mow strip with grout-filled leave-outs around the posts. Details of this testing are presented below.

7.1 TEST FACILITY

The tests were conducted at the Texas Transportation Institute's Proving Grounds. The test facilities at the Proving Grounds consist of an 809 hectare (2000 acre) complex of research and training facilities situated 16 km (10 miles) northwest of the main campus of Texas A&M University. The site, formerly an Air Force Base, has large expanses of concrete runways and parking aprons well suited for experimental research and testing of roadside safety hardware. The site selected for construction of the guardrail-mow strip test installations was along a wide out-of-service apron. The apron consists of an unreinforced jointed concrete pavement in 3.8 m × 4.6 m (12.5 ft × 15 ft) blocks nominally 203305 mm (812 in.) deep. The apron is about 50 years old and the joints have some displacement, but are otherwise flat and level.

7.2 CRASH TEST CONDITIONS

NCHRP Report 350 recommends two tests for Test Level 3 evaluation of longitudinal barriers:

> ***NCHRP Report 350* test designation 3-10:** This test involves an 820 kg (1806 lb) passenger car impacting the critical impact point (CIP) in the length of need (LON) of the longitudinal barrier at a nominal speed and angle of 100 km/h (62 mph) and 20 degrees. The purpose of this test is to evaluate the overall performance of the LON section in general and occupant risks in particular.
>
> ***NCHRP Report 350* test designation 3-11:** This test involves a 2000 kg (4405 lb) pickup truck impacting the CIP in the LON of the longitudinal barrier at a nominal speed and angle of 62 mph (100 km/h) and 25 degrees. The test is

intended to evaluate the strength of the section for containing and redirecting the pickup truck.

Both crash tests conducted under this study correspond to *NCHRP Report 350* test designation 3-11. Test 3-11 is believed to be the critical test for evaluating guardrail encased in mow strip because of the large impact loads and large deflections that must be accommodated.

The crash test and data analysis procedures followed under this study were in accordance with guidelines presented in *NCHRP Report 350*. Appendix C presents brief descriptions of these procedures.

7.3 EVALUATION CRITERIA

The performance evaluation of the guardrail in mow strip configurations met with *NCHRP Report 350* specifications. As stated in *NCHRP Report 350*, "Safety performance of a highway appurtenance cannot be measured directly but can be judged on the basis of three factors: structural adequacy, occupant risk, and vehicle trajectory after collision." Accordingly, researchers used the safety evaluation criteria from Table 5.1 of *NCHRP Report 350* to evaluate the crash tests reported herein.

7.4 STEEL POST W-BEAM GUARDRAIL CRASH TEST

7.4.1 Test Article

The first crash test was performed on a W-beam guardrail mounted on W150×13 (W6×9) steel posts that were encased in a concrete mow strip with grout-filled leave-outs. The W150×13 (W6×9) steel posts were placed in 457 mm (18 in.) diameter holes to a depth of 1.1 m (3.6 ft). The void surrounding the post was backfilled with *Report 350* standard soil that was compacted in 152 mm (6 in.) lifts through hand-tamping. The spacing of the posts was 1.9 m (6 ft-3 in.). A 12-gage W-beam guardrail was mounted to the posts at a height of 686 mm (27 in.) to the top of the rail. The rail was offset from the posts using 356 mm (14-in.) long, 203 mm (8-in.) deep routed wood blockouts.

A concrete mow strip was formed and placed adjacent to the test apron along the guardrail length of need. The mow strip was 30.5 m (100 ft) long, 1.1 m (3 ft-6 in.) wide, and

128 mm (5 in.) thick. It was constructed using TxDOT Class B riprap concrete with a minimum 28-day a compressive strength of 14 MPa (2031 psi). To help avoid shrinkage cracking and separation of the mow strip from the adjacent test apron, a single layer of W6×W6 welded wire fabric was used to reinforce the concrete mow strip.

Leave-out sections, 457 mm × 457 mm (18 in. × 18 in.), were formed around the guardrail posts. The traffic face of the posts was offset 3 in. from the front edge of the leave-out. The top 102 mm (4 in.) of the leave-out was backfilled with a two-sack grout mixture with a 28-day compressive strength of approximately 0.85 MPa (120 psi).

An 11.4 m (37.5 ft) LET end terminal was placed on each end of the guardrail in the mow strip to anchor the system, making the total length of the test installation 53.3 m (175 ft). Figure 62 shows additional details of the test installation. Figure 63 shows photos of the completed test installation.

7.4.2 Test Vehicle

A 1997 Chevrolet 2500 pickup truck, shown in Figures 64 and 65, was used for the crash test. Test inertia mass of the vehicle was 2045 kg (4524 lb), and its gross static mass was 2045 kg (4524 lb). The height to the lower edge of the vehicle bumper was 390 mm (15.4 in.), and the height to the upper edge of the bumper was 670 mm (26.4 in.). Additional dimensions and information on the vehicle are given in Appendix D, Figure 80. The vehicle was directed into the installation using a cable reverse tow and guidance system, and was released to be free-wheeling and unrestrained just prior to impact.

7.4.3 Soil and Weather Conditions

The test was performed on the morning of June 26, 2002. No rainfall occurred during the 10 days prior to the test. Moisture content of the *NCHRP Report 350* soil in which the device was installed was 5.8 percent. Weather conditions at the time of testing were as follows: Wind speed: 4 km/h (2 mph); Wind direction: 320 degrees with respect to the vehicle (vehicle was traveling in a southwesterly direction); Temperature: 31°C (88°F); Relative humidity: 67 percent.

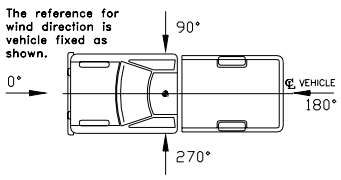

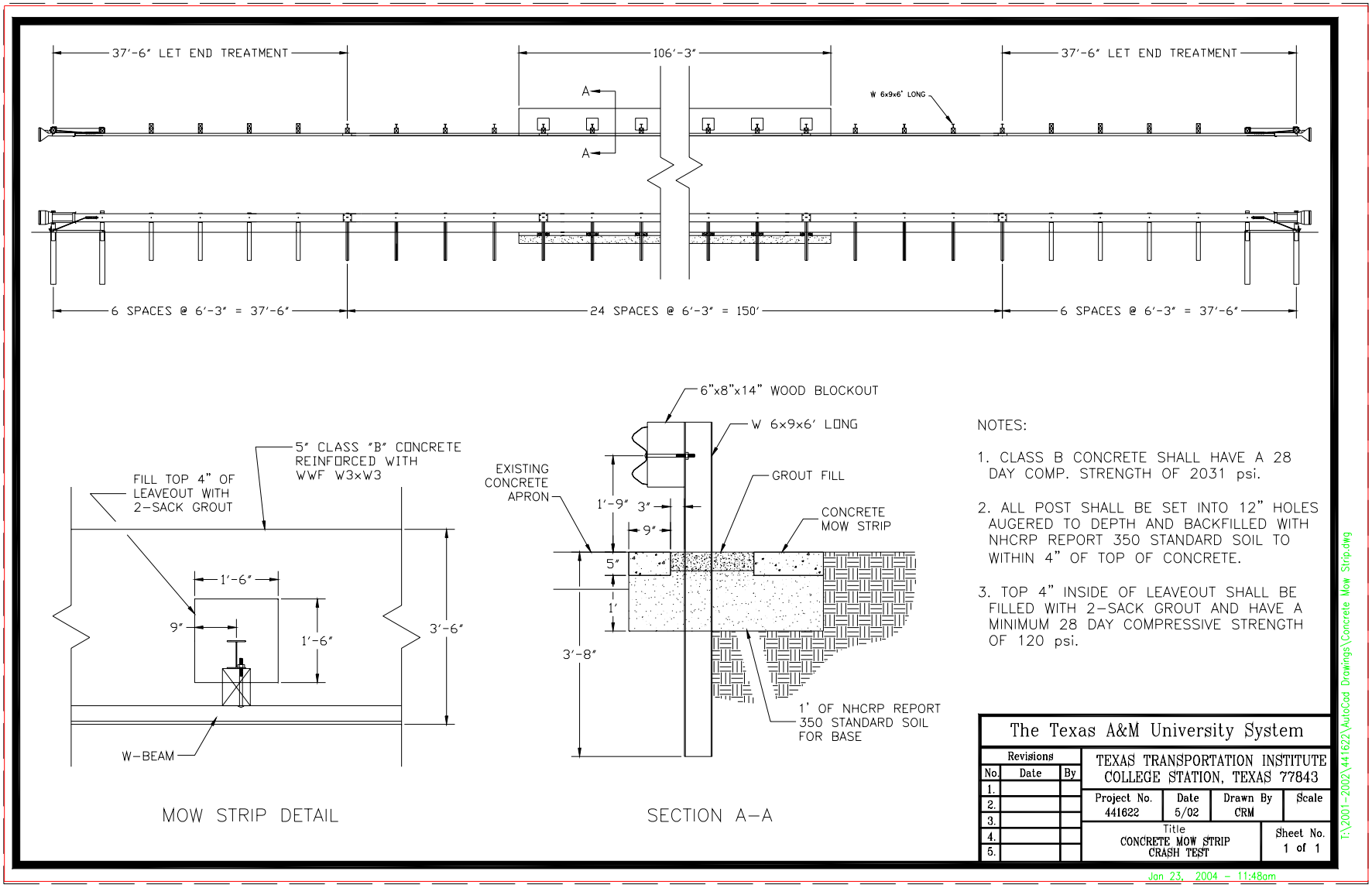

Figure 62. Details of the Steel Post Guardrail in Mow Strip Installation.

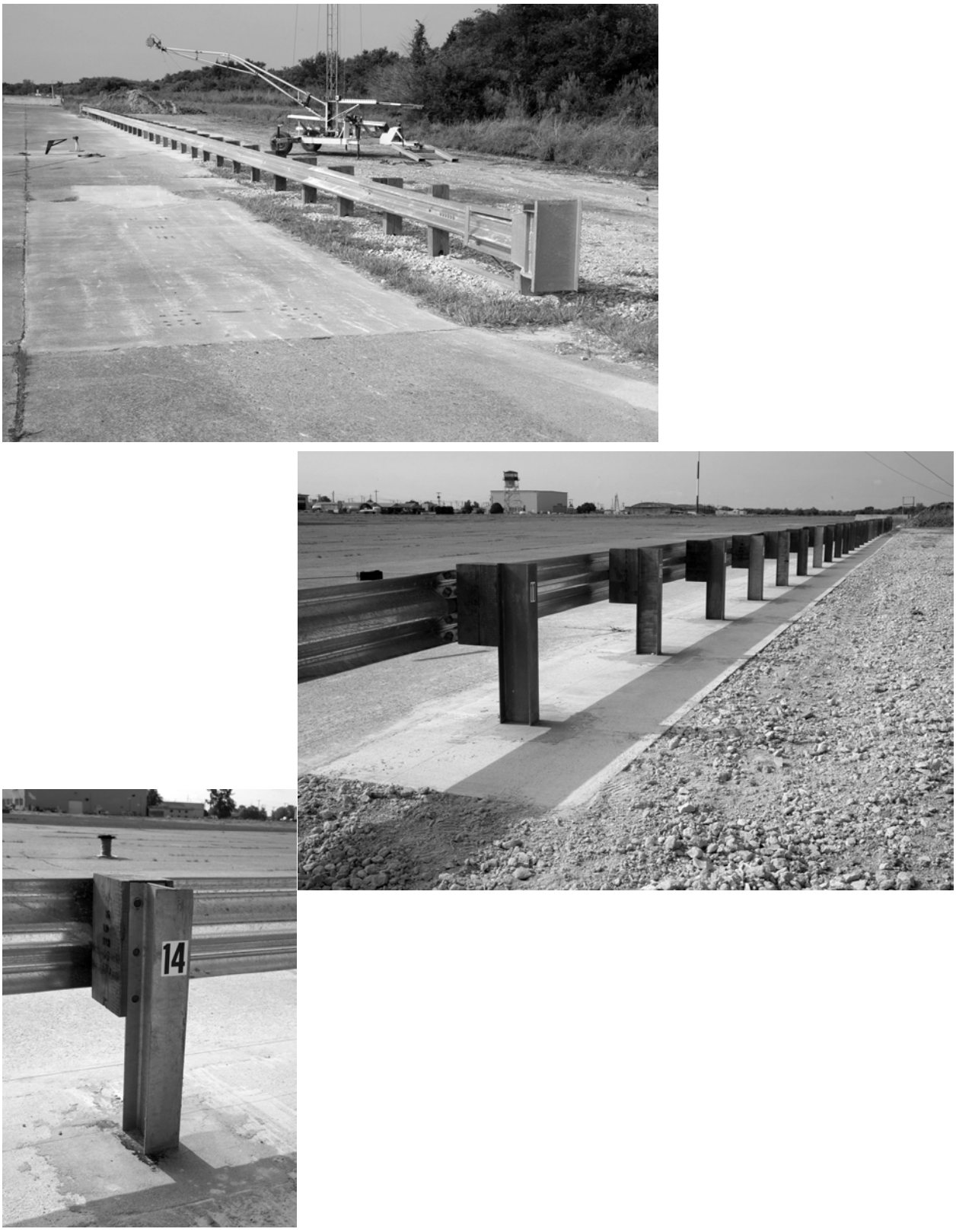

Figure 63. Mow Strip Installation before Test 441622-1.

Figure 64. Vehicle/Installation Geometrics for Test 441622-1.

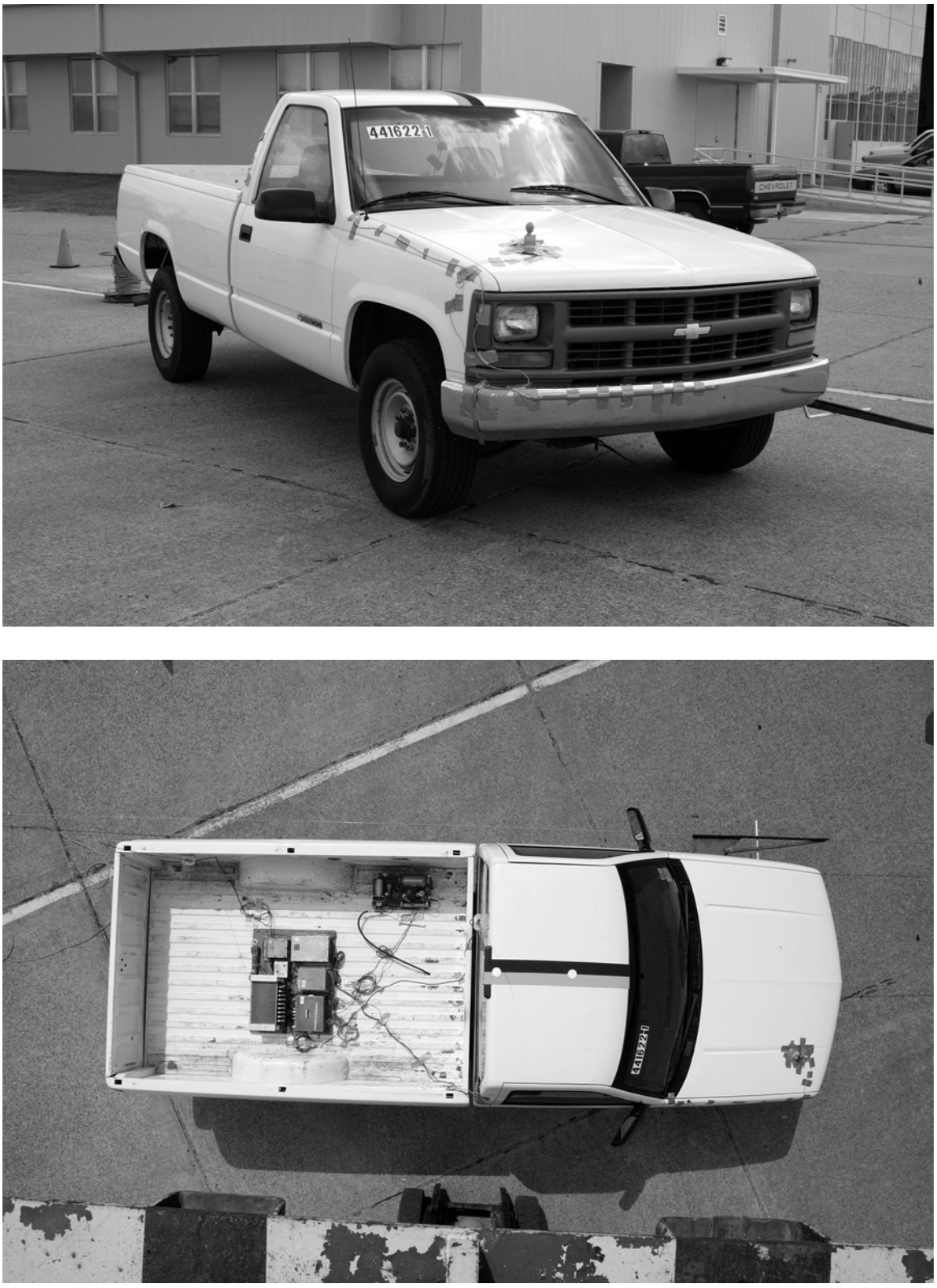

Figure 65. Vehicle before Test 441622-1.

7.4.4 Test Description

The vehicle, traveling at a speed of 99.7 km/h (62.0 mph), impacted the guardrail 0.68 m (2.2 ft) upstream of post 13 at an impact angle of 25.4 degrees. Shortly after impact, post 13 began to deflect toward the field side, and at 0.027 s the vehicle began to redirect. Post 14 began to deflect toward the field side at 0.056 s, and the right front tire contacted post 14 at 0.080 s. At 0.091 s, the W-beam rail element separated from post 14, and at 0.096 s post 15 began to deflect toward the field side. The blockouts detached from post 14 and post 15 at 0.143 s and 0.194 s, respectively. At 0.305 s, the vehicle was traveling parallel with the guardrail at a speed of 53.8 km/h (33.4 mph). The vehicle lost contact with the guardrail at 0.548 s at a speed of 53.6 km/h (33.3 mph) and an exit angle of 15.4 degrees. Brakes on the vehicle were applied 1.5 s after impact. The vehicle subsequently came to rest 43.5 m (142.6 ft) downstream of impact and 19.1 m (62.6 ft) forward of the traffic face of the rail. Sequential photographs of the test period are shown in Appendix E, Figures 82 and 83.

7.4.5 Damage to Test Installation

Damage to the guardrail and mow strip installation is shown in Figures 66 and 67. The grout around posts 11 through 17 was either cracked or broken up, and the mow strip pad was slightly disturbed. Posts 11 and 12 were disturbed, post 13 was deflected toward the field side 45 mm (1.8 in.) (measured at ground level), and posts 14 and 15 were rotated and deflected toward the field side 57 mm and 60 mm (2.2 in. and 2.4 in.), respectively. Post 16 was deformed, rotated, and deflected toward the field side 84 mm (3.3 in.). The blockouts at posts 14 and 15 were detached from the posts and rail with one coming to rest 5.7 m (18.7 ft) behind the rail between posts 17 and 18 and the other 13.7 m (44.9 ft) behind post 21. The rail mounting bolt pulled out of the rail at post 17, and the post was deflected toward the field side 5 mm (0.2 in.). The W-beam rail element was torn on the lower edge from the downstream end of the splice at post 15 and extended over a distance of 1.5 m (4.9 ft). On the upstream terminal, post 1 moved longitudinally 32 mm (1.25 in.), and posts 3 and 4 were split along the longitudinal axis. No movement or damage was noted on the downstream terminal. Maximum dynamic deflection during the test was 0.58 m (1.90 ft), and maximum permanent deformation after the test was 0.34 m (1.1 ft).

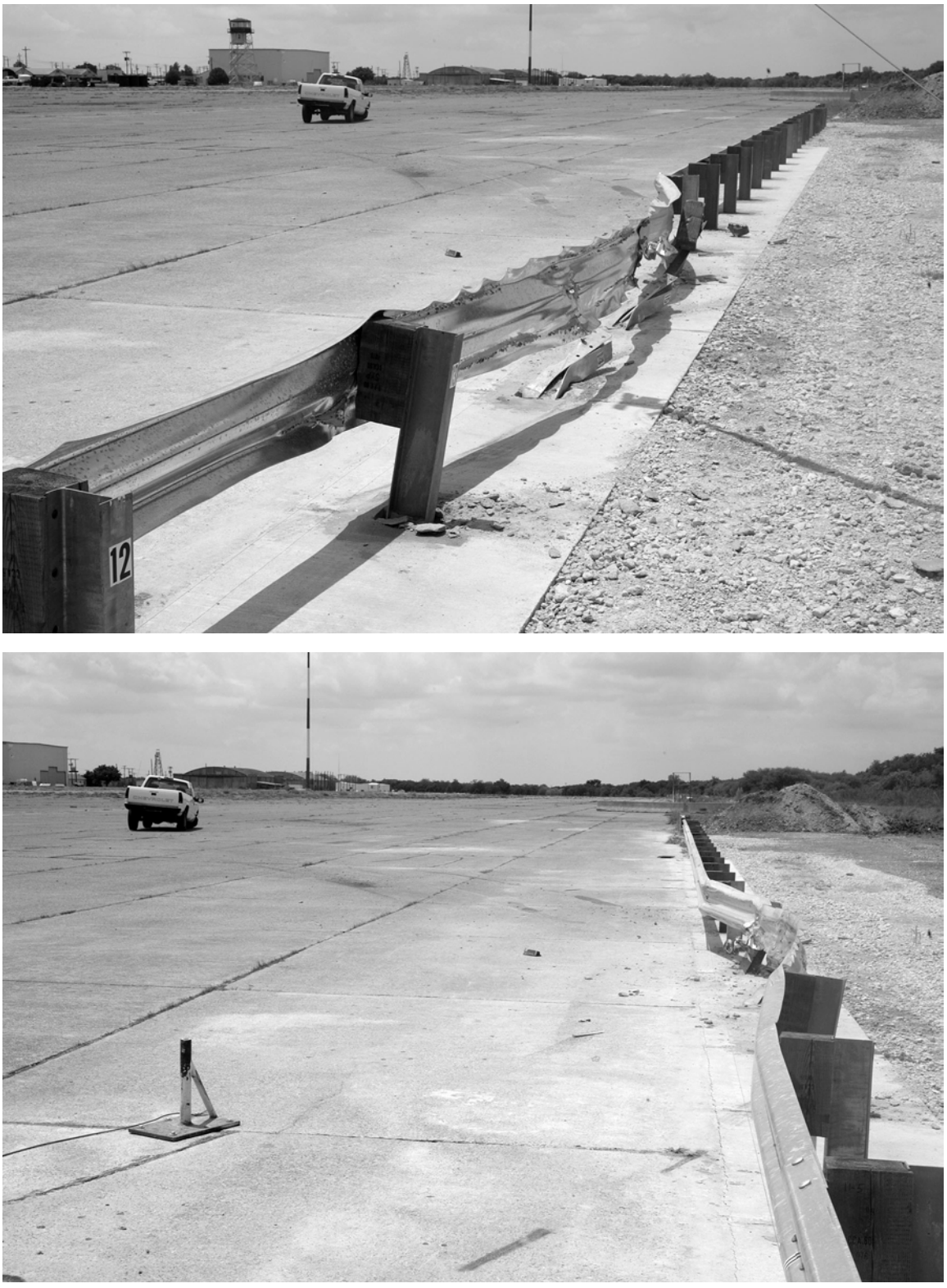

Figure 66. After Impact Trajectory for Test 441622-1.

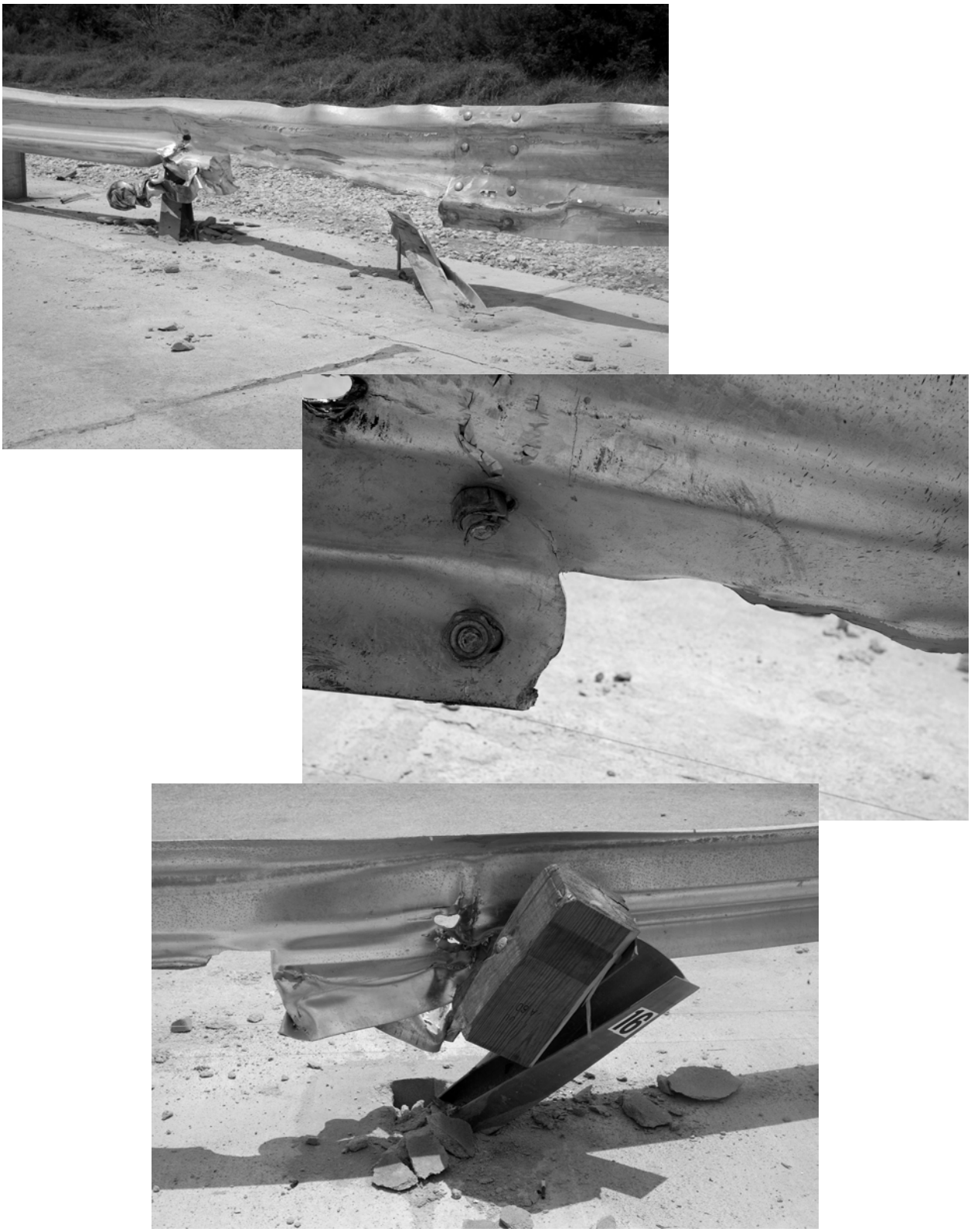

Figure 67. Installation after Test 441622-1.

7.4.6 Vehicle Damage

Structural damage was imparted to the right upper and lower A-arms, right side ball joints and rod ends, the stabilizer bar, and the right front frame member of the vehicle. Also damaged were the front bumper, radiator, fan, right front quarter panel, right door, and right front tire and wheel (see Figure 68). Maximum exterior crush sustained by the vehicle was 410 mm (16.1 in.) in the frontal plane near the right front corner at bumper height, and 350 mm (13.8 in.) in the side plane at the right front corner at 700 mm (27.6 in.) above the ground. Maximum occupant compartment deformation was 20 mm (0.8 in.) in the center front floor pan area over the transmission tunnel. Photographs of the interior of the vehicle are shown in Figure 69. Exterior crush measurements and occupant compartment deformation are shown in Appendix D, Tables 10 and 11.

7.4.7 Occupant Risk Factors

Data from the triaxial accelerometer located at the vehicle center of gravity were digitized to compute occupant impact velocity and ridedown accelerations. Only the occupant impact velocity and ridedown accelerations in the longitudinal axis direction are required from these data for evaluation of criterion L of *NCHRP Report 350*. In the longitudinal direction, occupant impact velocity was 5.7 m/s (18.7 ft/s) at 0.146 s, maximum 0.010-s ridedown acceleration was 14.6 g's from 0.340 to 0.350 s, and the maximum 0.050-s average was –6.6 g's between 0.272 and 0.322 s. In the lateral direction, the occupant impact velocity was 4.5 m/s (14.8 ft/s) at 0.146 s, the highest 0.010-s occupant ridedown acceleration was –9.1 g's from 0.323 to 0.333 s, and the maximum 0.050-s average was –4.8 g's between 0.178 and 0.228 s. These data and other information pertinent to the test are presented in Figure 70. Vehicle angular displacements and accelerations versus time traces are shown in Appendix F, Figures 85 through 91.

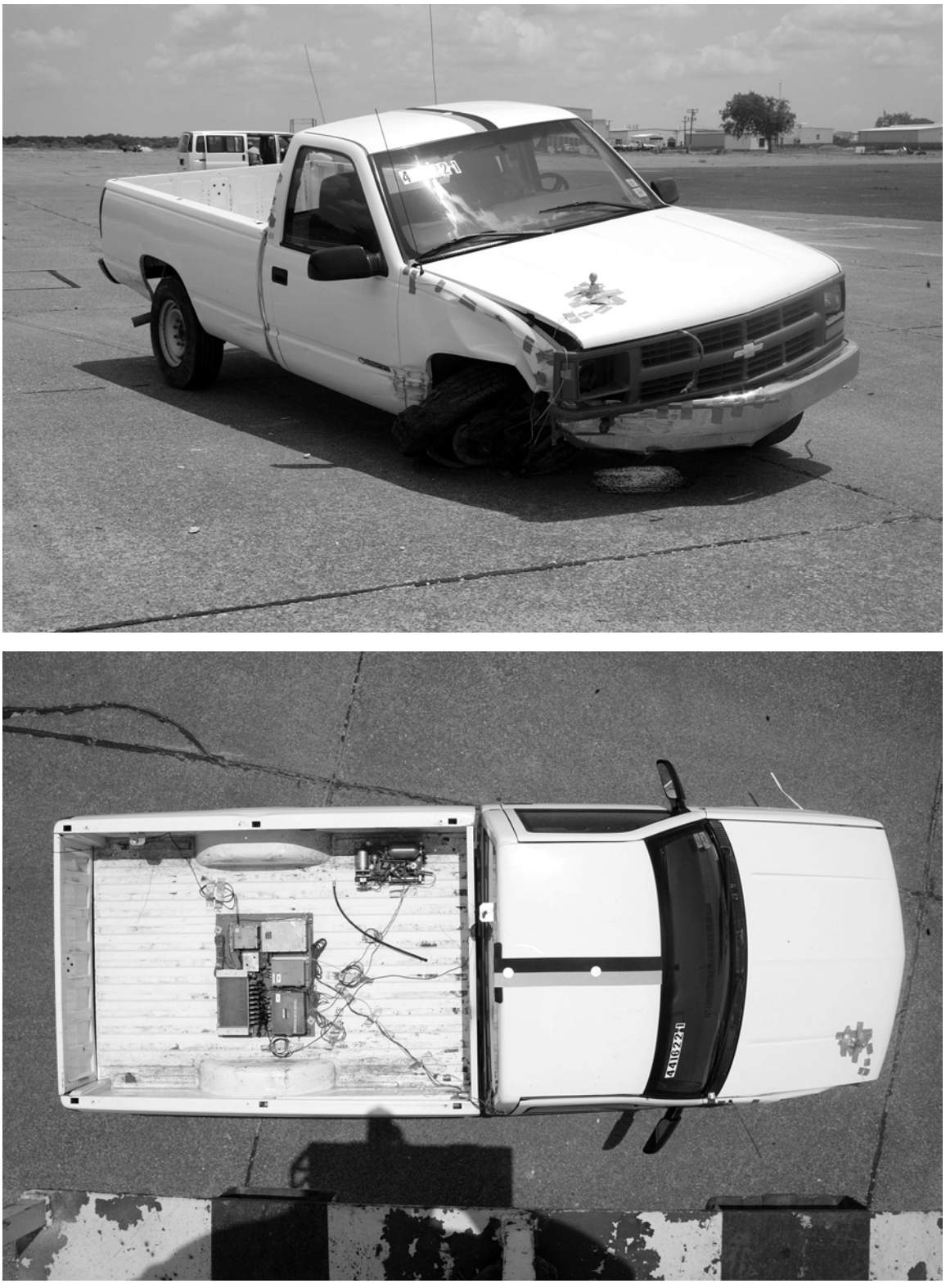

Figure 68. Vehicle after Test 441622-1.

Before test

After test

Figure 69. Interior of Vehicle for Test 441622-1.

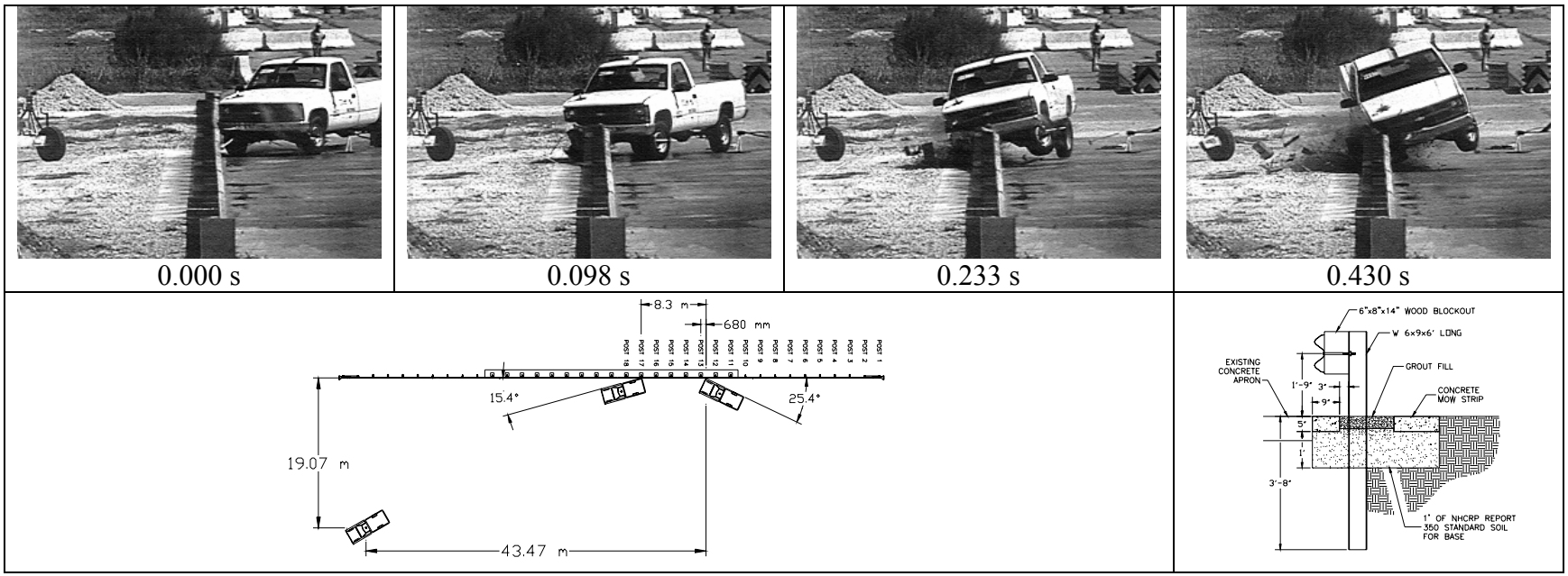

General Information	
Test Agency	Texas Transportation Institute
Test No.	441622-1
Date	06-26-2002
Test Article	
Type	Guardrail
Name	Mod. G4(1S) on Concrete Mow Strip
Installation Length	225 ft (68.6 m)
Material or Key Elements	W-Beam on Steel Posts with Wood Blockouts in Concrete Mow Strip
Soil Type and Condition	Std Soil w/Concrete Mow Strip, Dry
Test Vehicle	
Type	Production
Designation	2000P
Model	1997 Chevrolet 2500
Mass	
Curb	2131 kg (4694 lb)
Test Inertial	2045 kg (4504 lb)
Dummy	No Dummy
Gross Static	2045 kg (4504 lb)

Impact Conditions	
Speed (km/h (mph))	99.7 (62.0)
Angle	25.4
Exit Conditions	
Speed (km/h (mph))	53.6 (33.3)
Angle	15.4
Occupant Risk Values	
Impact Velocity (m/s (ft/s))	
Longitudinal	5.7 (18.7)
Lateral	4.5 (14.8)
THIV (km/h)	24.7
Ridedown Accelerations (g's)	
Longitudinal	-14.6
Lateral	-9.1
PHD (g's)	15.1
ASI	0.69
Max. 0.050-s Average (g's)	
Longitudinal	-6.6
Lateral	-4.8
Vertical	-3.3

Test Article Deflections (mm (in))	
Dynamic	584 (23.0)
Permanent	84 (3.3)
Working Width	1046 (41.2)
Vehicle Damage	
Exterior	
VDS	01RFQ4
CDC	01FYEW3
Maximum Exterior Vehicle Crush	410 mm (16.1 in.)
Interior	
OCDI	FS0000100
Maximum Occupant Compartment. Deformation	20 mm (0.8 in.)
Post-Impact Behavior	
(during 1.0 sec after impact)	
Max. Yaw Angel (deg)	-79.6
Max. Pitch Angle (deg)	-13.9
Max. Roll Angle (deg)	22.2

Figure 70. Summary of Results for Test 441622-1, *NCHRP Report 350* Test 3-11.

7.4.8 Assessment of Test Results

An assessment of the test based on the applicable *NCHRP Report 350* safety evaluation criteria is provided below.

Structural Adequacy

A. Test article should contain and redirect the vehicle; the vehicle should not penetrate, underride, or override the installation although controlled lateral deflection of the test article is acceptable.

Results: The W-beam guardrail with steel posts in mow strip contained and redirected the pickup truck. The vehicle did not penetrate, underride, or override the guardrail. Maximum dynamic deflection was 0.58 m (1.90 ft). *(Pass)*

Occupant Risk

D. Detached elements, fragments, or other debris from the test article should not penetrate or show potential for penetrating the occupant compartment, or present an undue hazard to other traffic, pedestrians, or personnel in a work zone. Deformation of, or intrusions into, the occupant compartment that could cause serious injuries should not be permitted.

Results: Two blockouts became detached from the posts and were thrown behind the guardrail. These blockouts did not penetrate nor show potential for penetrating the occupant compartment. As these blockouts remained behind the guardrail, they did not present undue hazard to others in the area. Maximum occupant compartment deformation was 20 mm (0.8 in.). *(Pass)*

F. The vehicle should remain upright during and after collision although moderate roll, pitching, and yawing are acceptable.

Results: The 2045 kg (4504 lb) pickup truck remained upright during and after the collision event. *(Pass)*

Vehicle Trajectory

K. After collision, it is preferable that the vehicle's trajectory not intrude into adjacent traffic lanes.

Results: The pickup truck came to rest 43.47 m (142.61 ft) downstream of impact and 19.07 m (62.56 ft) forward of the traffic face of the rail. *(Fail)*

L. The occupant impact velocity in the longitudinal direction should not exceed 12 m/s and the occupant ridedown acceleration in the longitudinal direction should not exceed 20 g's.

Results: Longitudinal occupant impact velocity was 5.7 m/s (18.7 ft/s) and longitudinal occupant ridedown acceleration was 14.6 g's. *(Pass)*

M. The exit angle from the test article preferably should be less than 60 percent of the test impact angle, measured at time of vehicle loss of contact with the test device.

Results: Exit angle at loss of contact was 15.4 degrees, which was 61 percent of the impact angle. *(Marginal)*

The following supplemental evaluation factors and terminology, as presented in the FHWA memo entitled "Action: Identifying Acceptable Highway Safety Features," were used for visual assessment of test results. *(37)* Factors underlined pertain to the test reported herein.

Passenger Compartment Intrusion

1. *Windshield Intrusion*
   - *a. No windshield contact*
   - *b. Windshield contact, no damage*
   - *c. Windshield contact, no intrusion*
   - *d. Device embedded in windshield, no significant intrusion*
   - *e. Complete intrusion into passenger compartment*
   - *f. Partial intrusion into passenger compartment*
2. *Body Panel Intrusion* — *yes* or *no*

Loss of Vehicle Control

1. *Physical loss of control*
2. *Loss of windshield visibility*
3. *Perceived threat to other vehicles*
4. *Debris on pavement*

Physical Threat to Workers or Other Vehicles

1. *Harmful debris that could injure workers or others in the area*
2. *Harmful debris that could injure occupants in other vehicles*

Two blockouts detached from the posts, but remained behind the guardrail.

Vehicle and Device Condition

1. *Vehicle Damage*
   - *a. None*
   - *b. Minor scrapes, scratches or dents*
   - *c. Significant cosmetic dents*
   - *d. Major dents to grill and body panels*
   - *e. Major structural damage*

2. Windshield Damage

a. None
b. Minor chip or crack
c. Broken, no interference with visibility
d. Broken or shattered, visibility restricted but remained intact
e. Shattered, remained intact but partially dislodged
f. Large portion removed
g. Completely removed

3. Device Damage

a. None
b. Superficial
c. Substantial, but can be straightened
d. Substantial, replacement parts needed for repair
e. Cannot be repaired

7.5 WOOD POST GUARDRAIL CRASH TEST

7.5.1 Test Article

The second crash test was performed on a W-beam guardrail mounted on 178 mm (7 in.) diameter round wood posts that were encased in a concrete mow strip with grout-filled leave-outs. The researchers selected 178 mm (7 in.) diameter round wood post over a 152 mm × 203 mm (6 in. × 8 in.) wood post because it has less flexural capacity and, thus, is more likely to fracture when confined within a mow strip.

With the exception of the post type, the details of the guardrail and mow strip test installation are the same as those used for the first crash test of the steel post guardrail system. Because it was undamaged in the first test, the same concrete mow strip was used for the second crash test. The steel posts were removed and the two-sack grout backfill material was cleaned out of the leave-out sections. A 457 mm (18 in.) diameter auger was used to drill new holes for placement of the 178 mm (7 in.) diameter round wood posts. The void surrounding the post was backfilled with *NCHRP Report 350* standard soil that was compacted in 152 mm (6 in.) lifts through hand-tamping. The top 102 mm (4 in.) of the leave-outs were then backfilled with a two-sack grout mixture.

Additional details of the test installation are shown in Figure 71. Photos of the completed test installation are shown in Figure 72.

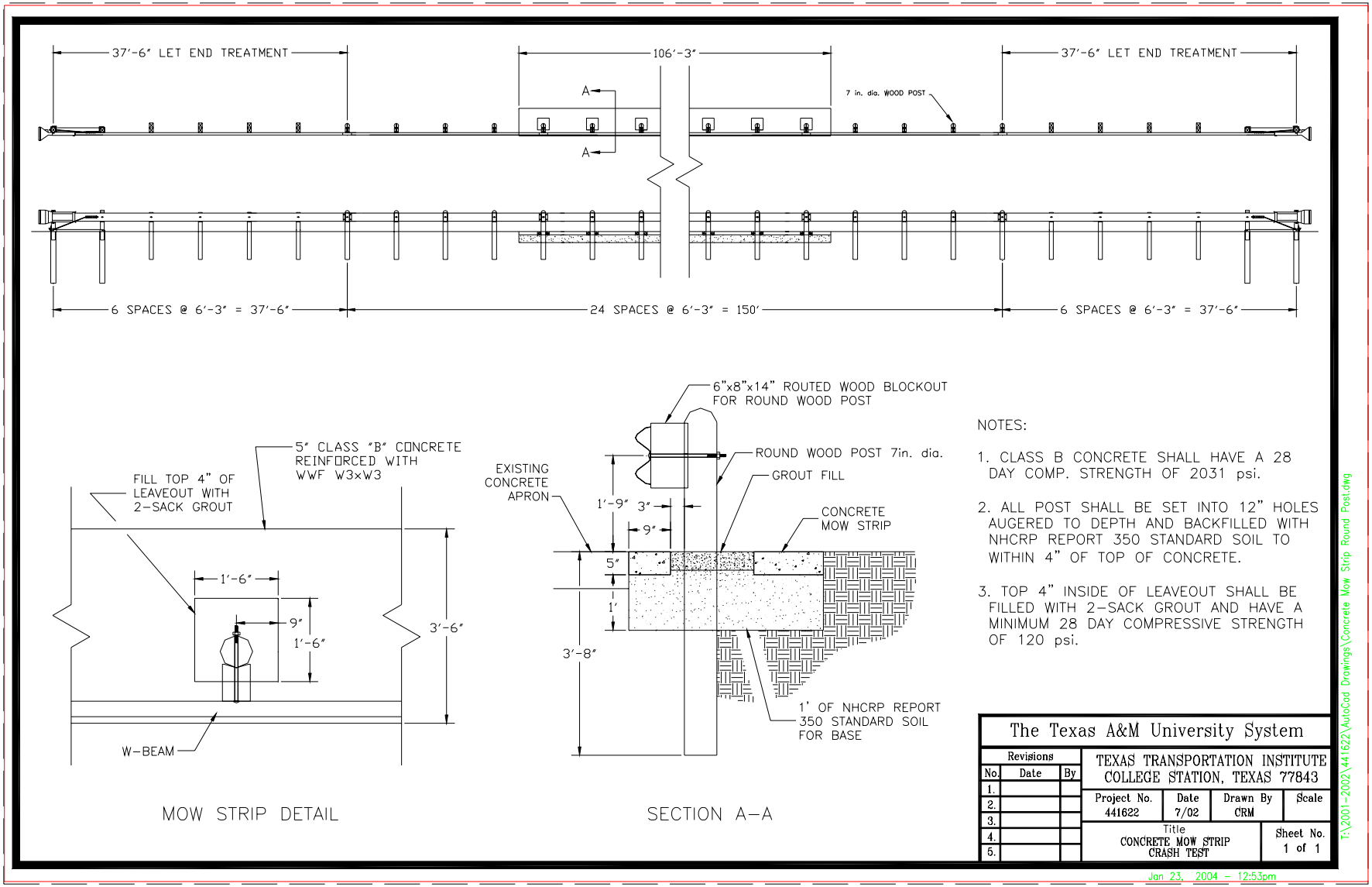

Figure 71. Details of the Wood Post Guardrail in Mow Strip Installation.

Figure 72. Mow Strip Installation before Test 441622-2.

7.5.2 Test Vehicle

A 1997 Chevrolet 2500 pickup truck, shown in Figures 73 and 74, was used for the crash test. Test inertia mass of the vehicle was 2042 kg (4498 lb), and its gross static mass was 2042 kg (4498 lb). The height to the lower edge of the vehicle bumper was 370 mm (14.6 in.), and the height to the upper edge of the bumper was 650 mm (25.6 in.). Additional dimensions and information on the vehicle are given in Appendix D, Figure 81. The vehicle was directed into the installation using a cable reverse tow and guidance system, and was released to be free-wheeling and unrestrained just prior to impact.

7.5.3 Soil and Weather Conditions

The test was performed on the morning of August 22, 2002. No rainfall occurred for the 10 days prior to the test. Moisture content of the *NCHRP Report 350* soil in which the device was installed was 5.8 percent. Weather conditions at the time of testing were as follows: Wind speed: 6 km/h (4 mph); Wind direction: 320 degrees with respect to the vehicle (vehicle was traveling in a southwesterly direction); Temperature: 32°C (90°F); Relative humidity: 68 percent.

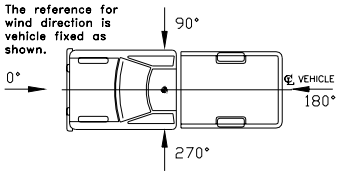

7.5.4 Test Description

The vehicle, traveling at a speed of 101.7 km/h (63.2 mph), impacted the guardrail 650 mm (25.6 in.) upstream of post 13 at an impact angle of 25.8 degrees. Shortly after impact, post 13 began to deflect toward the field side, and at 0.050 s post 14 began to deflect toward the field side. At 0.059 s, the vehicle began to redirect, and at 0.060 s the left front wheel steered into the rail. Post 15 began to deflect toward the field side at 0.099 s, followed by post 16 at 0.177 s. At 0.281 s, the vehicle became parallel with the rail and was traveling at a speed of 65.3 km/h (40.6 mph). At 0.603 s, the vehicle lost contact with the rail and was traveling at a speed of 59.4 km/h (36.9 mph) and an exit angle of 21.2 degrees. As the vehicle continued forward, it immediately began to yaw clockwise toward the rail. Brakes on the vehicle were not applied and the vehicle contacted the rail a second time at post 32. The vehicle subsequently came to rest with the right front quarter against the rail element at post 35. Sequential photographs of the test period are shown in Appendix E, Figure 84.

Figure 73. Vehicle/Installation Geometrics for Test 441622-2.

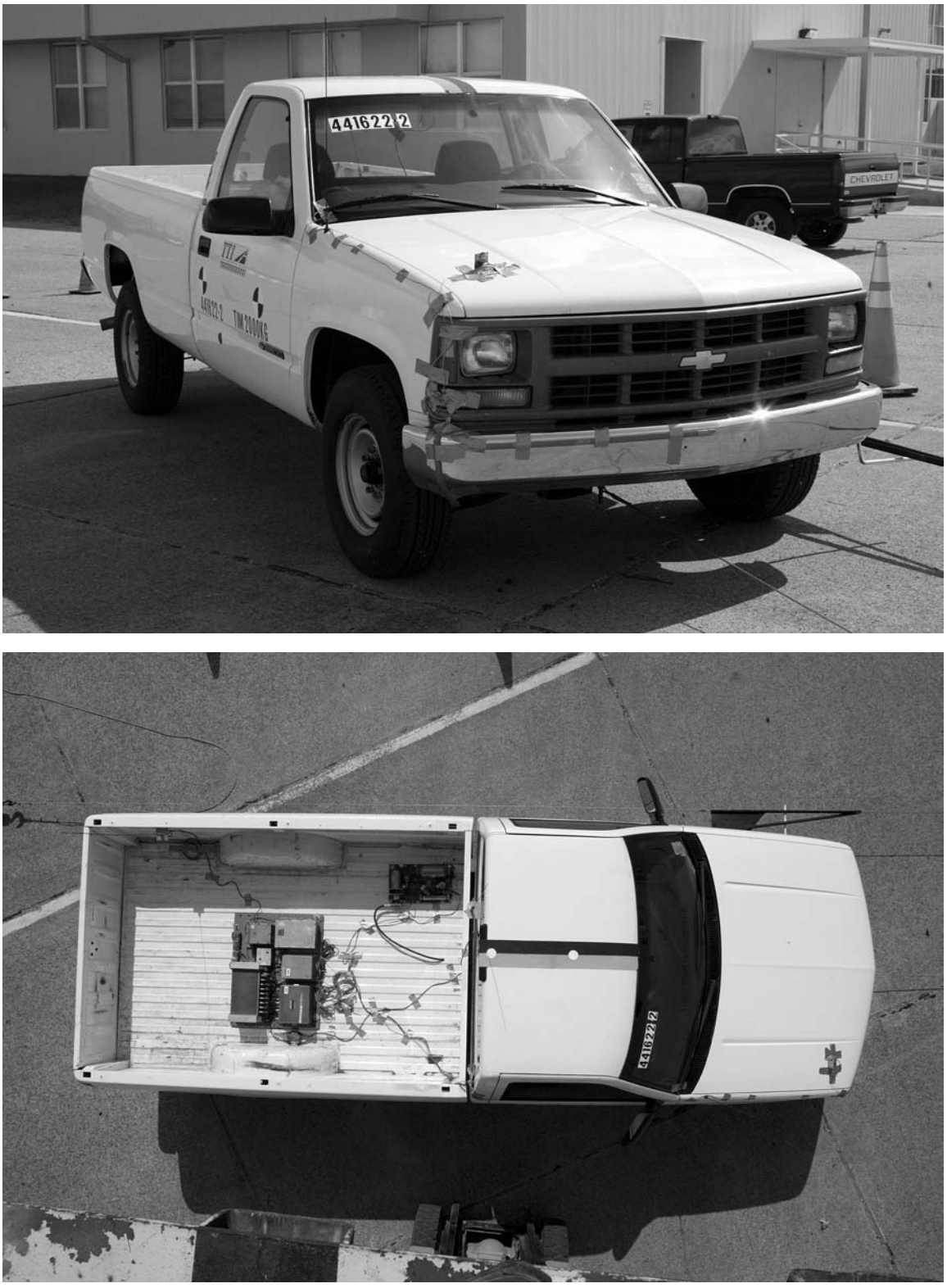

Figure 74. Vehicle before Test 441622-2.

7.5.5 Damage to Test Installation

Damage to the installation is shown in Figures 75 and 76. Posts 11 and 12 were slightly rotated and deflected toward the field of the barrier. Posts 14 and 15 fractured at and below ground level and came to rest behind the guardrail. Post 16 was deflected toward field side 80 mm (3.2 in.) (dynamic was 150 mm (5.9 in.)), and post 17 was deflected toward the field side 7 mm (0.3 in.). At the upstream terminal, post 1 moved longitudinally 10 mm (0.4 in.), and post 2 moved longitudinally 20 mm (0.8 in.). The rail tabs into which the cable anchor bracket sits were slightly torn, and the mounting bolt at post 2 pulled out of the rail element. Posts 3, 5, and 6 were split along the longitudinal axis, and post 4 was cracked. The downstream terminal was only slightly disturbed. Length of contact of the vehicle with the guardrail was 4.5 m (14.6 ft). Maximum dynamic deflection of the rail element was 0.69 m (2.26 ft), and maximum permanent deformation was 0.57 m (1.87 ft).

7.5.6 Vehicle Damage

Structural damage included damage to the right A-arm, tie rod, sway bar, and right front frame rail of the vehicle. The right front bumper, grill, radiator, fan, hood, right front quarter panel, right door, and right side of the bed were deformed, and the right front tire and wheel were damaged (see Figure 77). Maximum exterior crush was 630 mm (24.8 in.) in the side plane at the right front corner and 620 mm (24.4 in.) in the front plane at the right front corner, both near bumper height. Maximum occupant compartment deformation was 24 mm (0.9 in.) in the center front floor pan area over the transmission tunnel. Photographs of the interior of the vehicle are shown in Figure 78. Exterior crush measurements and occupant compartment deformation are presented in Appendix D, Tables 12 and 13.

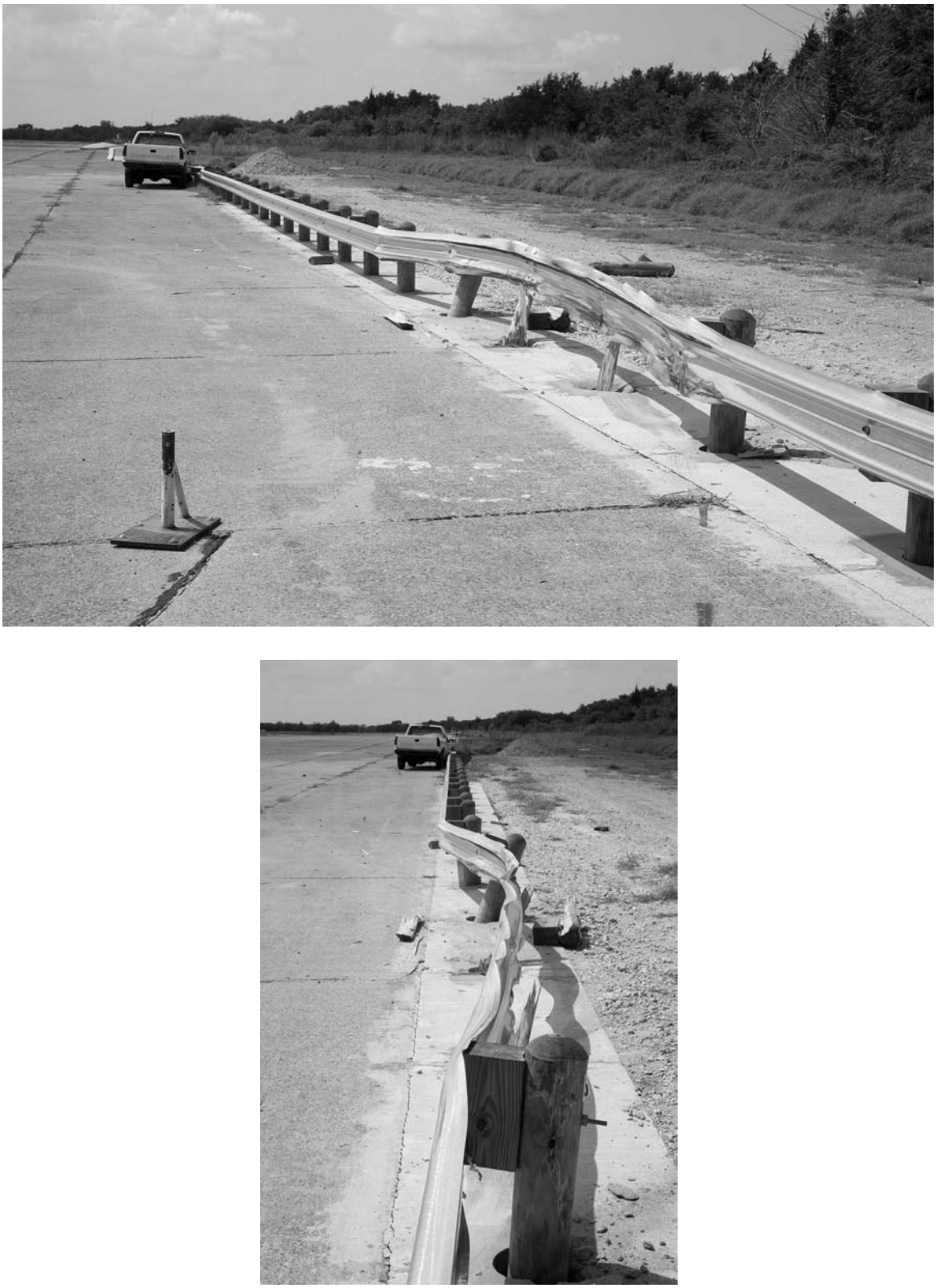

Figure 75. After Impact Trajectory for Test 441622-2.

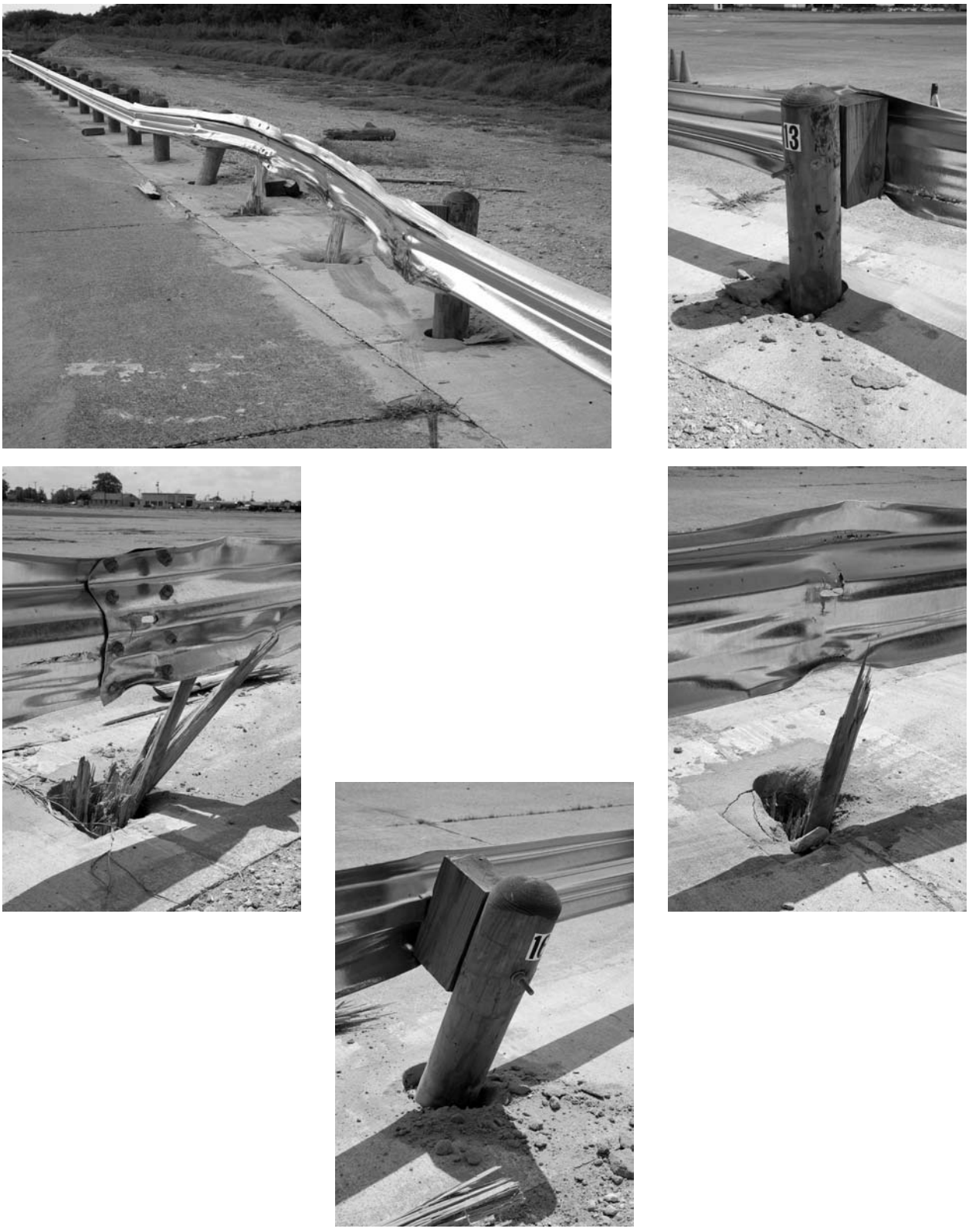

Figure 76. Installation after Test 441622-2.

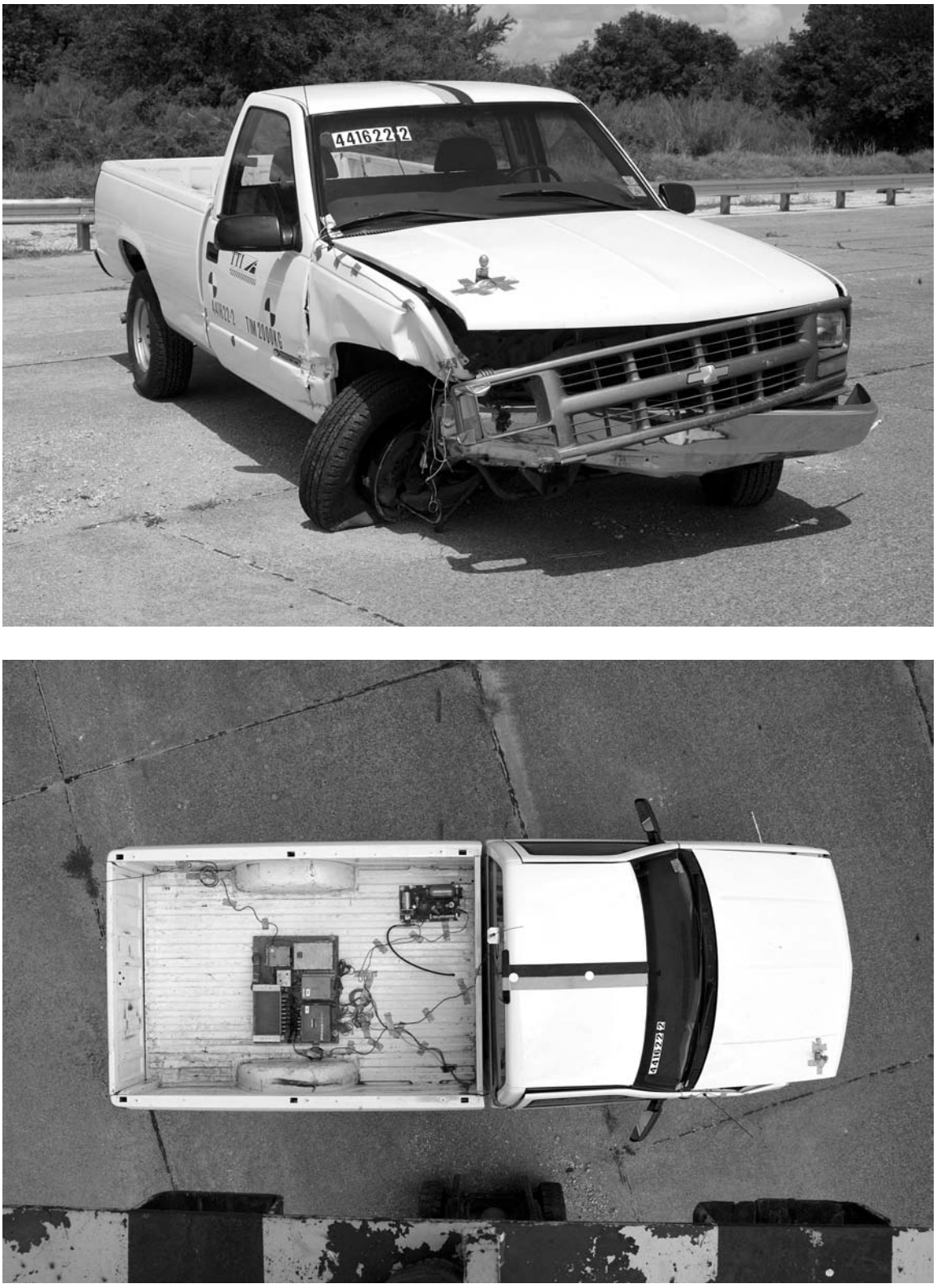

Figure 77. Vehicle after Test 441622-2.

Before test

After test

Figure 78. Interior of Vehicle for Test 441622-2.

7.5.7 Occupant Risk Factors

Data from the triaxial accelerometer located at the vehicle center of gravity were digitized to compute occupant impact velocity and ridedown accelerations. Only the occupant impact velocity and ridedown accelerations in the longitudinal axis are required from these data for evaluation of criterion L of NCHRP Report 350. In the longitudinal direction, occupant impact velocity was 5.8 m/s (19.0 ft/s) at 0.142 s, maximum 0.010-s ridedown acceleration was –7.6 g's from 0.176 to 0.186 s, and the maximum 0.050-s average was –6.5 g's between 0.062 and 0.112 s. In the lateral direction, the occupant impact velocity was 4.9 m/s (16.1 ft/s) at 0.142 s, the highest 0.010-s occupant ridedown acceleration was –8.3 g's from 0.151 to 0.161 s, and the maximum 0.050-s average was –6.1 g's between 0.144 and 0.194 s. These data and other information pertinent to the test are presented in Figure 79. Vehicle angular displacements and accelerations versus time traces are shown in Appendix F, Figures 92 through 98.

7.5.8 Assessment of Test Results

An assessment of the test based on the applicable *NCHRP Report 350* safety evaluation criteria is provided below.

Structural Adequacy

B. Test article should contain and redirect the vehicle; the vehicle should not penetrate, underride, or override the installation although controlled lateral deflection of the test article is acceptable.

Results: The W-beam guardrail with round wood posts in mow strip contained and redirected the pickup truck. The vehicle did not penetrate, underride, or override the guardrail. Maximum dynamic deflection was 0.69 m (2.26 ft). *(Pass)*

Occupant Risk

E. Detached elements, fragments, or other debris from the test article should not penetrate or show potential for penetrating the occupant compartment, or present an undue hazard to other traffic, pedestrians, or personnel in a work zone. Deformation of, or intrusions into, the occupant compartment that could cause serious injuries should not be permitted.

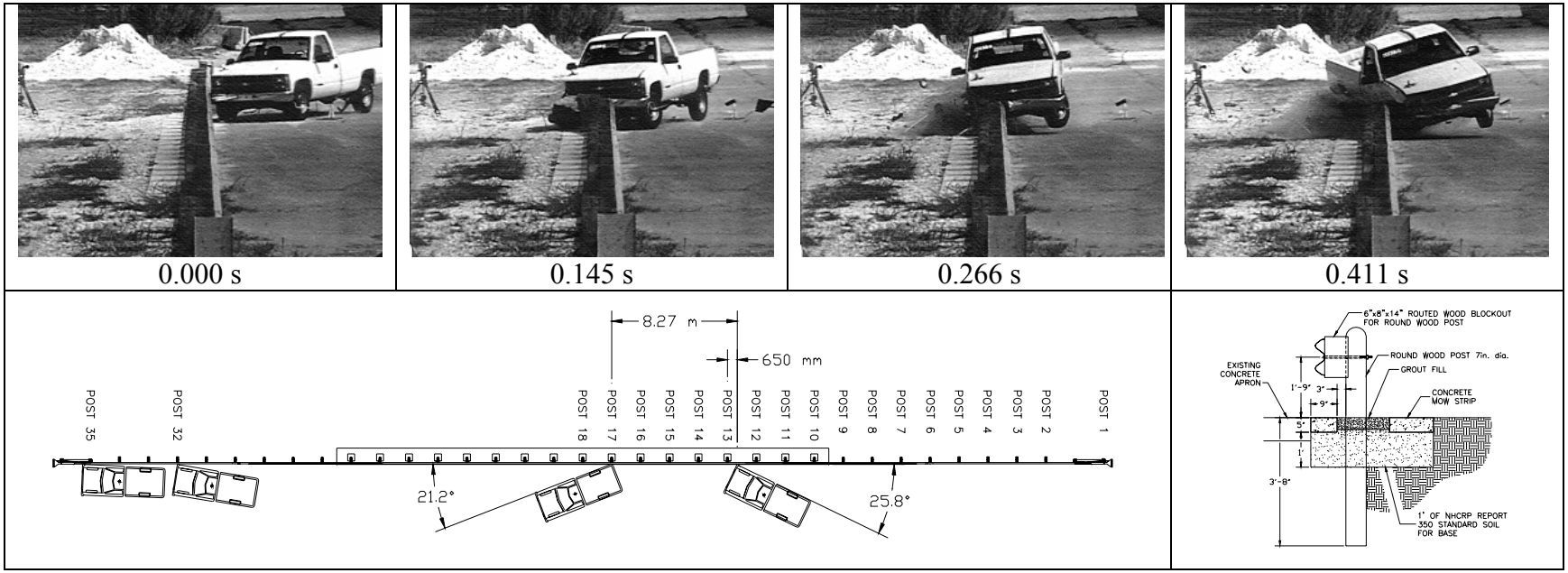

General Information	
Test Agency	Texas Transportation Institute
Test No.	441622-2
Date	08-22-2002
Test Article	
Type	Guardrail
Name	W-beam on Round Posts in Mow Strip
Installation Length	225 ft (68.6 m)
Material or Key Elements	W-Beam on Round Posts with Wood Blockouts in Concrete Mow Strip
Soil Type and Condition	Std Soil w/Concrete Mow Strip, Dry
Test Vehicle	
Type	Production
Designation	2000P
Model	1997 Chevrolet 2500
Mass	
Curb	2094 kg (4612 lb)
Test Inertial	2042 kg (4498 lb)
Dummy	No Dummy
Gross Static	2042 kg (4498 lb)

Impact Conditions	
Speed (km/h (mph))	101.7 (63.2)
Angle	25.8
Exit Conditions	
Speed (km/h (mph)	59.4 (36.9)
Angle	21.2
Occupant Risk Values	
Impact Velocity (m/s (ft/s))	
Longitudinal	5.8 (19.0)
Lateral	4.9 (16.1)
THIV (km/h)	25.1
Ridedown Accelerations (g's)	
Longitudinal	-7.6
Lateral	-8.3
PHD (g's)	10.4
ASI	0.82
Max. 0.050-s Average (g's)	
Longitudinal	-6.5
Lateral	-6.1
Vertical	3.8

Test Article Deflections (mm (in))	
Dynamic	688 (27.1)
Permanent	89 (3.5)
Working Width	1184 (46.6)
Vehicle Damage	
Exterior	
VDS	01RFQ5
CDC	01FYEW4
Maximum Exterior Vehicle Crush	630 mm (24.8 in.)
Interior	
OCDI	FS0000100
Maximum Occupant Compartment. Deformation	24 mm (0.9 in.)
Post-Impact Behavior	
(during 1.0 sec after impact)	
Max. Yaw Angel (deg)	-43.3
Max. Pitch Angle (deg)	-9.2
Max. Roll Angle (deg)	21.7

Figure 79. Summary of Results for Test 441622-2, *NCHRP Report 350* Test 3-11.

Results: Two posts fractured at and below ground level, but came to rest behind the guardrail. These posts did not penetrate, nor show potential for penetrating the occupant compartment, nor present undue hazard to others in the area. Maximum occupant compartment deformation was 24 mm (0.9 in.). *(Pass)*

F. The vehicle should remain upright during and after collision although moderate roll, pitching, and yawing are acceptable.

Results: The pickup truck remained upright during and after the collision. *(Pass)*

♦ **Vehicle Trajectory**

K. After collision, it is preferable that the vehicle's trajectory not intrude into adjacent traffic lanes.

Results: The vehicle did not intrude into adjacent traffic lanes as it traveled alongside the guardrail and came to rest against the rail. *(Pass)*

L. The occupant impact velocity in the longitudinal direction should not exceed 12 m/s and the occupant ridedown acceleration in the longitudinal direction should not exceed 20 g's.

Results: Longitudinal occupant impact velocity was 5.8 m/s (19.0 ft/s) and longitudinal occupant ridedown acceleration was –7.6 g's. *(Pass)*

M. The exit angle from the test article preferably should be less than 60 percent of the test impact angle, measured at time of vehicle loss of contact with the test device.

Results: Exit angle at loss of contact was 21.2 degrees, which was 82 percent of the impact angle. However, immediately after loss of contact, the vehicle yawed toward the rail. *(Fail)*

The following supplemental evaluation factors and terminology, as presented in the FHWA memo entitled "Action: Identifying Acceptable Highway Safety Features," were used for visual assessment of test results. Factors underlined pertain to the test reported herein.

Passenger Compartment Intrusion

1. *Windshield Intrusion*
   - *a. No windshield contact*
   - *b. Windshield contact, no damage*
   - *c. Windshield contact, no intrusion*
   - *d. Device embedded in windshield, no significant intrusion*
   - *e. Complete intrusion into passenger compartment*
   - *f. Partial intrusion into passenger compartment*
2. *Body Panel Intrusion*

yes or *no*

Loss of Vehicle Control

1. *Physical loss of control*
2. *Loss of windshield visibility*
3. *Perceived threat to other vehicles*
4. *Debris on pavement*

Physical Threat to Workers or Other Vehicles

1. *Harmful debris that could injure workers or others in the area*
2. *Harmful debris that could injure occupants in other vehicles*

Two posts fractured at and below ground level, but remained behind the installation.

Vehicle and Device Condition

1. *Vehicle Damage*
   - *a. None*
   - *b. Minor scrapes, scratches or dents*
   - *c. Significant cosmetic dents*
   - *d. Major dents to grill and body panels*
   - *e. Major structural damage*
2. *Windshield Damage*
   - *a. None*
   - *b. Minor chip or crack*
   - *c. Broken, no interference with visibility*
   - *d. Broken or shattered, visibility restricted but remained intact*
   - *e. Shattered, remained intact but partially dislodged*
   - *f. Large portion removed*
   - *g. Completely removed*
3. *Device Damage*
   - *a. None*
   - *b. Superficial*
   - *c. Substantial, but can be straightened*
   - *d. Substantial, replacement parts needed for repair*
   - *e. Cannot be repaired*

CHAPTER 8. SUMMARY AND CONCLUSIONS

Provided a guardrail is crashworthy, there are other factors that merit consideration, such as the cost and related safety concerns associated with routine maintenance (e.g., mowing) and repair operations. Encasing the guardrail in a mow strip can help address some of these issues. However, there are no national standards for this practice, and the effect of mow strips on impact performance had not been previously investigated.

The performance of guardrails encased in pavement mow-strip was researched using component tests, component simulations, predictive full-scale simulations, and full-scale crash testing. Nonlinear finite element analysis methods were used successfully as a design tool for selecting a working mow strip design for both steel and wood post guardrail systems. Two full-scale crash tests were successfully conducted in accordance with *NCHRP Report 350* to verify the impact performance of both steel post and wood post guardrail systems encased in a concrete mow strip with grout-filled leave-outs around the posts.

The grout material in the leave-out sections surrounding the posts failed as designed, permitting the posts in the impact region to rotate in the soil and help dissipate the lateral energy of the vehicle. A partial tear was observed in the W-beam rail after the steel post guardrail test, but the rail maintained its integrity and did not rupture. Two posts fractured during the wood post test, but the vehicle did not pocket into or rupture the rail. Although a couple of the posts contacted the back edge of the leave-out during testing, there was no damage to the concrete mow strip in either test. The repair would consist of removing the damaged guardrail components and grout, and resetting the system within the existing leave-outs.

Tables 8 and 9 provide a summary of the impact performance evaluation for the steel and wood post guardrail tests, respectively. Both guardrail systems met all the required evaluation criteria of *NCHRP Report 350* and demonstrated low maintenance/repair costs under design impact conditions.

The direct encasement of guardrail posts in a mow strip without leave-outs around the posts is a common practice. To investigate the impact performance of this practice, a finite element model of a full-scale guardrail system encased in a rigid mow strip was constructed and used to perform impact simulations. The results indicate that this system has a low probability of meeting *NCHRP Report 350* evaluation criteria and its use is highly discouraged.

Table 8. Performance Evaluation Summary for Test 441622-1, *NCHRP Report 350* Test 3-11.

Test Agency: Texas Transportation Institute | Test No.: 441622-1 | Test Date: 06/26/2002

***NCHRP Report 350* Test 3-11 Evaluation Criteria**	**Test Results**	**Assessment**
Structural Adequacy		
A. Test article should contain and redirect the vehicle; the vehicle should not penetrate, underride, or override the installation although controlled lateral deflection of the test article is acceptable.	The W-beam guardrail in mow strip contained and redirected the pickup truck. The vehicle did not penetrate, underride, or override the guardrail. Maximum dynamic deflection was 0.58 m (1.90 ft).	Pass
Occupant Risk		
D. Detached elements, fragments, or other debris from the test article should not penetrate or show potential for penetrating the occupant compartment, or present an undue hazard to other traffic, pedestrians, or personnel in a work zone. Deformations of, or intrusions into, the occupant compartment that could cause serious injuries should not be permitted.	Two blockouts became detached from the posts and were thrown behind the guardrail. These blockouts did not penetrate nor show potential for penetrating the occupant compartment. As these blockouts remained behind the guardrail, they did not present undue hazard to others in the area. Maximum occupant compartment deformation was 20 mm (0.8 in).	Pass
F. The vehicle should remain upright during and after collision although moderate roll, pitching, and yawing are acceptable.	The pickup truck remained upright during and after the collision event.	Pass
Vehicle Trajectory		
K. After collision it is preferable that the vehicle's trajectory not intrude into adjacent traffic lanes.	The pickup truck came to rest 43.5 m (142.6 ft) downstream of impact and 19.1 m (62.6 ft) forward of the traffic face of the rail.	Fail*
L. The occupant impact velocity in the longitudinal direction should not exceed 12 m/s and the occupant ridedown acceleration in the longitudinal direction should not exceed 20 g's.	Longitudinal occupant impact velocity was 5.7 m/s (18.7 ft/s) and longitudinal occupant ridedown acceleration was 14.6 g's.	Pass
M. The exit angle from the test article preferably should be less than 60 percent of test impact angle, measured at time of vehicle loss of contact with test device.	Exit angle at loss of contact was 15.4 degrees, which was 61 percent of the impact angle.	Marginal*

* Criterion K and M are preferable, not required.

Table 9. Performance Evaluation Summary for Test 441622-2, *NCHRP Report 350* Test 3-11.

Test Agency: Texas Transportation Institute | Test No.: 441622-2 | Test Date: 08/22/2002

***NCHRP Report 350* Test 3-11 Evaluation Criteria**	**Test Results**	**Assessment**
Structural Adequacy		
A. Test article should contain and redirect the vehicle; the vehicle should not penetrate, underride, or override the installation although controlled lateral deflection of the test article is acceptable.	The W-beam guardrail with round wood posts in mow strip contained and redirected the pickup truck. The vehicle did not penetrate, underride, or override the guardrail. Maximum dynamic deflection was 0.69 m (2.26 ft).	Pass
Occupant Risk		
D. Detached elements, fragments, or other debris from the test article should not penetrate or show potential for penetrating the occupant compartment, or present an undue hazard to other traffic, pedestrians, or personnel in a work zone. Deformations of, or intrusions into, the occupant compartment that could cause serious injuries should not be permitted.	Two posts fractured at and below ground level, but came to rest behind the guardrail. These posts did not penetrate, nor show potential for penetrating the occupant compartment, nor present undue hazard to others in the area. Maximum occupant compartment deformation was 24 mm (0.9 in).	Pass
F. The vehicle should remain upright during and after collision although moderate roll, pitching, and yawing are acceptable.	The pickup truck remained upright during and after the collision event.	Pass
Vehicle Trajectory		
K. After collision it is preferable that the vehicle's trajectory not intrude into adjacent traffic lanes.	The vehicle did not intrude into adjacent traffic lanes as it traveled alongside the guardrail and came to rest against the rail.	Pass*
L. The occupant impact velocity in the longitudinal direction should not exceed 12 m/s and the occupant ridedown acceleration in the longitudinal direction should not exceed 20 g's.	Longitudinal occupant impact velocity was 5.8 m/s (19.0 ft/s) and longitudinal occupant ridedown acceleration was –7.6 g's.	Pass
M. The exit angle from the test article preferably should be less than 60 percent of test impact angle, measured at time of vehicle loss of contact with test device.	Exit angle at loss of contact was 21.2 degrees, which was 82 percent of the impact angle. However, immediately after loss of contact, the vehicle yawed toward the rail.	Fail*

* Criterion K and M are preferable, not required.

CHAPTER 9. IMPLEMENTATION RECOMMENDATIONS

The successfully tested mow strip systems shown in Figures 62 and 71 are suitable for immediate implementation on the national highway system. In addition to providing greatly enhanced impact performance, it is believed that mow strip configurations featuring leave-outs are also more practical based on ease of repair after an impact.

The tested configurations are considered to be representative of the most severe confinement conditions allowable. Any increase in post confinement beyond that provided by the grout backfill material used in the leave-out sections formed around the guardrail posts should undergo additional analysis and/or testing. This applies to systems featuring guardrail posts directly encased in concrete or asphalt.

While the number of full-scale crash tests conducted was limited, the structure of subcomponent analysis and testing provided additional insight into the performance of guardrail encased in mow strip. Some recommendations resulting from this research regarding acceptable ranges for some key mow strip parameters, including mow strip material and dimensions, leave-out dimensions, leave-out backfill material, and guardrail post location are provided below. These recommendations are intended to give highway designers and maintenance engineers some flexibility in mow strip design in order to accommodate varying site conditions, construction practices, and maintenance objectives without affecting impact performance.

9.1 MOW STRIP MATERIAL

One of the objectives of the mow strip research was to develop mow strip configurations that incurred minimal damage during an impact to reduce the cost and worker exposure associated with repairs after an impact. Because dynamic bogie testing indicated that a concrete mow strip is more likely to become damaged in an impact, it was chosen for full-scale testing to assess the magnitude and extent of repairs required after a design impact event. In the full-scale tests of both the steel and wood post guardrail systems, no posts impacted the concrete mow strip with sufficient force to damage the concrete. Only the sacrificial leave-out material was damaged. Because of this, it is anticipated that little or no repair of the mow strip should be required when either asphalt or concrete is used as the mow strip material. However, to avoid damage to the concrete mow strip layer, the concrete should be at least as strong as the welded

wire fabric reinforced TxDOT Class B concrete used in the crash test. Asphalt is also considered to be an acceptable mow strip material.

9.2 MOW STRIP DIMENSIONS

The mow strip systems that were crash tested were 1.1 m (3.5 ft) wide. This width is based on two factors. First, this width of mow strip layer provides adequate clearance behind the guardrail posts to allow for the wheel of a mower deck to ride on the mow strip surface. This allows the mower to cut grass right up to the edge of the paved surface eliminating the need for any roadside hand mowing. Second, the layer of concrete provided behind the grout leave-out is wide enough to prevent significant concrete failure during design impact conditions. If damage to the concrete mow strip layer can be avoided during an impact, repair efforts will be significantly reduced. However, the overall mow strip dimensions can be varied without effecting impact performance, provided a leave-out with dimensions equal to or exceeding those used in the crash test are provided around the guardrail posts.

The depth of the concrete mow strip used in the crash test installations was 127 mm (5 in.). Because the energy dissipating ability of a mow strip system depends primarily on the leave-out material and dimensions, the mow strip depth is not critical to system performance within reasonable bounds. The point of rotation of the post is approximately two-thirds of the post embedment depth, and the first point of contact of the post with the mow strip will always be the upper edge. The primary reason for a mow strip depth requirement is the prevention of damage during an impact. Concrete mow strip depths less than 127 mm (5 in.) may result in some damage to the concrete under design impact conditions, but will not adversely affect impact performance. Bogie impacts of posts in asphalt mow strips were conducted using mow strip depths up to 203 mm (8 in.). Acceptable post behavior was observed in these tests. Therefore, mow strip depths of 203 mm (8 in.) or less are considered acceptable from an impact performance standpoint. Mow strip depths significantly greater than 203 mm (8 in.) may warrant further investigation since the additional soil confinement may begin to restrict movement of the post.

9.3 LEAVE-OUT DIMENSIONS

Both steel and wood post systems were tested with 457 mm × 457 mm (18 in. × 18 in.) square leave-outs. A 457 mm (18 in.) diameter round leave-out provides approximately the same area of leave-out material around the post and is considered to be an acceptable alternative to the square leave-out. Without further testing, these are considered to be the minimum acceptable dimensions for the leave-outs. However, larger leave-out dimensions are considered acceptable from both an impact performance and maintenance/repair standpoint. Under severe impact conditions, larger leave-outs would provide more distance for the post to rotate before bottoming out on the mow strip material. If desired, it is considered acceptable to extend the leave-out to the back edge of the mow strip. However, while offering potential improvement in impact performance, this practice may make the leave-out backfill material more subject to cracking or other forms of long-term degradation.

9.4 LEAVE-OUT BACKFILL MATERIAL

The material used to backfill the leave-outs is a standard two-sack grout mixture. Tests indicated a maximum 28-day compressive strength of 0.85 MPa (120 psi) for this material. Other leave-out backfill materials (e.g. foams) may be accepted as alternatives to the two-sack grout provided their compressive strength does not exceed that of the grout. The strength of an alternative leave-out backfill material can be demonstrated through laboratory and/or dynamic bogie vehicle testing. Alternative leave-out backfill materials should also have a demonstrated ability to resist vegetation growth. Approval of a backfill material with a compressive strength exceeding that of the two-sack grout (i.e., greater than 0.85 MPa (120 psi)) would require a full-scale crash test.

The depth of leave-out backfill material used in the crash tests was 102 mm (4 in.). This depth should be sufficient to resist cracking and growth of vegetation. Shallower depths of leave-out material are acceptable from an impact performance standpoint. However, the long-term durability of a shallow grout layer is not known and any degradation of the leave-out material would likely reduce its resistance to vegetation growth over time. Backfill depths significantly greater than 102 mm (4 in.) may warrant further investigation through a dynamic bogie vehicle test to assess the effects on the force-deflection characteristics of the post.

9.5 GUARDRAIL POST TYPE

Full-scale crash tests were successfully conducted with both W150×13 (W6×9) steel and 178 mm (7 in.) diameter round wood guardrail posts. Both of these post types are considered to be acceptable alternatives for use with the recommended mow strip configurations described above.

The full-scale crash test (test no. 441622-2) of the wood post guardrail system was conducted using 178 mm (7 in.) diameter round wood posts because it was considered to represent a more critical condition than a 152 mm × 203 mm (6 in. × 8 in.) rectangular wood post for the mow strip application. For a given grade of wood post, a 152 mm × 203 mm (6 in. × 8 in.) rectangular cross-section has more bending strength than a 178 mm (7 in.) diameter round cross-section. Therefore, the 178 mm (7 in.) diameter round wood post is more likely to fracture under increased confinement and result in vehicular pocketing. Since a 178 mm (7 in.) diameter round wood post was successfully crash tested, a 152 mm × 203 mm (6 in. × 8 in.) rectangular wood post is also considered to be an acceptable post type.

9.6 GUARDRAIL POST LOCATION

The front (traffic) face of the guardrail posts should be placed approximately 76 mm (3 in.) from the front edge of the leave-out. This location was selected to maximize the available post deflection distance while providing sufficient room to permit proper tamping of the soil in front of posts installed by drilling and backfilling. If the posts are installed by driving, the 76 mm (3 in.) offset between the front edge of the leave-out and the front face of the post is not required and the overall dimensions of the leave-out can be accordingly reduced, as long as the distance between the back face of the post and the back edge of the leave-out is maintained.

The offset of the face of the post from the front edge of the leave-out can be increased provided the overall depth of the leave-out is also increased so as to maintain a deflection distance between the back face of the post and the back edge of the leave-out that is equal to or greater than 178 mm (7 in.).

REFERENCES

1. Ross, H. E., "Evolution of roadside safety," *Transportation Research Circular*, Transportation Research Board, Washington, D. C., 435(2), 5-16, 1995.

2. Ross, H. E., Sicking, D. L., Zimmer, R. A., and Michie, J. D., "Recommended procedures for the safety performance evaluation of highway features," *National Cooperative Highway Research Program Report 350*, Transportation Research Board, Washington, D. C., 1993.

3. *LS-DYNA keyword user's manual: Nonlinear dynamic analysis of structures in three dimensions,* Version 960, Volumes I and II, Livermore Software Technology Company, Livermore, California, 2001.

4. Mak, K. K., Bligh, R. P., and Menges, W. L., "Crash testing and evaluation of existing guardrail systems," *Report No. RF 471470*, Texas Transportation Institute, Texas A&M University, College Station, Texas, 1995.

5. Green, D. W., and Kretschmann, D. E., "Moisture content and the properties of clear southern pine," *Research Paper FPL-RP-531*, United States Department of Agriculture, Forest Service, Forest Products Laboratory, Madison, Wisconsin, 1994.

6. Dewey, J. F., Jeyapalan, J. K., Hirsch, T. J., and Ross, H. E., "A study of the soil-structure interaction of guardrail posts," *Report No. FHWA/TX-84/12+343-1*, Texas Transportation Institute, Texas A&M University, College Station, Texas, 1983.

7. Hallquist, J. O., *LS-DYNA Theoretical manual,* Livermore Software Technology Company, Livermore, California, 1998.

8. Habibagahi, K., and Lagner, J. A., "Horizontal subgrade modulus of granular soil," *Laterally loaded deep foundations: Analysis and performance,* J.A. Langner, E.T. Mosley, and C.D. Thompson, eds., ASTM, West Conshohoken, Pennsylvania, 21-34, 1984.

9. Patzner, G. S., Plaxico, C. A. and Ray, M. H., "Effect of post and soil strength on the performance of a guardrail terminal," *Engineering mechanics: A Force for the 21st Century*, Proceedings of 12th Engineering Mechanics Conference, ASCE, New York, New York, 1998.

10. Tabiei, A., and Wu, J., "Evaluation of G4 strong-post guardrail for truck rollover and snagging using finite element simulation," *FHWA Report No. DTFh61-97-X-0027*, Center of Excellence in Transportation Computational Mechanics, The University of Cincinnati, Cincinnati, Ohio, 2000.

11. Tabiei, A., and Wu, J., "Roadmap for crashworthiness finite element simulation of roadside safety structures," *Finite Elements in Analysis and Design*, 34(2), 145-157, 2000.

12. Plaxico, C. A., Ray, M. H., and Hiranmayee, K., "Comparison of the impact performance of the G4(1W) and G4(2W) guardrail systems under NCHRP Report 350 test 3-11 conditions," *Transportation Research Record,* Transportation Research Board, Washington, D. C., 2000.

13. Eskandarian, A., Marzougui, D., Bedewi, N. E., "Finite element model and validation of a surrogate crash test vehicle for impacts with roadside objects," *International Journal of Crashworthiness*, 2(3), 37-50, 1997.

14. Mak, K. K., and Menges, W. L., "Crash testing and evaluation of strong-post W-beam guardrails," *Transportation Research Record*, Transportation Research Board, Washington, D.C., 1994.

15. Bullard, D. L., Menges, W. L., and Alberson, D. C., "NCHRP Report 350 compliance Test 3-11 of the modified G4(1S) guardrail with timber blockouts," *Report No. RF 405421-1*, Texas Transportation Institute, Texas A&M University, College Station, Texas, 1996.

16. Bligh, R. P. and Menges, W. L., "Testing and evaluation of a modified steel post W-beam guardrail with recycled polyethylene blockouts," *Report No. 400001-MPT*, Texas Transportation Institute, Texas A&M University, College Station, Texas, 1997.

17. Bligh, R. P., Menges, W. L., and Butler, B. G., "Evaluation of a modified steel post W-beam guardrail system," *Report No. 3963-S*, Texas Transportation Institute, Texas A&M University, College Station, Texas, 1997.

18. Alberson, D. C., Menges, W. L., Schoeneman, S. K., "NCHRP Report 350 Test 3-11 of the strong post W-beam guardrail with Trinity composite blockout," *Report No. 400001-TRB3*, Texas Transportation Institute, Texas A&M University, College Station, Texas, 2001.

19. Williams, W. F., Menges, W. L., and Haug, R. R., "NCHRP Report 350 Test 3-11 of the G-4 W-beam guardrail with Mondo recycled polymer offset block," *Report No. 400001-MON1*, Texas Transportation Institute, Texas A&M University, College Station, Texas, 2002.

20. Hamilton, M. E., "Simulation of the T-6 bridge rail using LS-DYNA," MS thesis, Texas A&M University, College Station, Texas, 1999.

21. Alberson, D. C., Bullard, D. L., and Zimmer, R. A., "Testing and validation of a surrogate crash vehicle," *Unpublished Report*, Texas Transportation Institute, Texas A&M University, College Station, Texas. 1994.

22. Hinch, J., Manhard, G., Stout, D., and Owings, R., "FOIL construction laboratory procedures to determine the breakaway behavior of luminare supports in mini-sized vehicle collisions," Volumes I, II, and III. *Report Nos. FHWA/RD-86/105, 106, and 107*, Federal Highway Administration, Washington, D. C., 1987.

23. Hott, C., Brown, C., Totani, N., and Hansen, A., "Validation of a surrogate vehicle for verification testing of transformer base luminare supports," *Report No. FHWA/RD-87/034*, Federal Highway Administration, Washington, D. C., 1988.

24. Hott, C., Brown, C., Totani, N., and Hansen, A., "Crush characteristics of the breakaway bogie," *Report No. FHWA/RD-89/107*, Federal Highway Administration, Washington, D. C., 1990.

25. American Institute of Steel Construction (AISC), *Manual of steel construction: Load and resistance factor design,* 3rd Edition, Chicago, Illinois, 2002.

26. Hamilton, M. E., "Simulation of the T-6 bridge rail using LS-DYNA," MS thesis, Texas A&M University, College Station, Texas, 1999.

27. Eggers, D. W., and Hirsch, T. J., "The effects of embedment depth, soil properties, and post type on the performance of highway guardrail posts," *Report No. FHWA/TX-86/64+405-1*, Texas Transportation Institute, Texas A&M University, College Station, Texas, 1986.

28. Seckinger, N. R., and Roschke, P. N., "Numerical simulation of dynamic soil structure interaction using an explicit finite element code," *Proceedings of The Ninth International Conference on Computing in Civil and Building Engineering*, Taipei, Taiwan, 2002.

29. American Association of State Highway and Transportation Officials (AASHTO), "Aggregate and soil-aggregate subbase, base, and surface courses: M147-70," *Standard Specifications for Transportation Materials and Methods of Sampling and Testing*, Washington, D. C., 1990.

30. Jeyapalan, J. K., Dewey, J. F., Hirsch, T. J., and Ross, H. E., "Soil-foundation interaction behavior of highway guardrail posts," *Transportation Research Record*, Transportation Research Board, Washington, D. C., 1983.

31. United States Army Corps of Engineers (USACE), "Bearing capacity of soils," *Engineering Manual 1110-1-1905*, Washington, D. C., 1982.

32. Lade, P. V., and Duncan, J. M., "Elastoplastic stress-strain theory for cohesionless soils," *Journal of the Geotechnical Engineering Division*, ASCE, 101(10), 1037-1053, 1975.

33. Drucker, D. C., and Prager, W., "Soil mechanics and plastic analysis or limit design," *Quarterly of Applied Mathematics*, Vol. X, No. 2, 157-165, 1952.

34. American Association of State Highway and Transportation Officials (AASHTO), "Corrugated sheet steel beams for highway guardrails: M-180," *Standard Specifications for Transportation Materials and Methods of Sampling and Testing*, Washington, D. C., 1990.

35. Reid, J. D. and Sicking, D. L., "Design of the SKT-350 using LS-DYNA," *Transportation Research Record*, Transportation Research Board, Washington, D. C., 1997.

36. American Concrete Institute (ACI), "Building code requirements for reinforced concrete and commentary," *ACI 318-02/318R-02*, Farmington Hills, Michigan, 2002.

37. Federal Highway Administration Memorandum, from the Director, Office of Engineering, entitled: "ACTION: Identifying Acceptable Highway Safety Features," dated July 25, 1997.

APPENDIX A. STATE OF PRACTICE SURVEY

Texas Transportation Institute
The Texas A&M University System
3135 TAMUS
College Station, TX 77843-3135

979-845-6375:
Fax 979-845-6107
http://tti.tamu.edu

TxDOT MOW-STRIP SURVEY

Name_____Date_____

District _____

Phone _____ Fax_____

		Please Circle One	
1.	Does your District have a procedure for placing mow-strip around guard fence?	Y	N
2.	If yes, does a written detail or standard exist?	Y	N
A.	If yes, would you please provide a copy.		
B.	If a written detail or standard does not exist, would you please provide a brief description of the typical methodology used for a mow-strip application (Please attach other pages if needed): _____ _____ _____ _____		
3.	What material is typically used to construct the mow-strip? (e.g. Concrete, Asphalt, Rip Rap, etc.): _____		
4.	Is there an individual in your District that is familiar with the installation and repair of mow-strips? Name _____ Phone _____	Y	N
5.	Does your district incorporate "Leave-out" sections in your mow-strips? ("Leave-outs" are voids in the mow-strip around posts that facilitate removal and repair of damaged posts.)	Y	N
6.	If "Leave-out" sections are used, what material is used to backfill the void?_____		

Questions or Comments? Please contact Roger Bligh @ 979-845-4377 or Dean Alberson @ 979-458-3874

Safety and Structural Systems Division

APPENDIX B. SUBCOMPONENT IMPACT TESTING DRAWINGS

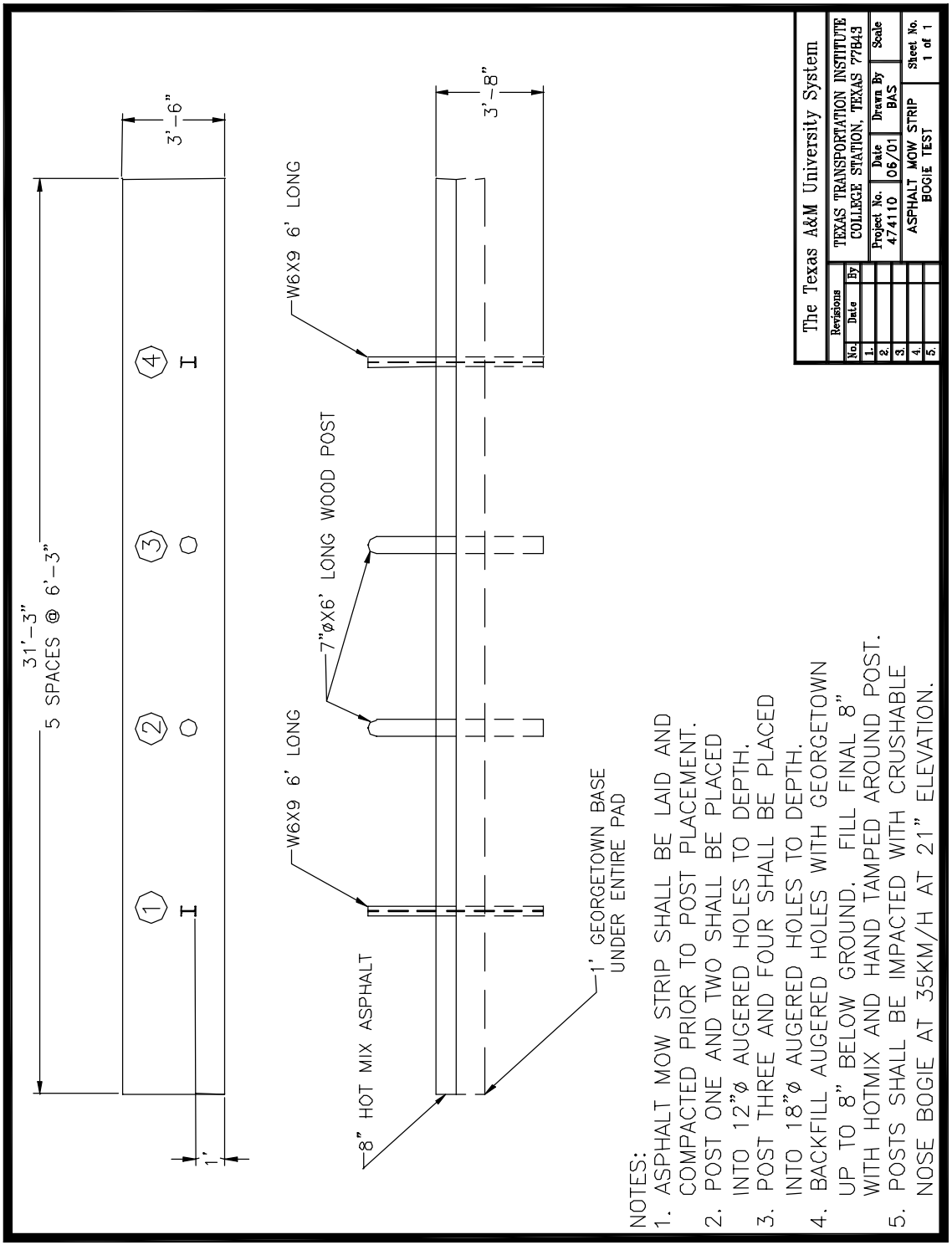

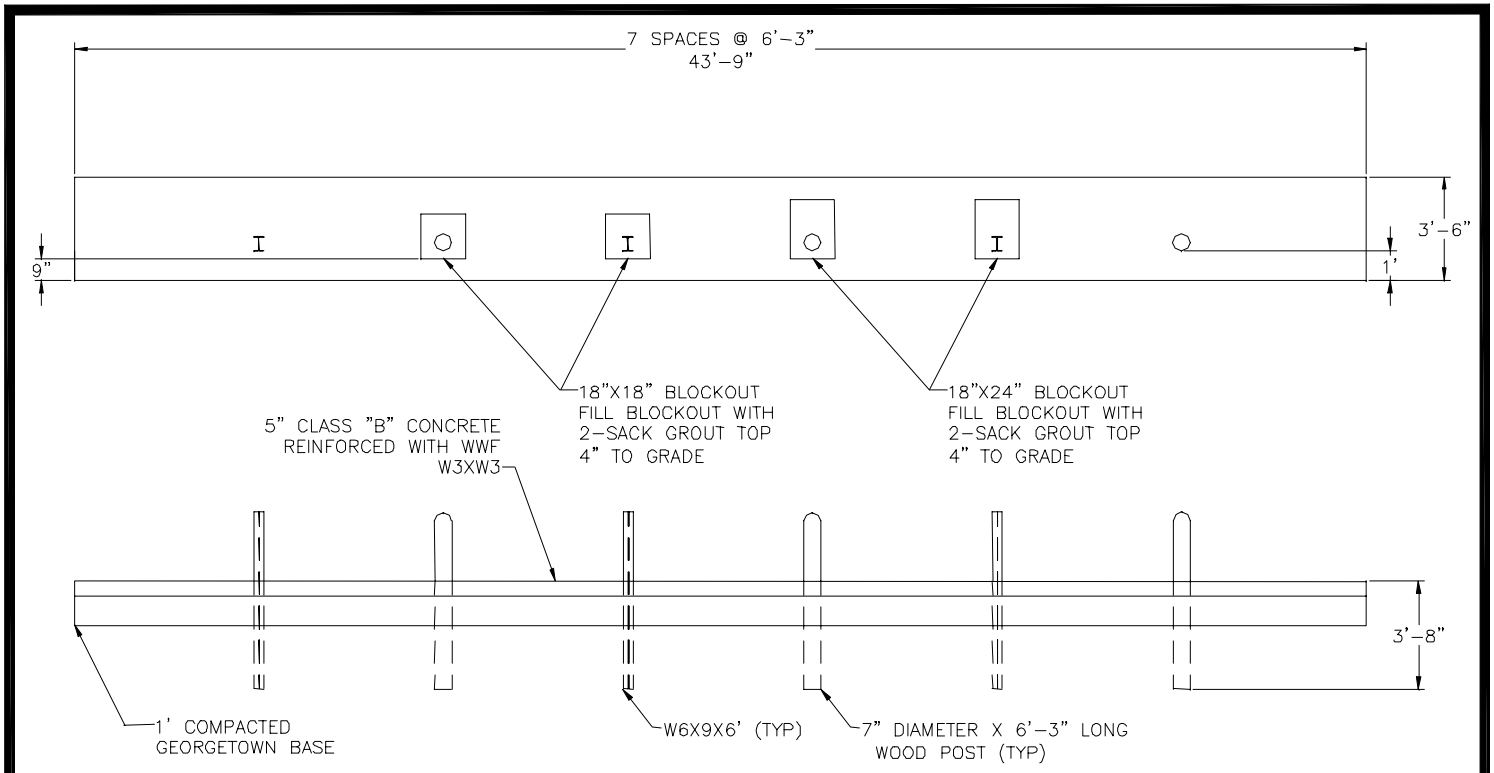

NOTES:
1. CLASS B CONCRETE SHALL HAVE A 28 DAY COMP. STRENGTH OF 14MPa (2031 PSI).
2. POST ARE TO BE IMPACTED AT 21" BY CRUSHABLE NOSE BOGIE AT 35 KM/HR.
3. ALL POST SHALL BE SET INTO 12" HOLES AUGERED TO DEPTH AND BACKFILLED WITH GEORGETOWN. THE CONCRETE SHALL BE PLACED AFTER POSTS ARE IN PLACE.

The Texas A&M University System

Revisions		
No.	Date	By
1.		
2.		
3.		
4.		
5.		

TEXAS TRANSPORTATION INSTITUTE
COLLEGE STATION, TEXAS 77843

Project No.	Date	Drawn By	Scale
474110	06/01	BAS	

CONCRETE MOW STRIP
BOGIE TEST

Sheet No. 1 of 1

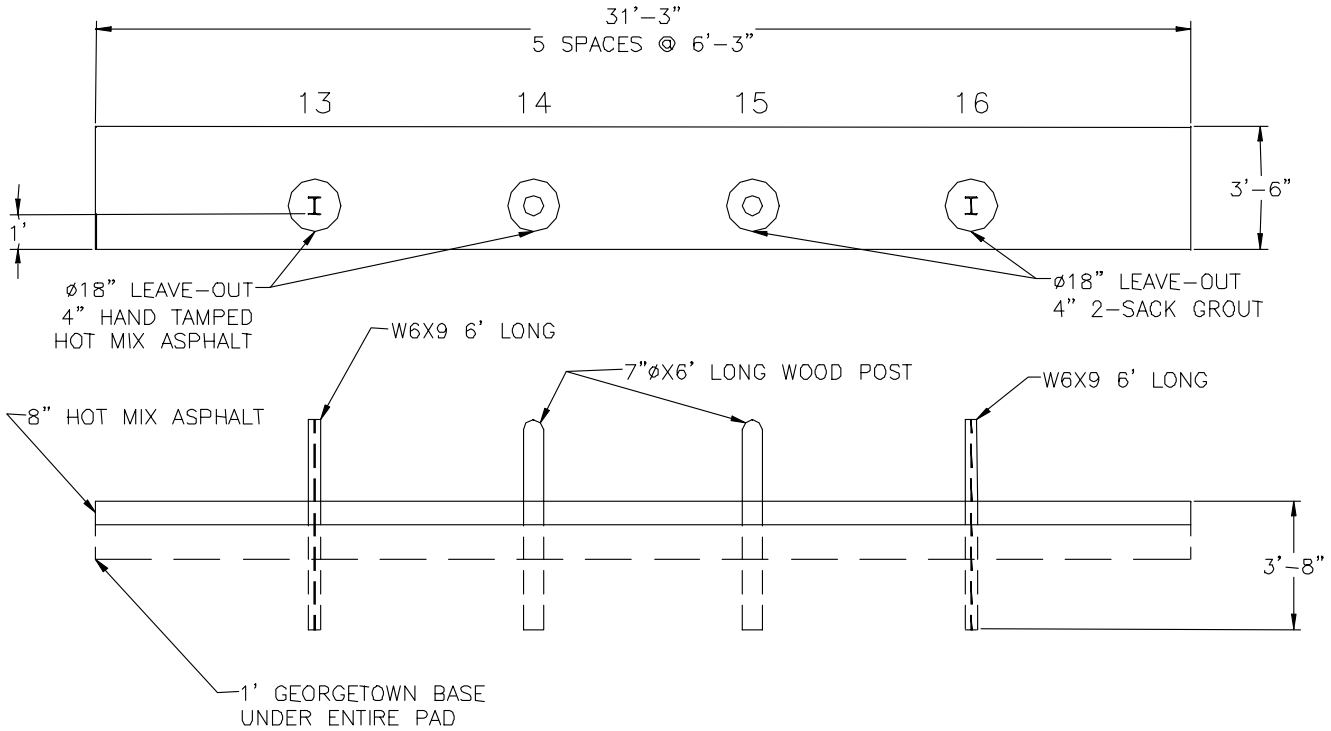

NOTES:

1. ASPHALT MOW STRIP SHALL BE LAID AND COMPACTED PRIOR TO POST PLACEMENT.
2. ALL POST SHALL BE PLACED IN 12ø AUGERED HOLES TO DEPTH.
3. BACKFILL AUGERED HOLES WITH GEORGETOWN UP TO 4" BELOW GROUND. FILL FINAL 4" WITH HOTMIX OR 2 SACK GROUT AS SHOWN.
4. POSTS SHALL BE IMPACTED WITH CRUSHABLE NOSE BOGIE AT 35KM/H AT 21" ELEVATION.

The Texas A&M University System

Revisions		
No.	Date	By
1.		
2.		
3.		
4.		
5.		

TEXAS TRANSPORTATION INSTITUTE
COLLEGE STATION, TEXAS 77843

Project No.	Date	Drawn By	Scale
441622	11/01	BAS	

ASPHALT MOW STRIP
BOGIE TEST

Sheet No. 1 of 1

APPENDIX C. CRASH TEST PROCEDURES AND DATA ANALYSIS

The crash test and data analysis procedures were in accordance with guidelines presented in *NCHRP Report 350*. Brief descriptions of these procedures are presented as follows.

ELECTRONIC INSTRUMENTATION AND DATA PROCESSING

The test vehicle was instrumented with three solid-state angular rate transducers to measure roll, pitch, and yaw rates; a triaxial accelerometer near the vehicle center of gravity (c.g.) to measure longitudinal, lateral, and vertical acceleration levels; and a backup biaxial accelerometer in the rear of the vehicle to measure longitudinal and lateral acceleration levels. These accelerometers were ENDEVCO® Model 2262CA, piezoresistive accelerometers with a ±100 g range.

The accelerometers are strain gage type with a linear millivolt output proportional to acceleration. Angular rate transducers are solid state, gas flow units designed for high-"g" service. Signal conditioners and amplifiers in the test vehicle increase the low-level signals to a ±2.5 volt maximum level. The signal conditioners also provide the capability of a resistance calibration (R-cal) or shunt calibration for the accelerometers and a precision voltage calibration for the rate transducers. The electronic signals from the accelerometers and rate transducers are transmitted to a base station by means of a 15-channel, constant bandwidth, Inter-Range Instrumentation Group (I.R.I.G.), FM/FM telemetry link for recording on magnetic tape and for display on a real-time strip chart. Calibration signals from the test vehicle are recorded before the test and immediately afterward. A crystal-controlled time reference signal is simultaneously recorded with the data. Wooden dowels actuate pressure-sensitive switches on the bumper of the impacting vehicle prior to impact by wooden dowels to indicate the elapsed time over a known distance to provide a measurement of impact velocity. The initial contact also produces an "event" mark on the data record to establish the instant of contact with the installation.

The multiplex of data channels, transmitted on one radio frequency, is received and demultiplexed onto separate tracks of a 28-track (I.R.I.G.) tape recorder. After the test, the data are played back from the tape machine and digitized. A proprietary software program (WinDigit) converts the analog data from each transducer into engineering units using the R-cal and pre-zero values at 10,000 samples per second, per channel. WinDigit also provides Society of Automotive Engineers SAE J211 class 180 phaseless digital filtering and vehicle impact velocity.

All accelerometers are calibrated annually according to the SAE J211 *4.6.1* by means of a ENDEVCO® 2901, precision primary vibration standard. This device and its support instruments are returned to the factory annually for a National Institute of Standards Technology (NIST) traceable calibration. The subsystems of each data channel are also evaluated annually, using instruments with current NIST traceability, and the results are factored into the accuracy of the total data channel, per SAE J211. Calibrations and evaluations are made any time data are suspect.

The Test Risk Assessment Program (TRAP) uses the data from WinDigit to compute occupant/compartment impact velocities, time of occupant/compartment impact after vehicle

impact, and the highest 10-millisecond (ms) average ridedown acceleration. WinDigit calculates change in vehicle velocity at the end of a given impulse period. In addition, maximum average accelerations over 50-ms intervals in each of the three directions are computed. For reporting purposes, the data from the vehicle-mounted accelerometers are filtered with a 60-Hz digital filter, and acceleration versus time curves for the longitudinal, lateral, and vertical directions are plotted using TRAP.

TRAP uses the data from the yaw, pitch, and roll rate transducers to compute angular displacement in degrees at 0.0001-s intervals and then plots yaw, pitch, and roll versus time. These displacements are in reference to the vehicle-fixed coordinate system with the initial position and orientation of the vehicle-fixed coordinate systems being initial impact.

ANTHROPOMORPHIC DUMMY INSTRUMENTATION

An Alderson Research Laboratories Hybrid II, 50th percentile male anthropomorphic dummy, restrained with lap and shoulder belts, was placed in the driver's position of the 820C vehicle. The dummy was uninstrumented. Use of a dummy in the 2000P vehicle is optional according to *NCHRP Report 350*, and there was no dummy used in the tests with the 2000P vehicle.

PHOTOGRAPHIC INSTRUMENTATION AND DATA PROCESSING

Photographic coverage of the test included three high-speed cameras: one overhead with a field of view perpendicular to the ground and directly over the impact point; one placed behind the installation at an angle; and a third placed to have a field of view parallel to and aligned with the installation at the downstream end. A flash bulb activated by pressure sensitive tape switches was positioned on the impacting vehicle to indicate the instant of contact with the installation and was visible from each camera. The films from these high-speed cameras were analyzed on a computer-linked Motion Analyzer to observe phenomena occurring during the collision and to obtain time-event, displacement, and angular data. A 16-mm movie cine, a BetaCam, a VHS-format video camera and recorder, and still cameras recorded and documented conditions of the test vehicle and installation before and after the test.

TEST VEHICLE PROPULSION AND GUIDANCE

The test vehicle was towed into the test installation using a steel cable guidance and reverse tow system. A steel cable for guiding the test vehicle was tensioned along the path, anchored at each end, and threaded through an attachment to the front wheel of the test vehicle. An additional steel cable was connected to the test vehicle, passed around a pulley near the impact point, through a pulley on the tow vehicle, and then anchored to the ground such that the tow vehicle moved away from the test site. A 2-to-1 speed ratio between the test and tow vehicle existed with this system. Just prior to impact with the installation, the test vehicle was released to be free-wheeling and unrestrained. The vehicle remained free-wheeling, i.e., no steering or braking inputs, until the vehicle cleared the immediate area of the test site, at which time brakes on the vehicle were activated to bring it to a safe and controlled stop.

APPENDIX D. TEST VEHICLE PROPERTIES AND INFORMATION

Date: 08-25-2003 Test No.: 441622-1 VIN No.: 1GCGC24R8VZ237123

Year: 1997 Make: Chevrolet Model: 2500 pickup truck

Tire Inflation Pressure: _____ Odometer: 178947 Tire Size: 245/75R16

Describe any damage to the vehicle prior to test: _____

• Denotes accelerometer location.

NOTES: _____

Engine Type: 8 cyl.
Engine CID: 5.7 liter
Transmission Type:
___ Auto
x Manual
Optional Equipment:
8 lug

Dummy Data:
Type: No dummy
Mass: N/A
Seat Position: N/A

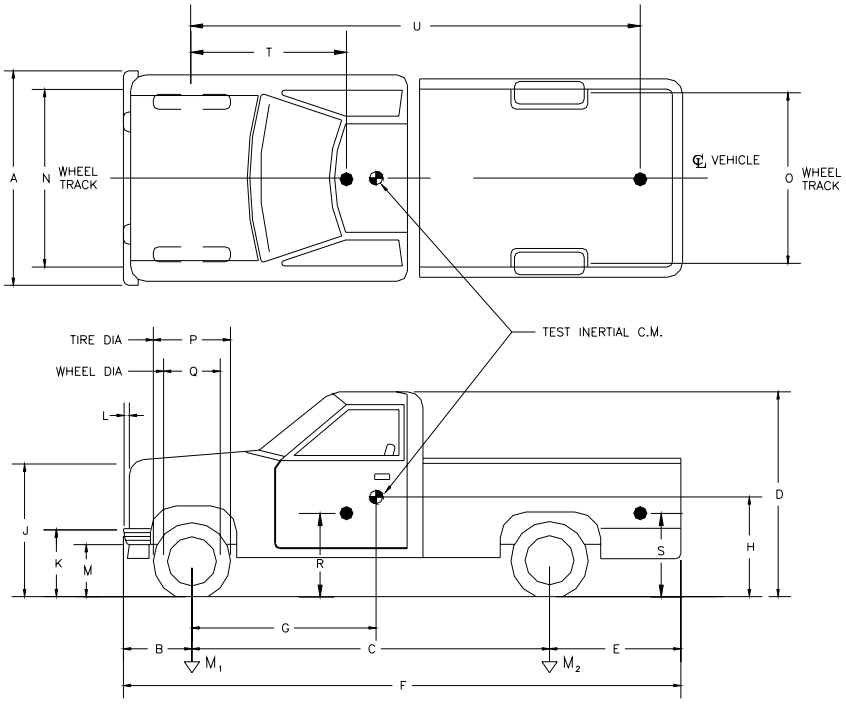

Geometry (mm)

A	1850	E	1310	J	1090	N	1610	R	760
B	860	F	5530	K	670	O	1620	S	910
C	3360	G	1480	L	90	P	750	T	1480
D	1820	H		M	390	Q	440	U	3400

Mass (kg)	Curb	Test Inertial	Gross Static
M_1	1239	1162	
M_2	892	883	
M_{Total}	2131	2045	

Mass Distribution (kg): LF: 587 RF: 575 LR: 445 RR: 438

Figure 80. Vehicle Properties for Test 441622-1.

Table 10. Exterior Crush Measurements for Test 441622-1.

VEHICLE CRUSH MEASUREMENT SHEET[1]

Complete When Applicable	
End Damage	Side Damage
Undeformed end width _____	Bowing: B1 _____ X1 _____
Corner shift: A1 _____	B2 _____ X2 _____
A2 _____	
End shift at frame (CDC)	Bowing constant
(check one)	$\frac{X1+X2}{2}$ = _____
< 4 inches _____	
≥ 4 inches _____	

Note: Measure C_1 to C_6 from Driver to Passenger Side in Front or Rear Impacts – Rear to Front in Side Impacts.

Specific Impact Number	Plane* of C-Measurements	Direct Damage		Field L**	C_1	C_2	C_3	C_4	C_5	C_6	±D
		Width** (CDC)	Max*** Crush								
1	Front Bumper	730	410	680	0	30	110	160	260	410	+280
2	700 Above Ground	870	350	1000	0	80	N/A	N/A	N/A	350	+1520

[1]Table taken from National Accident Sampling System (NASS).

*Identify the plane at which the C-measurements are taken (e.g., at bumper, above bumper, at sill, above sill, at beltline, etc.) or label adjustments (e.g., free space).

Free space value is defined as the distance between the baseline and the original body contour taken at the individual C locations. This may include the following: bumper lead, bumper taper, side protrusion, side taper, etc. Record the value for each C-measurement and maximum crush.

**Measure and document on the vehicle diagram the beginning or end of the direct damage width and field L (e.g., side damage with respect to undamaged axle).

***Measure and document on the vehicle diagram the location of the maximum crush.

Note: Use as many lines/columns as necessary to describe each damage profile.

Table 11. Occupant Compartment Measurements for Test 441622-1.

T R U C K

O c c u p a n t C o m p a r t m e n t D e f o r m a t i o n

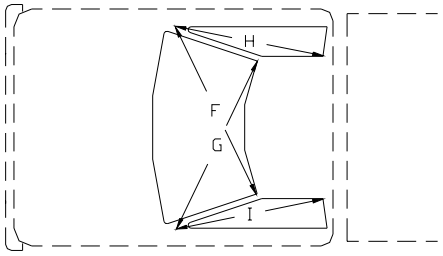

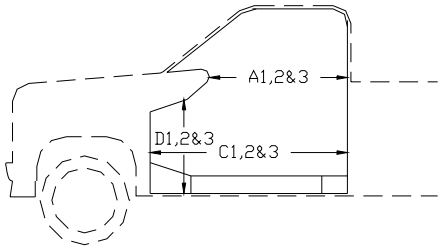

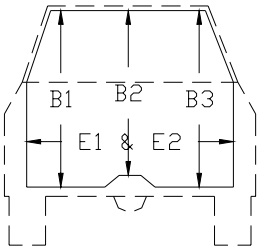

	BEFORE (mm)	AFTER (mm)
A1	910.0	910.0
A2	930.0	930.0
A3	920.0	920.0
B1	1110.0	1110.0
B2	1000.0	980.0
B3	1110.0	1110.0
C1	1380.0	1380.0
C2	1280.0	1280.0
C3	1390.5	1390.5
D1	310.5	310.5
D2	270.5	270.5
D3	320.0	320.0
E1	1580.0	1600.0
E2	1600.0	1600.0
F	1580.0	1580.0
G	1580.0	1580.0
H	750.0	750.0
I	750.0	750.0
J*	1510.5	1510.5

*Lateral area across the cab from
driver's side kickpanel to passenger's side kickpanel.

Date: 08-22-2003 Test No.: 441622-2 VIN No.: 1GCGC24R2WZ135849

Year: 1997 Make: Chevrolet Model: 2500 pickup truck

Tire Inflation Pressure: _____ Odometer: 202105 Tire Size: 245/75R16

Describe any damage to the vehicle prior to test: _____

• Denotes accelerometer location.

NOTES: _____

Engine Type: 8 cyl. G.M. 350
Engine CID: 5.7 liter
Transmission Type:
___ Auto
X Manual
Optional Equipment:
8 lug

Dummy Data:
Type: No dummy
Mass: N/A
Seat Position: N/A

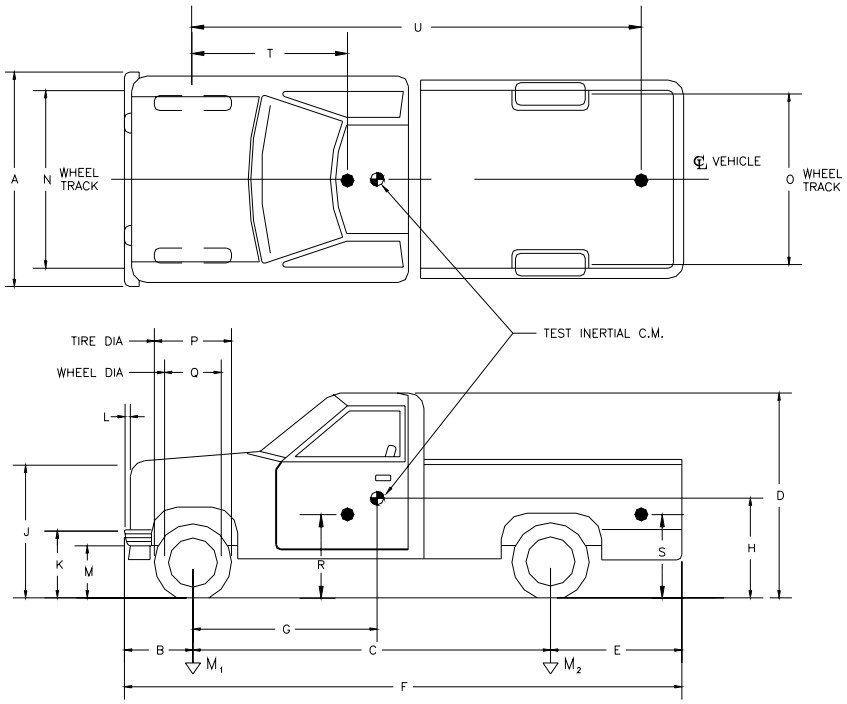

Geometry (mm)

A	1860	E	1325	J	1060	N	1590	R	730
B	830	F	5505	K	650	O	1625	S	910
C	3350	G	1402.66	L	80	P	740	T	1460
D	1820	H		M	370	Q	445	U	3385

Mass (kg)	Curb	Test Inertial	Gross Static
M_1	1222	1187	
M_2	872	855	
M_{Total}	2094	2042	

Mass Distribution (kg): LF: 593 RF: 594 LR: 424 RR: 431

Figure 81. Vehicle Properties for Test 441622-2.

Table 12. Exterior Crush Measurements for Test 441622-2.

VEHICLE CRUSH MEASUREMENT SHEET[1]

Complete When Applicable	
End Damage	Side Damage
Undeformed end width _____	Bowing: B1 _____ X1 _____
Corner shift: A1 _____	B2 _____ X2 _____
A2 _____	
End shift at frame (CDC)	Bowing constant
(check one)	$\frac{X1+X2}{2}$ = _____
< 4 inches _____	
≥ 4 inches _____	

Note: Measure C_1 to C_6 from Driver to Passenger Side in Front or Rear Impacts – Rear to Front in Side Impacts.

Specific Impact Number	Plane* of C-Measurements	Direct Damage		Field L**	C_1	C_2	C_3	C_4	C_5	C_6	±D
		Width** (CDC)	Max*** Crush								
1	Right Front Bumper	600	620	800	50	150	280	400	540	620	+0
2	Right Front Side	620	630	1200	630	360	260	N/A	N/A	25	+1700

[1]Table taken from National Accident Sampling System (NASS).

*Identify the plane at which the C-measurements are taken (e.g., at bumper, above bumper, at sill, above sill, at beltline, etc.) or label adjustments (e.g., free space).

Free space value is defined as the distance between the baseline and the original body contour taken at the individual C locations. This may include the following: bumper lead, bumper taper, side protrusion, side taper, etc. Record the value for each C-measurement and maximum crush.

**Measure and document on the vehicle diagram the beginning or end of the direct damage width and field L (e.g., side damage with respect to undamaged axle).

***Measure and document on the vehicle diagram the location of the maximum crush.

Note: Use as many lines/columns as necessary to describe each damage profile.

Table 13. Occupant Compartment Measurements for Test 441622-2.

T R U C K

O c c u p a n t C o m p a r t m e n t D e f o r m a t i o n

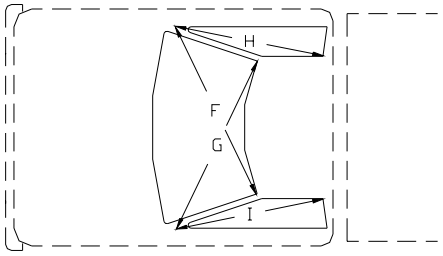

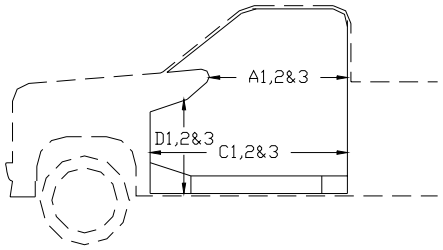

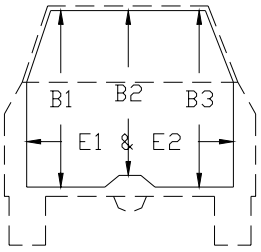

	BEFORE (mm)	AFTER (mm)
A1	909	909
A2	930	930
A3	920	920
B1	1077	1077
B2	1022	998
B3	1076	1071
C1	1386	1386
C2	1259	1250
C3	1393	1390
D1	319	319
D2	352	338
D3	318	320
E1	1590	1590
E2	1595	1595
F	1460	1460
G	1460	1460
H	900	900
I	900	900
J*	1520	1510

*Lateral area across the cab from
driver's side kickpanel to passenger's side kickpanel.

APPENDIX E. SEQUENTIAL PHOTOGRAPHS

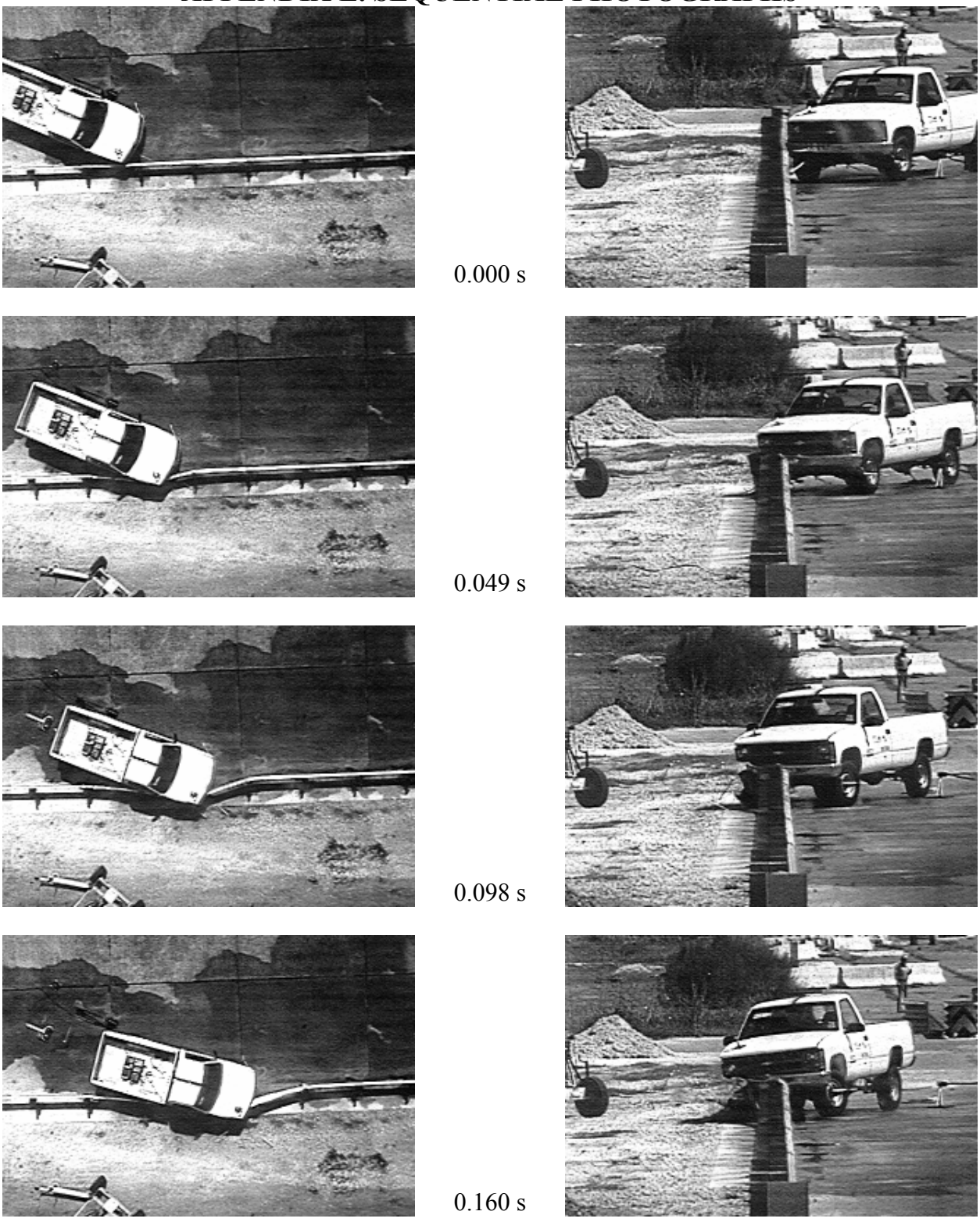

Figure 82. Sequential Photographs for Test 441622-1 (Overhead and Frontal Views).

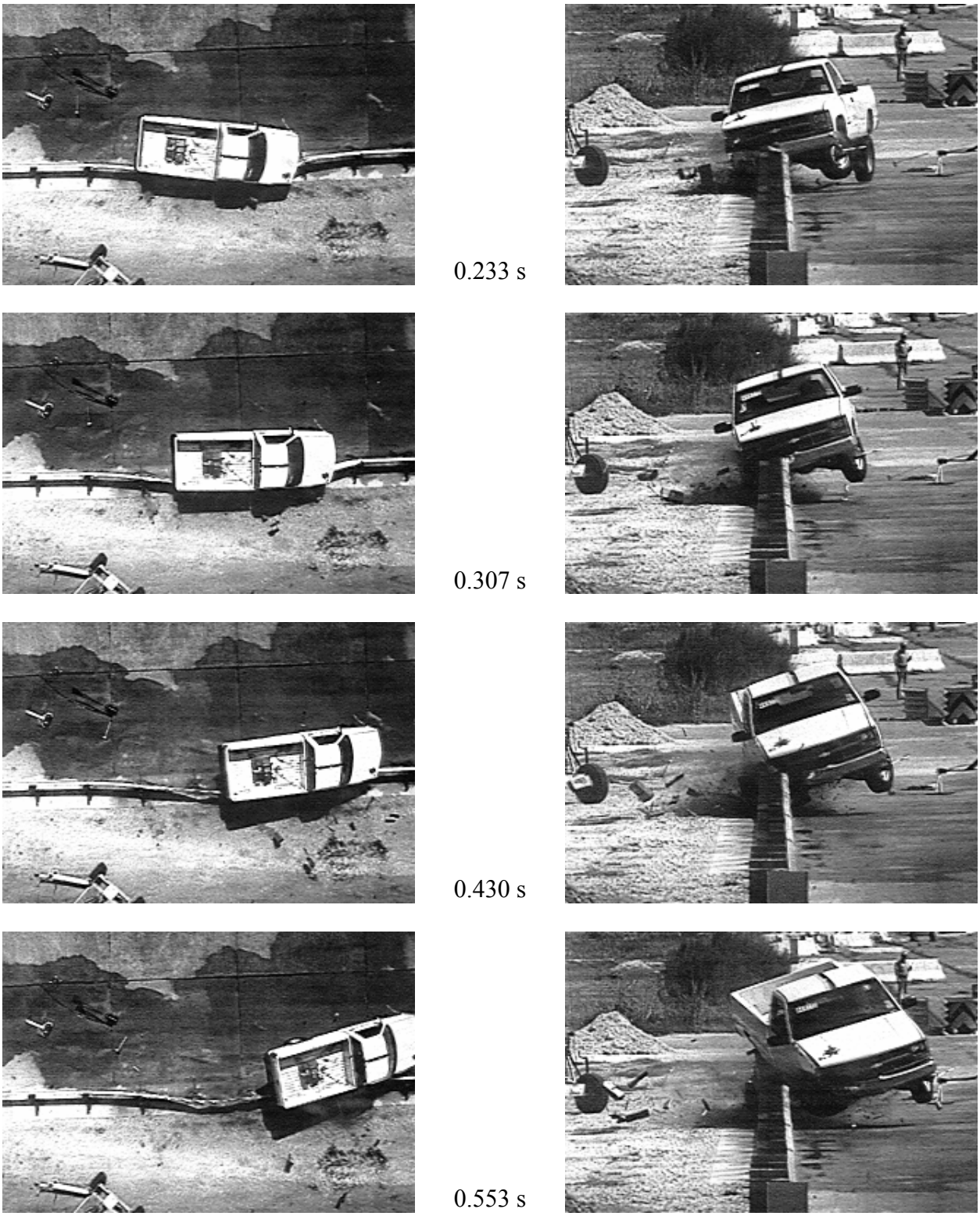

Figure 82. Sequential Photographs for Test 441622-1 (Overhead and Frontal Views) (Continued).


0.000 s


0.233 s


0.049 s


0.307 s


0.098 s


0.430 s


0.160 s


0.553 s

Figure 83. Sequential Photographs for Test 441622-1 (Rear View).

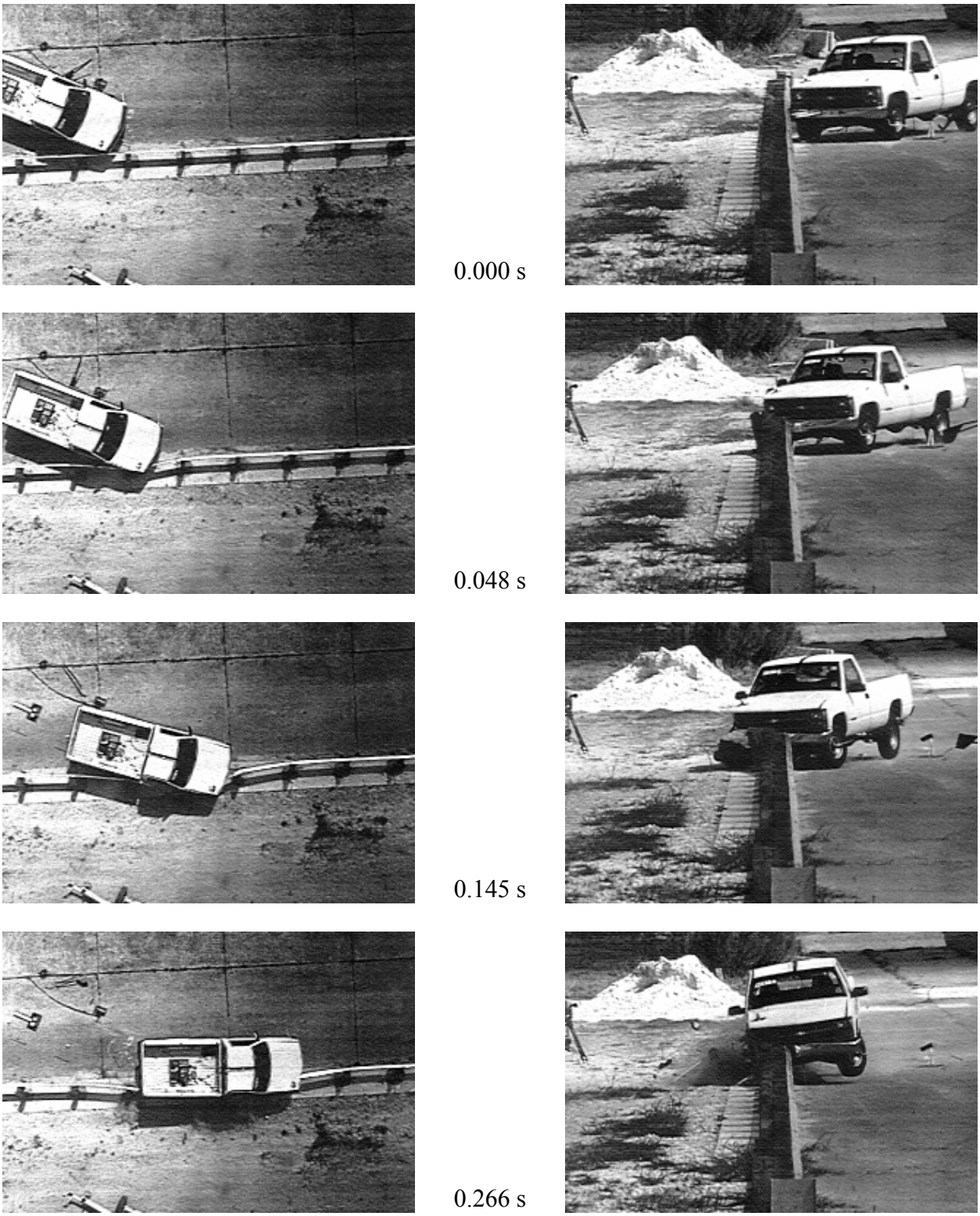

Figure 84. Sequential Photographs for Test 441622-2 (Overhead and Frontal Views).

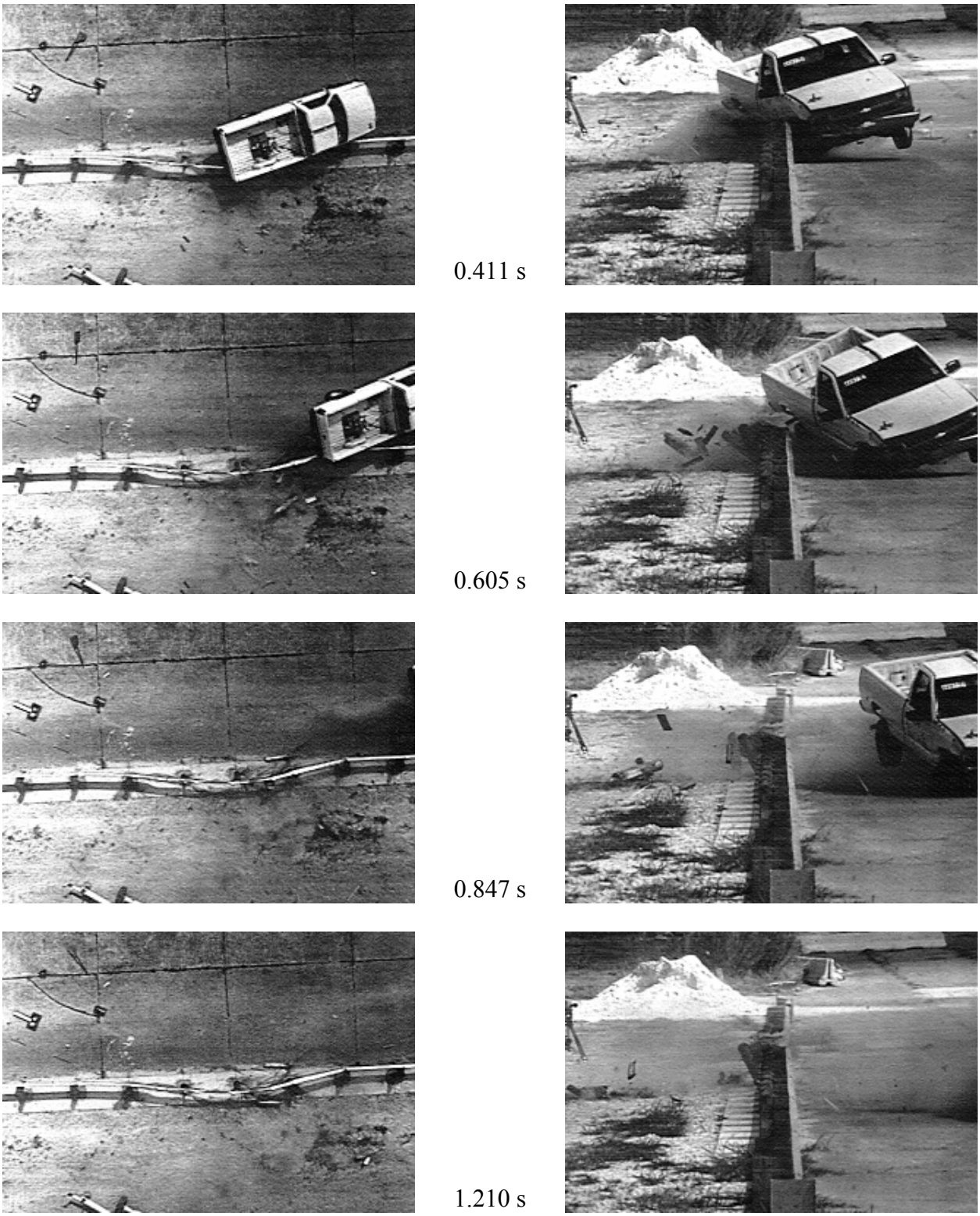

Figure 84. Sequential Photographs for Test 441622-2 (Overhead and Frontal Views) (Continued).

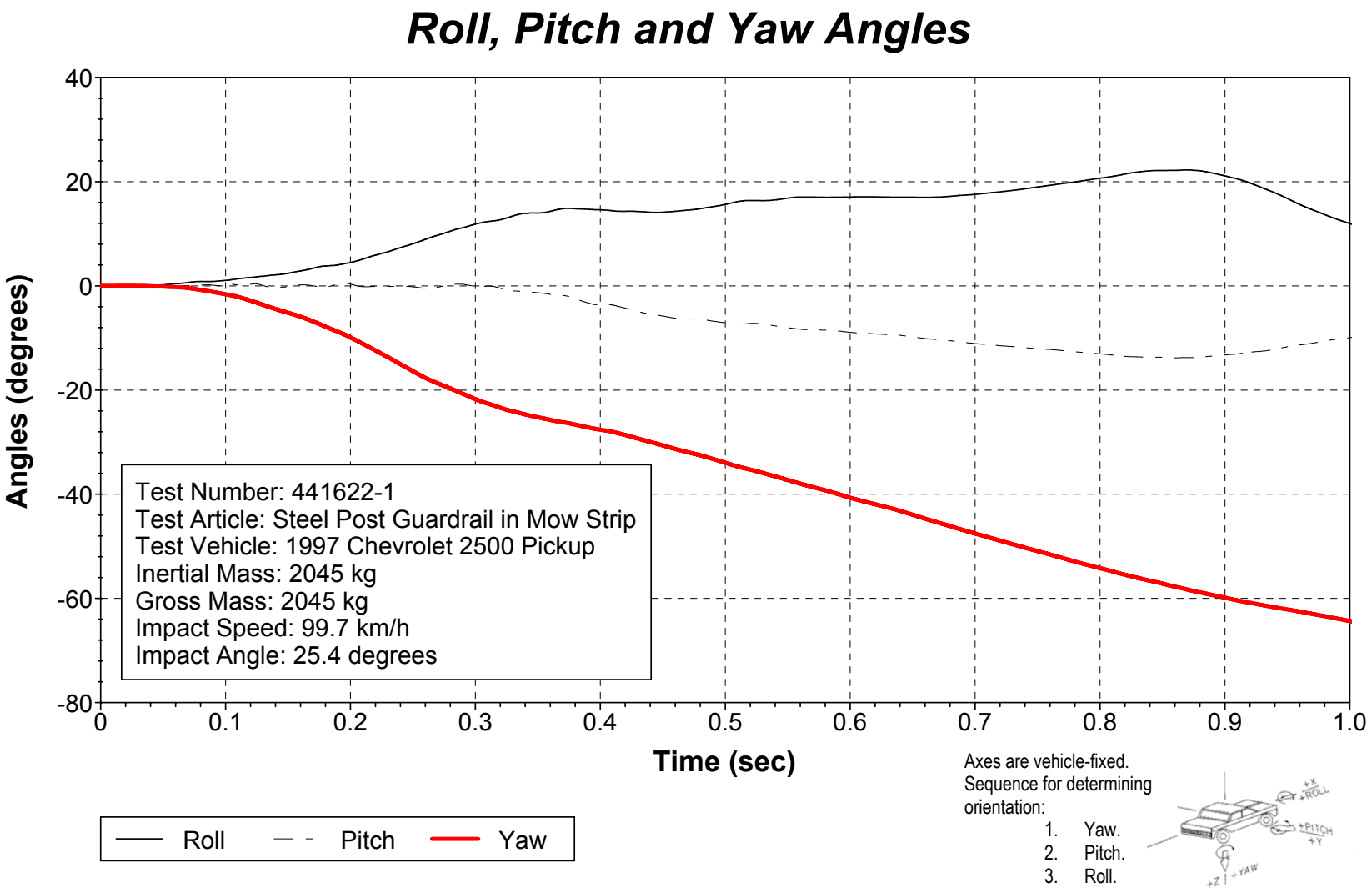

Figure 85. Vehicular Angular Displacements for Test 446122-1.

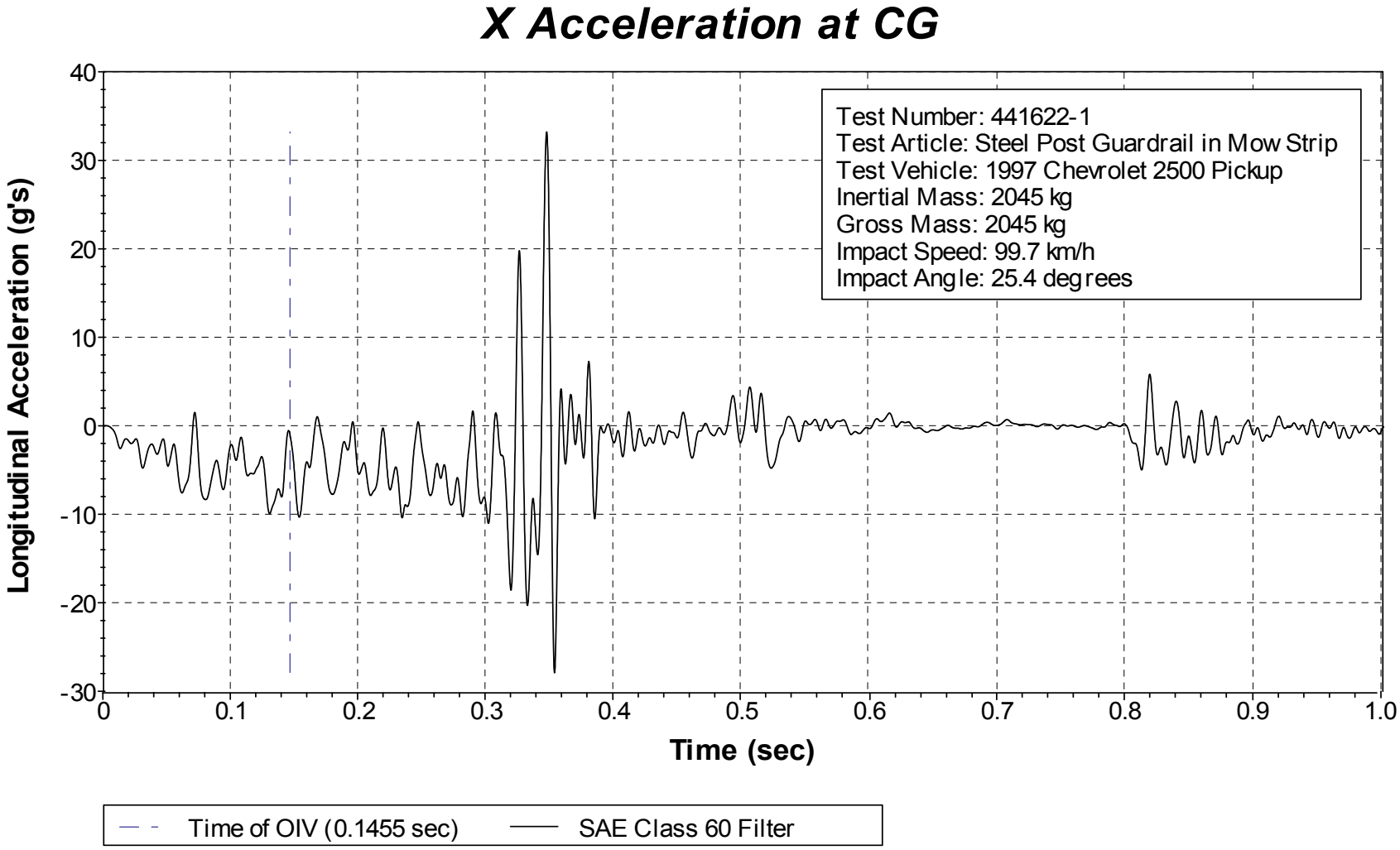

Figure 86. Vehicle Longitudinal Accelerometer Trace for Test 441622-1 (Accelerometer Located at Center of Gravity).

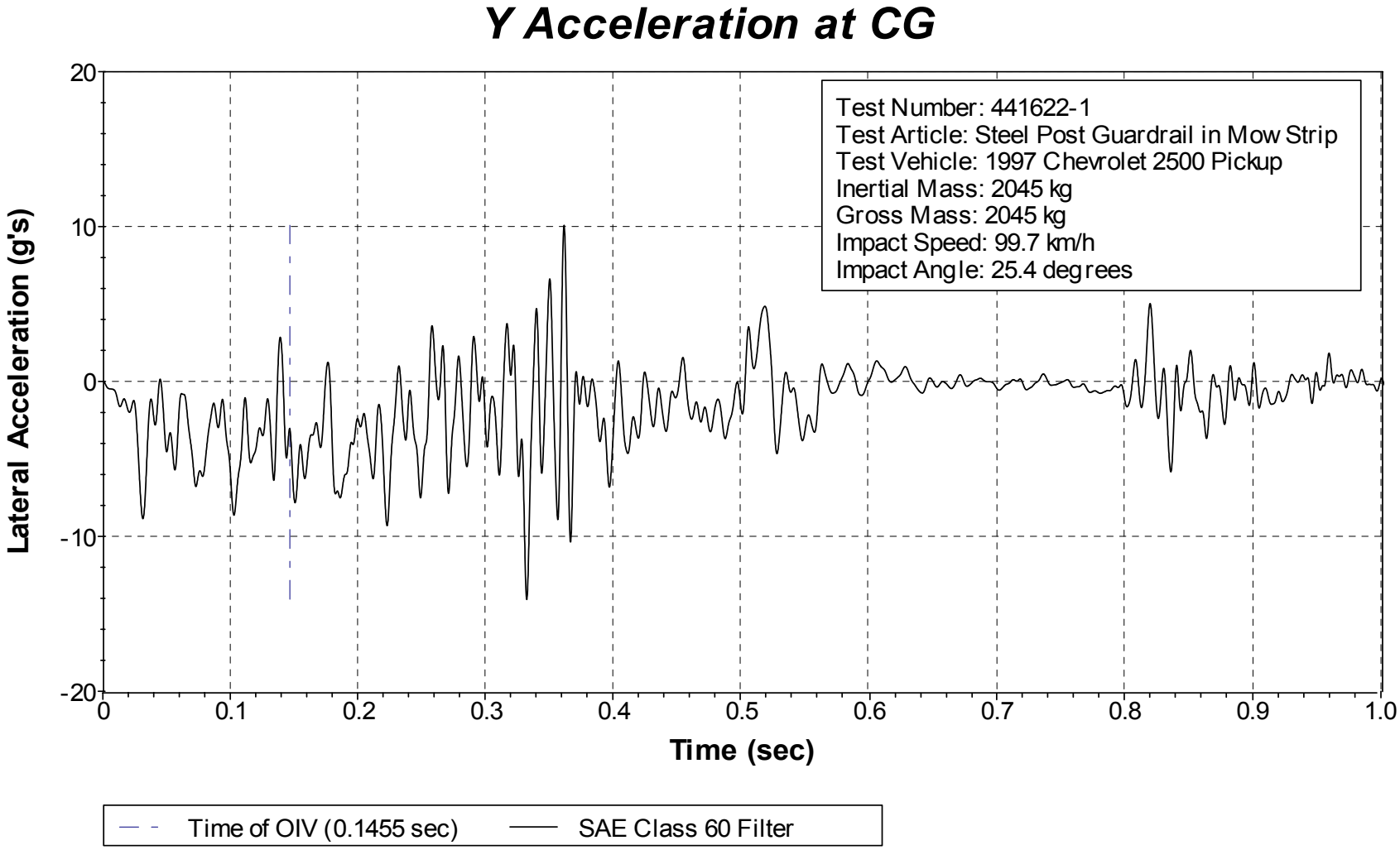

Figure 87. Vehicle Lateral Accelerometer Trace for Test 441622-1 (Accelerometer Located at Center of Gravity).

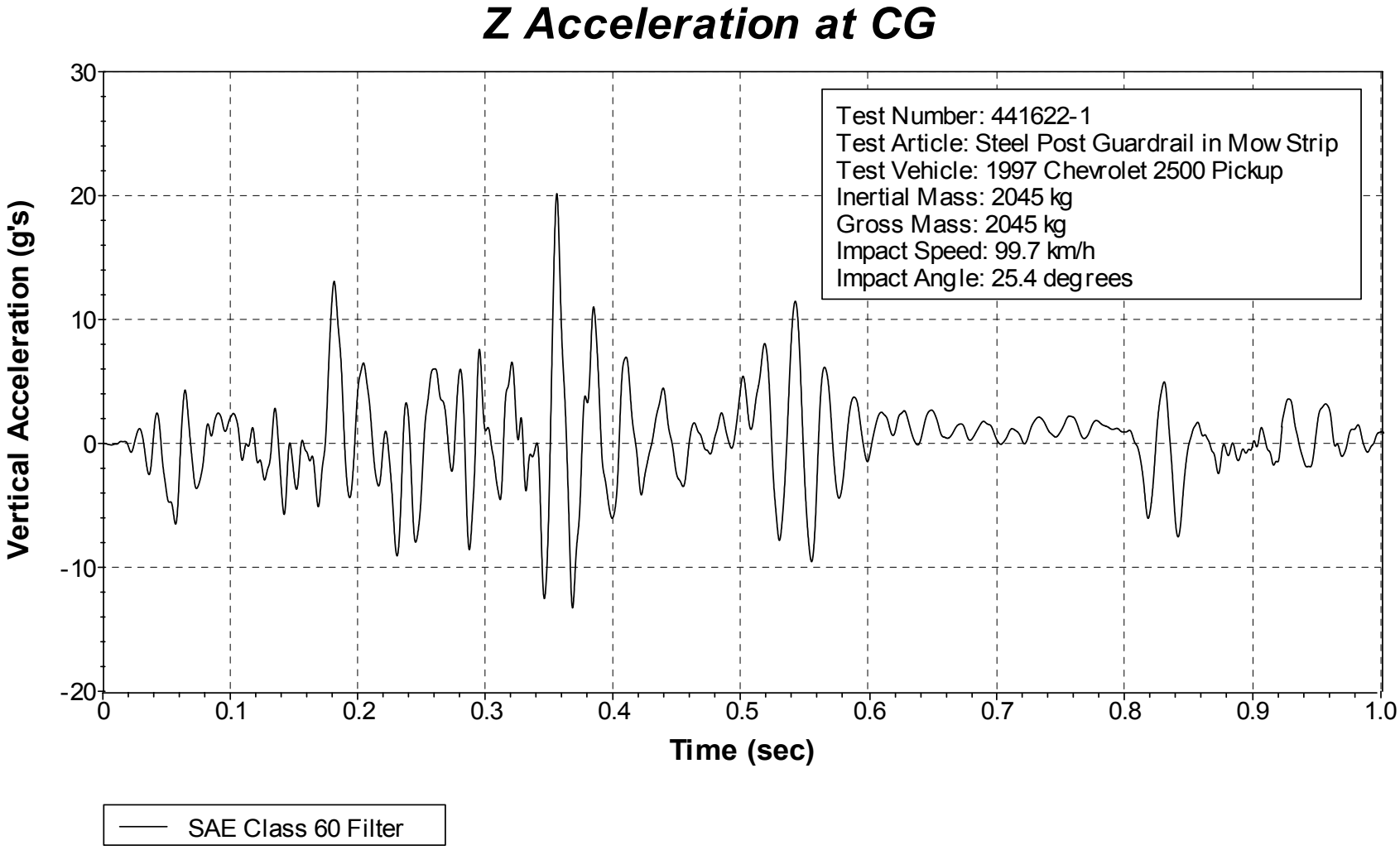

Figure 88. Vehicle Vertical Accelerometer Trace for Test 441622-1 (Accelerometer Located at Center of Gravity).

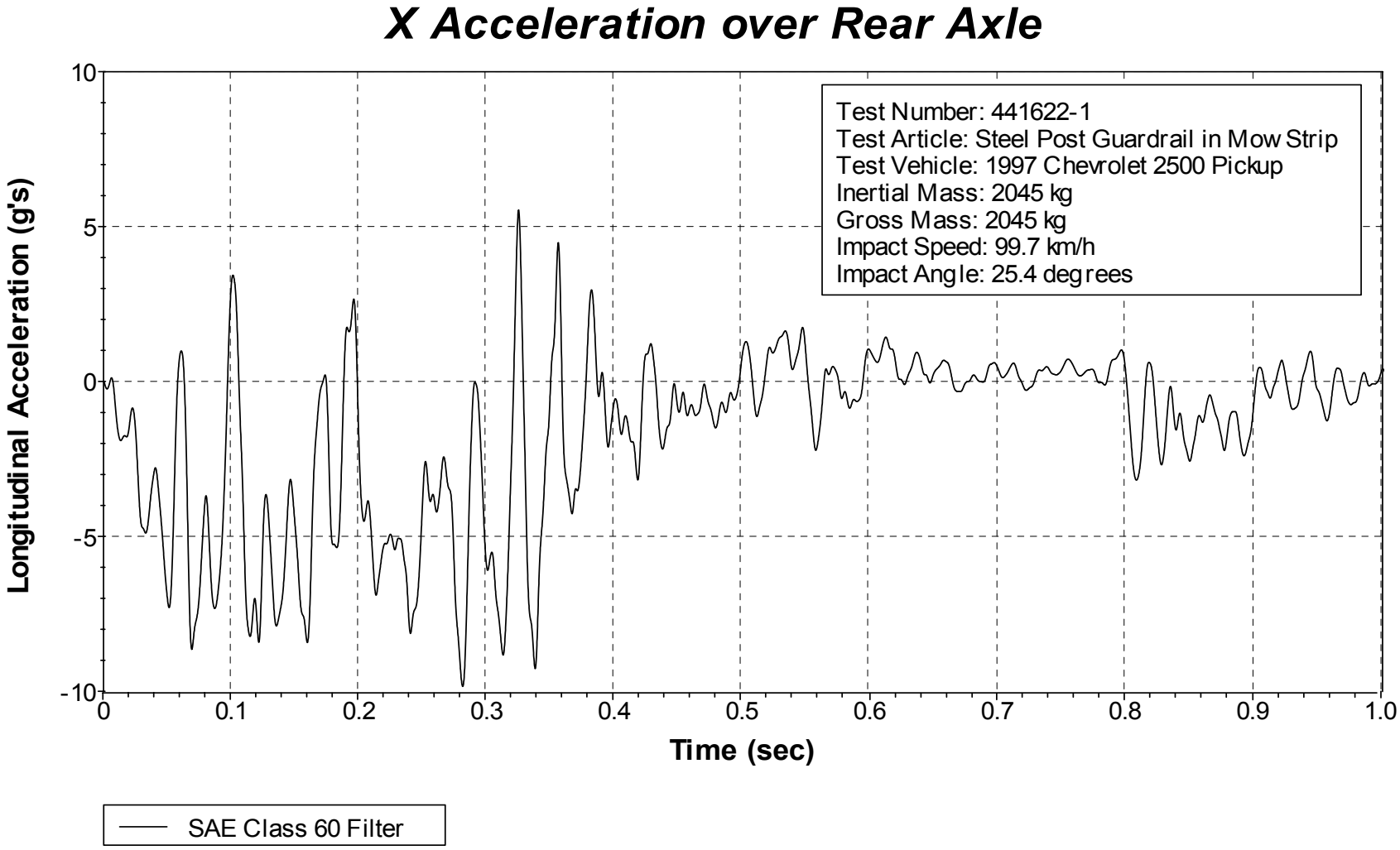

Figure 89. Vehicle Longitudinal Accelerometer Trace for Test 441622-1 (Accelerometer Located over Rear Axle).

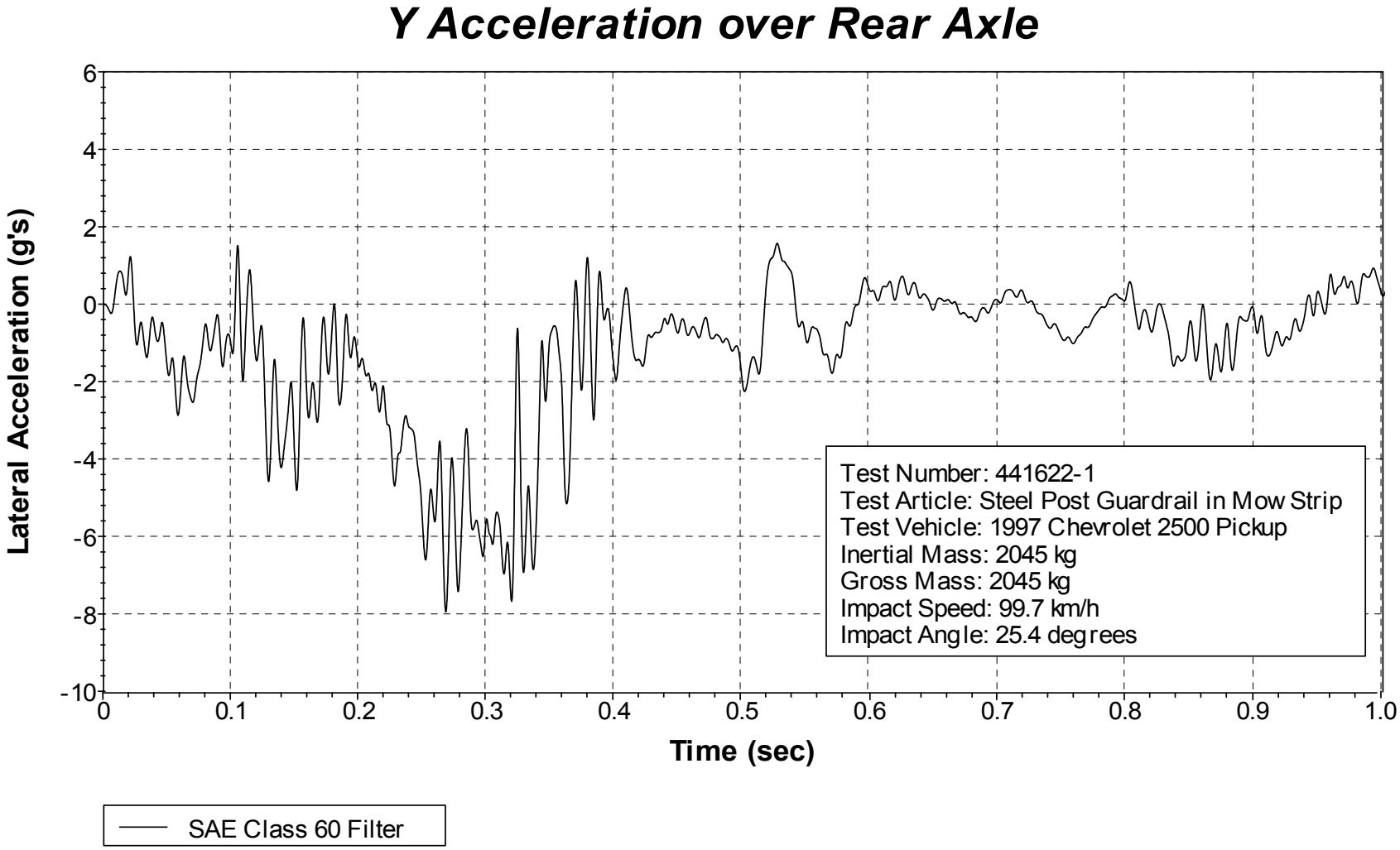

Figure 90. Vehicle Lateral Accelerometer Trace for Test 441622-1 (Accelerometer Located over Rear Axle).

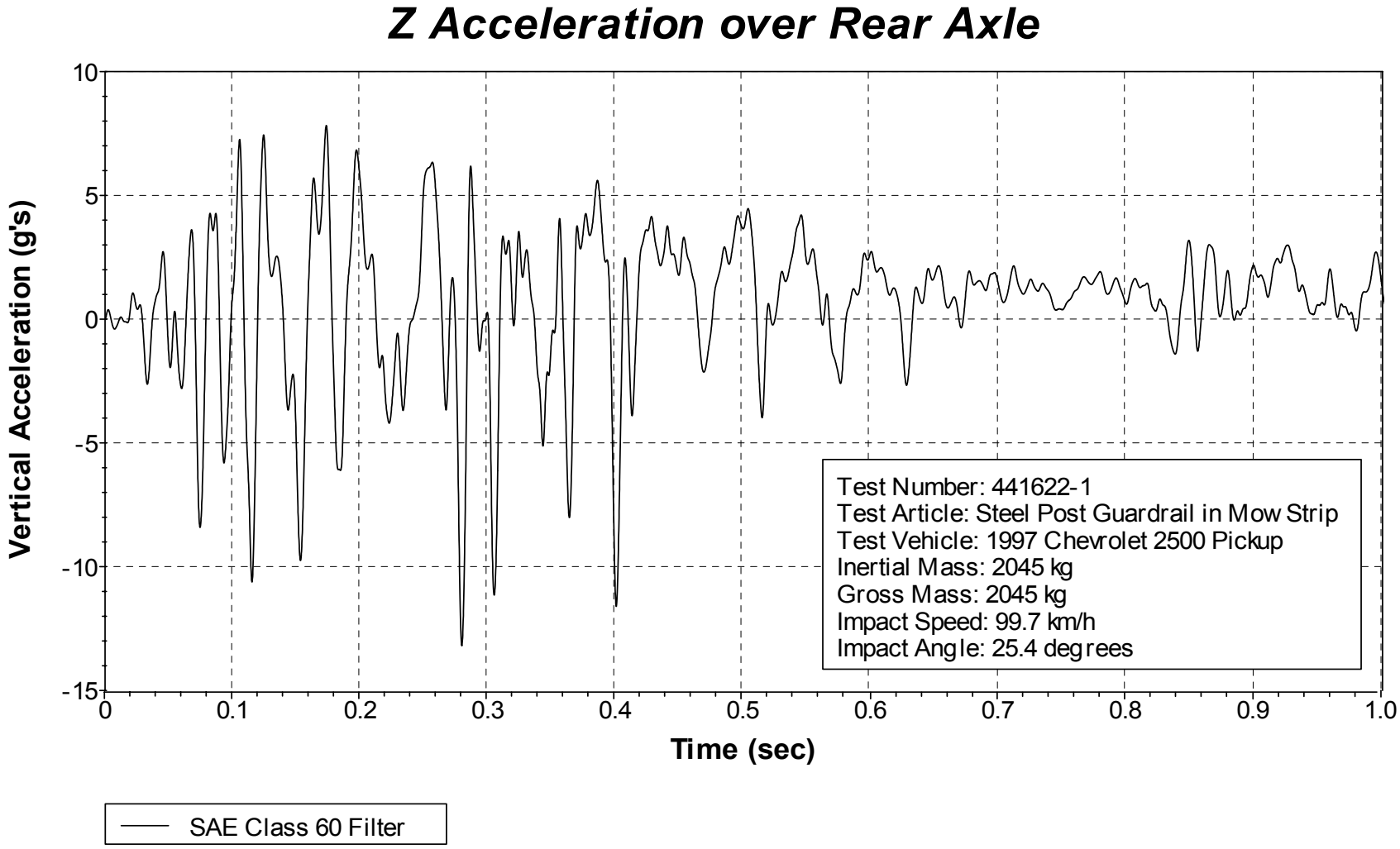

Figure 91. Vehicle Vertical Accelerometer Trace for Test 441622-1 (Accelerometer Located over Rear Axle).

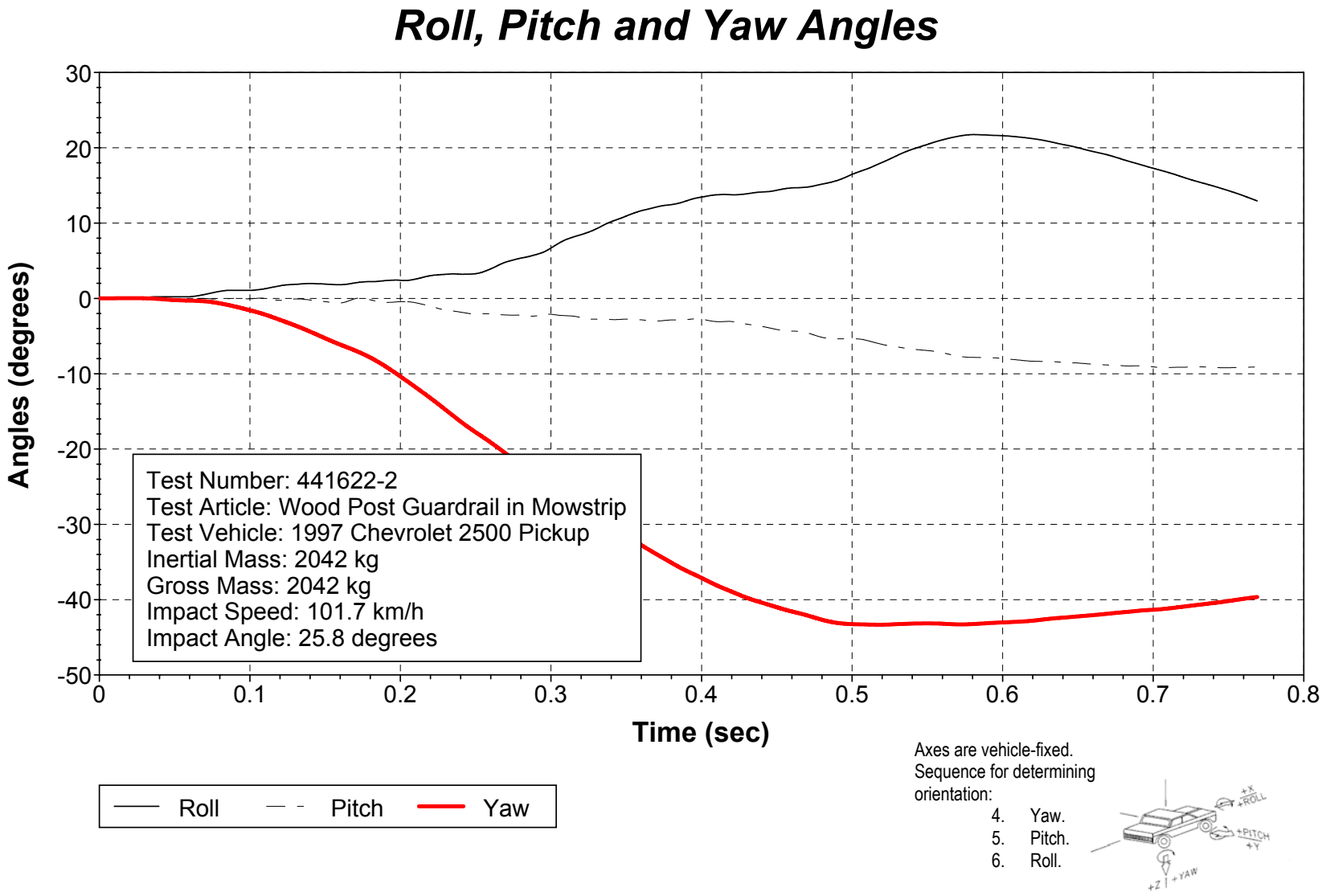

Figure 92. Vehicular Angular Displacements for Test 441622-2.

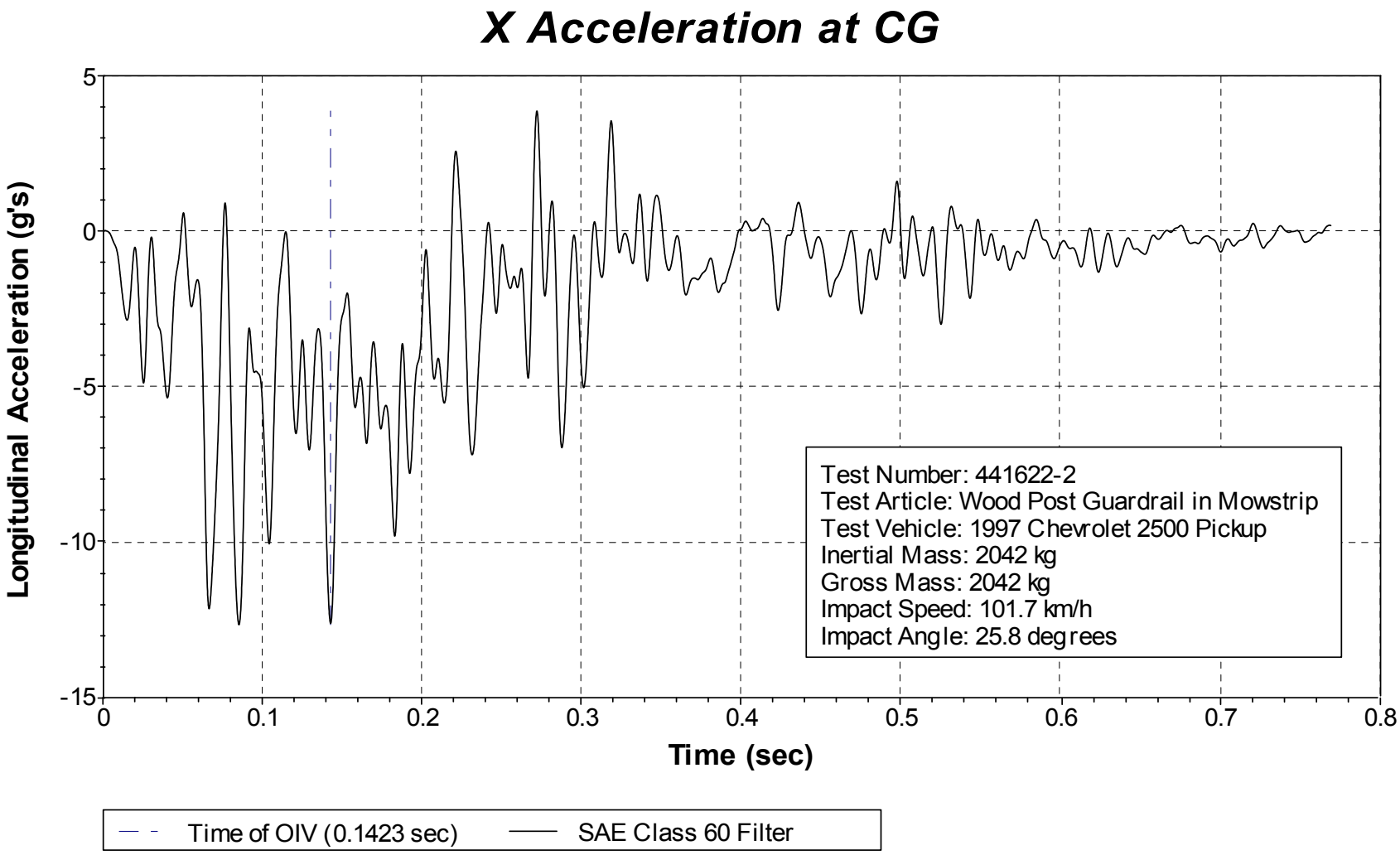

Figure 93. Vehicle Longitudinal Accelerometer Trace for Test 441622-2 (Accelerometer Located at Center of Gravity).

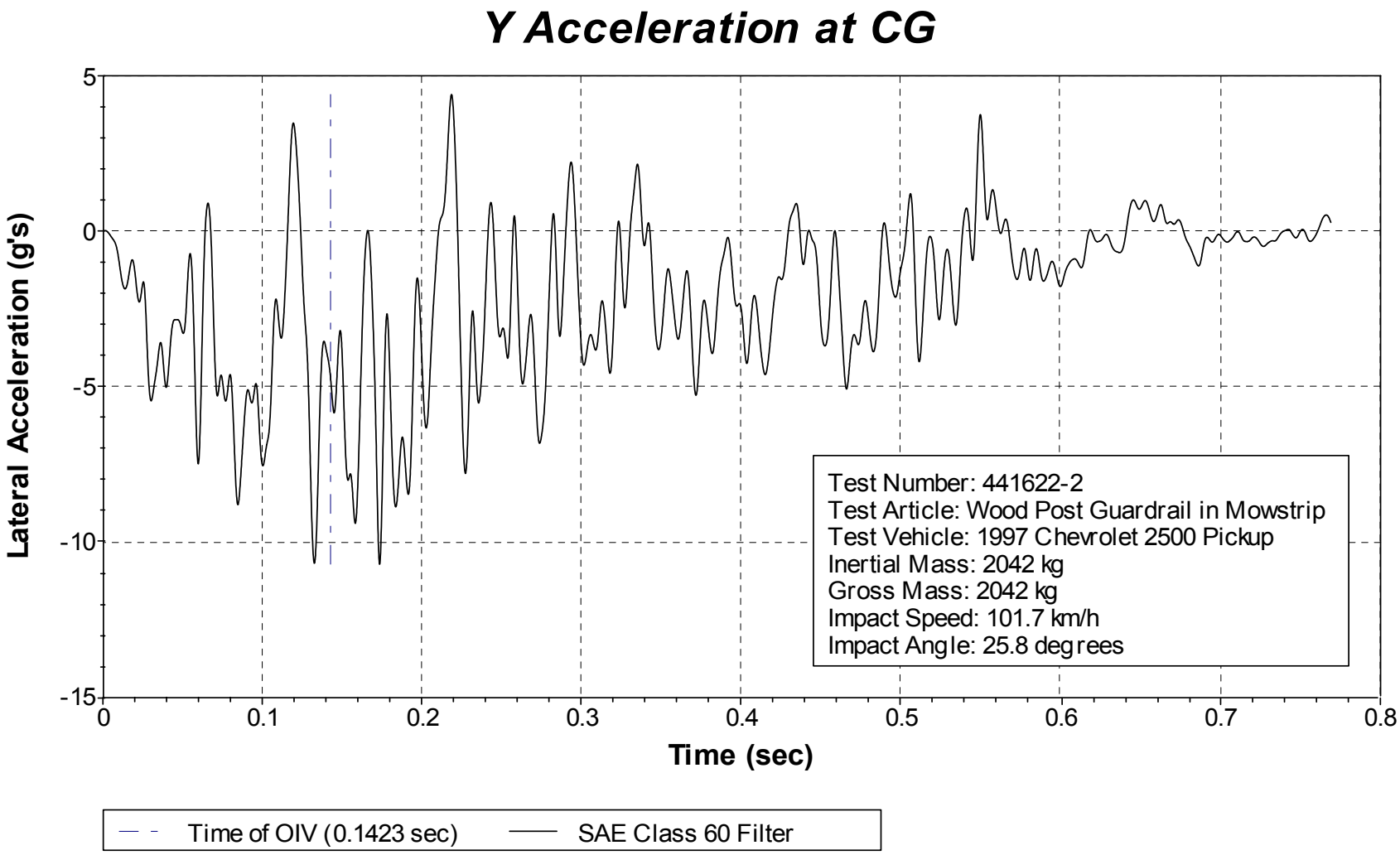

Figure 94. Vehicle Lateral Accelerometer Trace for Test 441622-2 (Accelerometer Located at Center of Gravity).

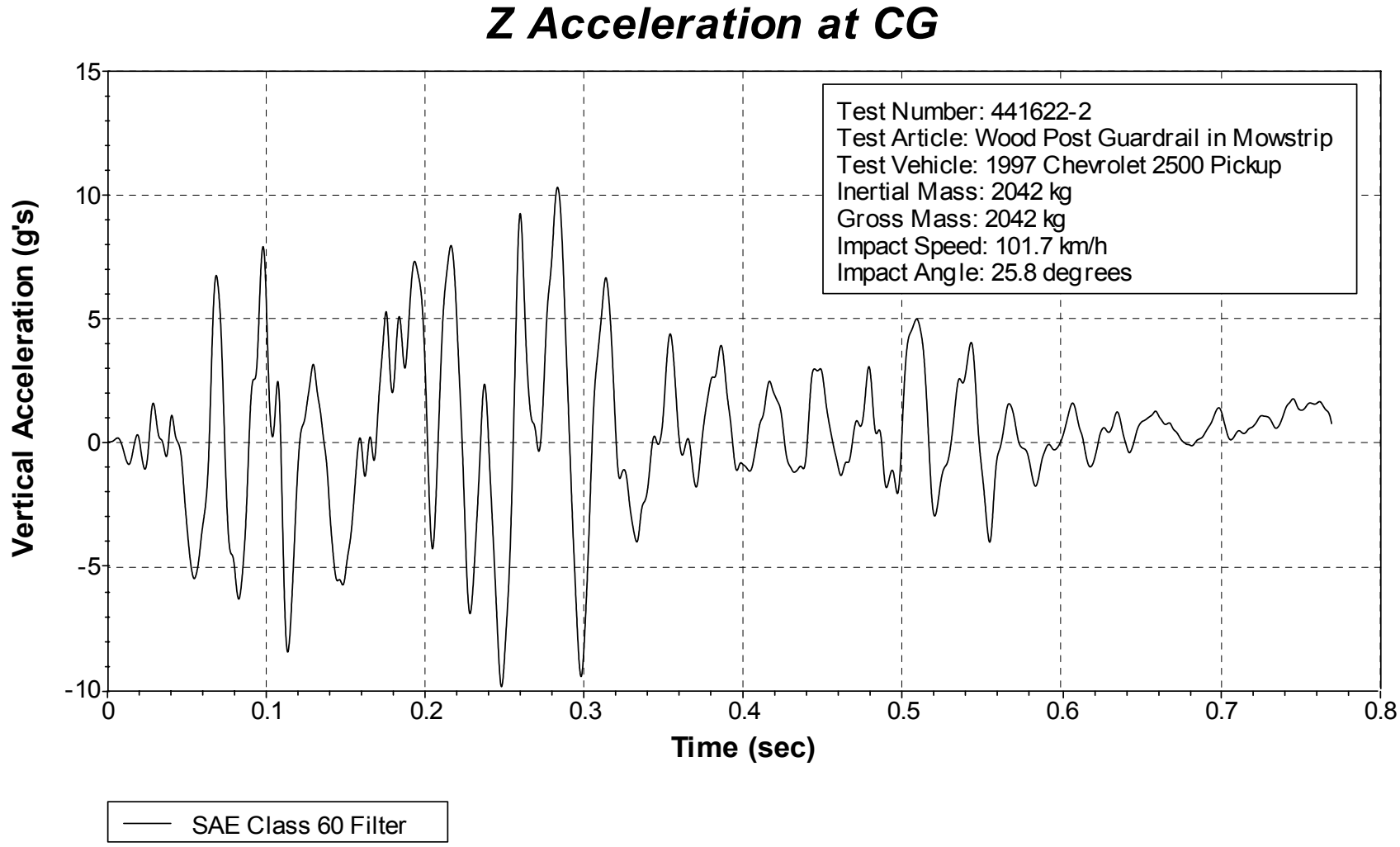

Figure 95. Vehicle Vertical Accelerometer Trace for Test 441622-2 (Accelerometer Located at Center of Gravity).

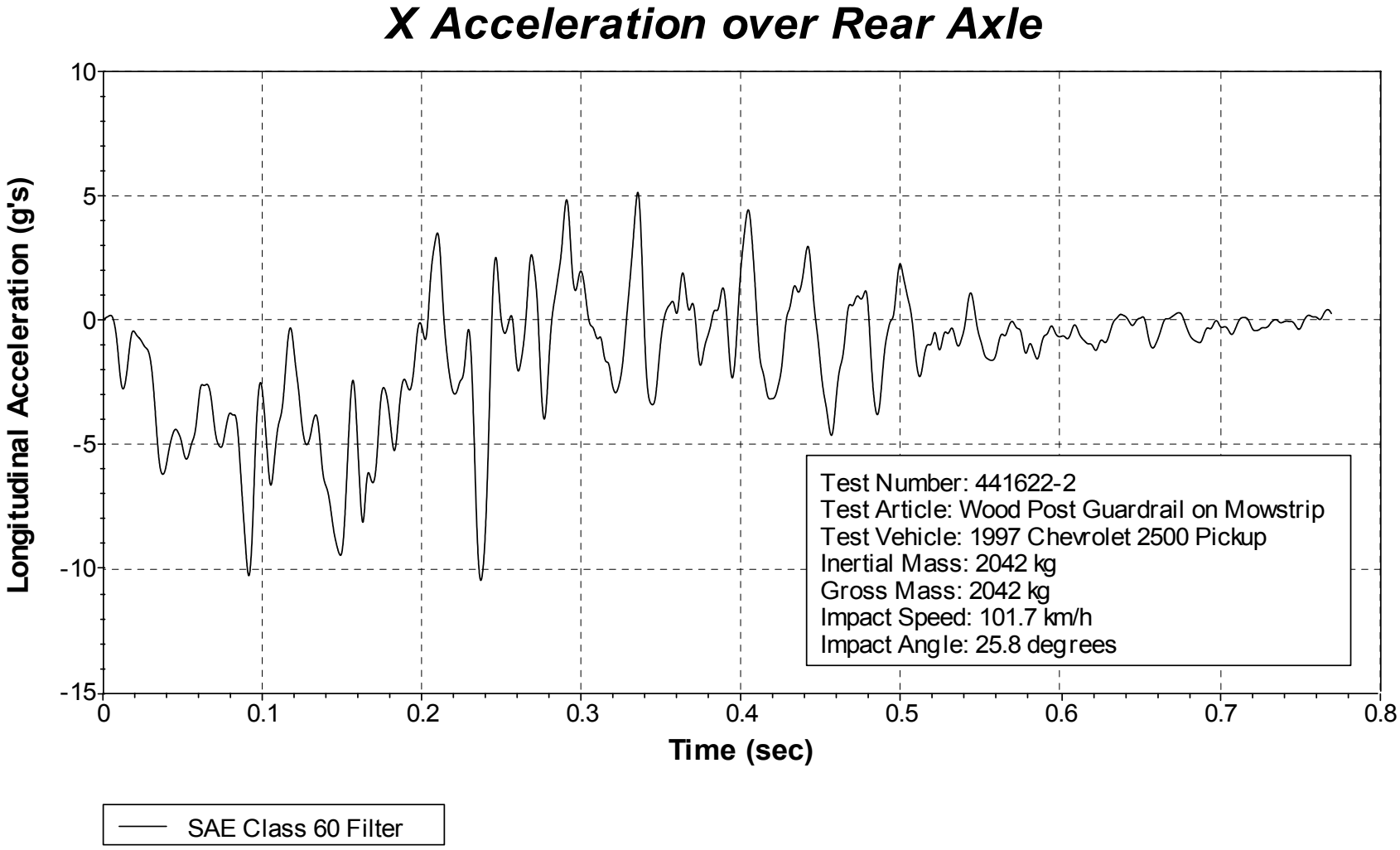

Figure 96. Vehicle Longitudinal Accelerometer Trace for Test 441622-2 (Accelerometer Located over Rear Axle).

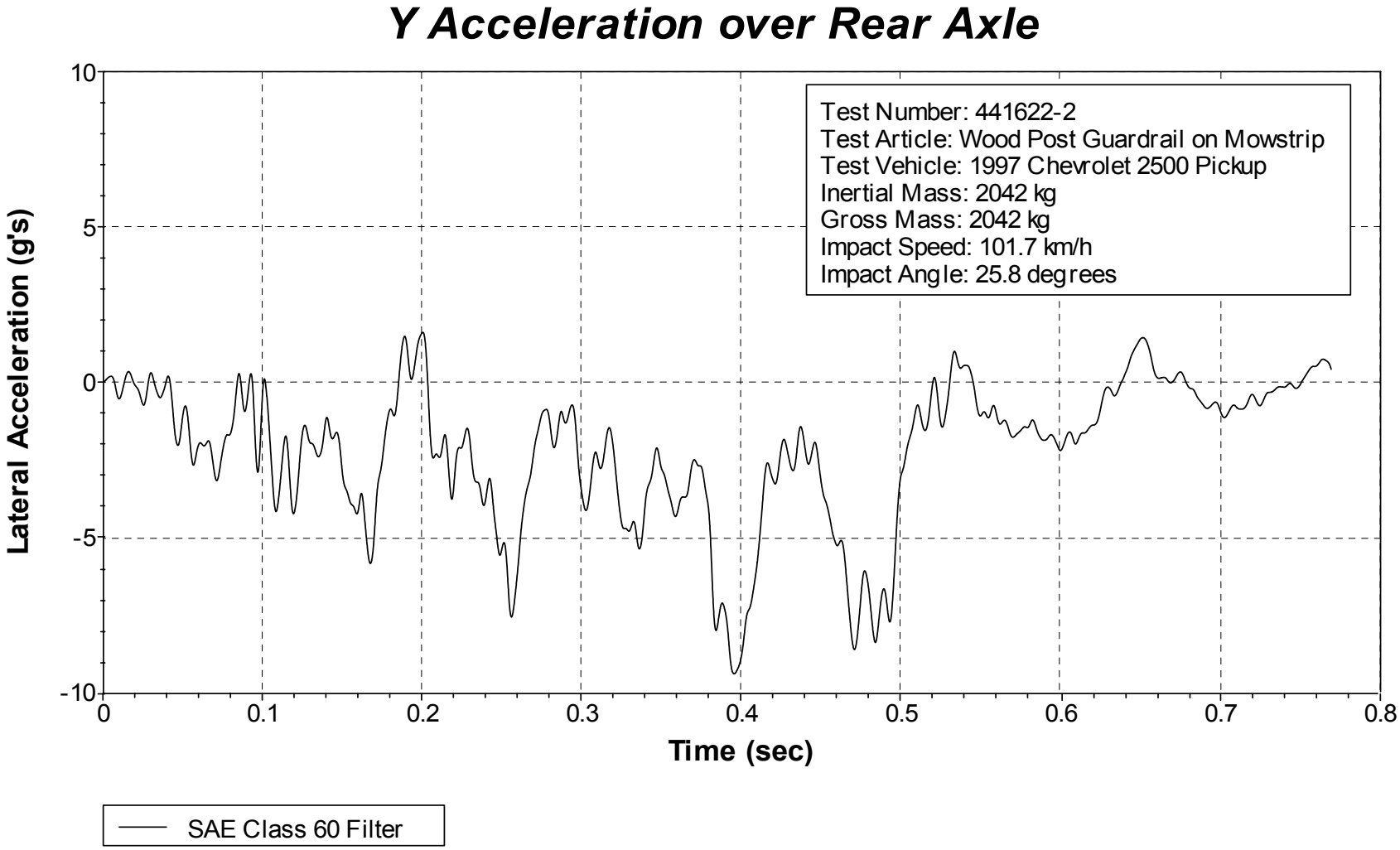

Figure 97. Vehicle Lateral Accelerometer Trace for Test 441622-2 (Accelerometer Located over Rear Axle).

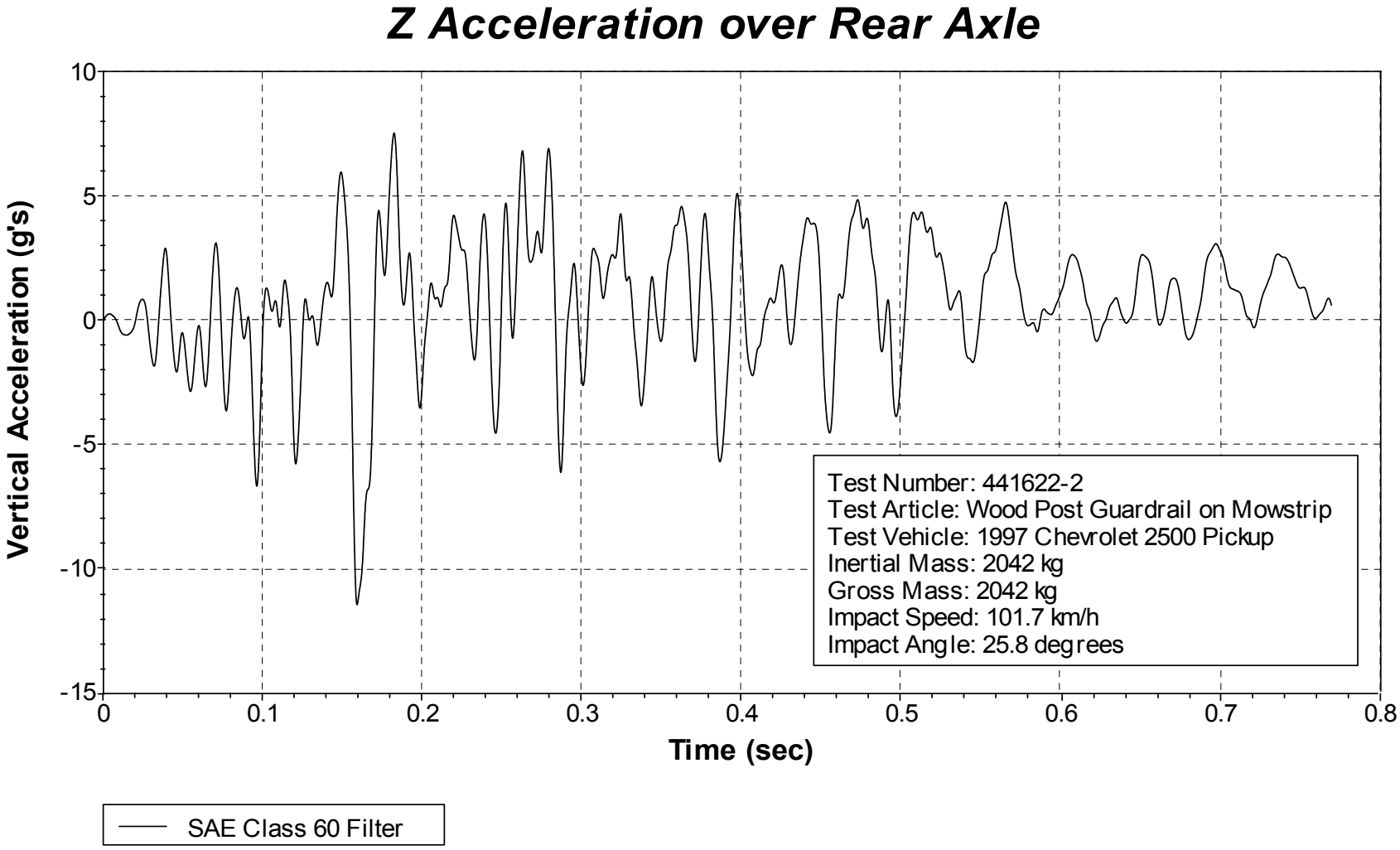

Figure 98. Vehicle Vertical Accelerometer Trace for Test 441622-2 (Accelerometer Located over Rear Axle).